ADDIS ABABA UNIVERSITY

ADDIS ABABA INSTITUTE OF TECHNOLOGY

SCHOOL OF MECHANICAL AND INDUSTRIAL ENGINEERING

GRADUATE PROGRAM IN RAILWAY ENGINEERING

Fatigue Failure Analysis on Curved Rail of Addis Ababa Light Rail Transit (AALRT)

A Research Paper Submitted to Addis Ababa Institute of Technology School of Graduate Studies, Addis Ababa University for Partial Fulfillment of the Requirements for Master of Science in Rolling Stock Engineering.

By

Gemechu Dugassa

Advisor

Dr. Daniel Tilahun

July 2017

ADDIS ABABA UNIVERSITY

Addis Ababa Institute of Technology

School of Mechanical and Industrial Engineering

Fatigue Failure Analysis on Curved Rail of Addis Ababa Light Rail Transit (AALRT)

By

Gemechu Dugassa

July 2017

Approved by Board of Examining:

Dr. Daniel Tilahun	_____	_____
Railway center, Head	Signature	Date
Dr. Daniel Tilahun	_____	_____
Advisor	Signature	Date
Mr. Haileloul Sahle	_____	_____
Internal Examiner	Signature	Date
Mr. Behailu Mamo	_____	_____
External Examiner	Signature	Date

DECLARATION

I, the undersigned, declare that this thesis is my original work and has not been presented for a degree in this or any other universities, and all sources of materials used for the thesis work have been fully acknowledged.

Gemechu Dugassa _____ _____

Name Signature Date

This thesis has been submitted for examination with my approval as a university advisor.

Dr. Daniel Tilahun _____ _____

Name Signature Date

ACKNOWLEDGEMENT

First of all, massive thanks to almighty God, for his countless help to complete my thesis successfully.

I would like to express my heart felt appreciation and gratitude to my Advisor Dr.Daniel Tilahun for his helpful advice and guidance, that he gave to me during my research work to be completed. I would also like to thank him for giving me valuable support with my research work and run with it which allowed me to proceed the research that much more. Without these ideas, this research paper would not have been the success that it has become and he initiates me for completion of the research.

I would like to thank Dawit Belachew in Addis Ababa light rail transit, kality depot construction department and Waquma in Addis Ababa light rail transit kality depot rolling stock department giving me data as per the requirement.

I would like to express my deepest gratitude to my brother Dessalegn Dugassa and my families who have been supported me emotionally and monetarily for many years.

I would like to thank my entire friends who have contributed to my education and have supported me through my graduate study.

ABSTRACT

The rails are the supporting parts with which the wheels are in contact. Rails, as the heart of the railway system, are subjected to very high service loads and harsh environmental conditions. Fatigue failure in rails can be initiated at the rail head, at the web and/or at the foot. The main objective of the study is analyzing fatigue on curved rail due to cyclic wheel load that causes failures and determining fatigue life of rail in Addis Ababa Light Rail Transit. The fatigue analysis on curved rail route on going with 3D modelling on CATIA V5 software and imported to ANSYSv16 workbench software for finite element analysis. The analysis deals with the curved rail route profile with fifty meter radius located at three places (stadium, saint lideta and autobistera) with working period during morning peak hour, day flat hour, and afternoon peak hour. During the analysis of wheel/rail contact in ANSYS software, the parameters have been used are wheel vertical load, wheel lateral load, angular velocity and gravitational acceleration. From ANSYS workbench software result at stadium during afternoon peak hour is highly exposed to the equivalent alternating stress, pressure distribution and fatigue damage than the result at saint lideta and autobistera. For this reason, the rail service life at stadium during afternoon peak hour is small as compared to the rail service life at saint lideta and autobistera curved rail route location. On the curved rail at autobistera: the equivalent alternating stress, pressure distribution and fatigue damage is small in comparison to the curved rail at stadium and saint lideta. The fatigue life will be better at autobistera.

Key words: Addis Ababa Light Rail Transit (AALRT), Fatigue failure on curved rail, Fatigue life.

TABLE OF CONTENTS

ACKNOWLEDGEMENT i
ABSTRACT ii
LIST OF TABLE v
LIST OF FIGURE vi
NOMENCLATURE xi
CHAPTER ONE 1
1. INTRODUCTION 1
1.1. Background of the Study 1
1.1.1. Loads on the track system 2
1.1.2. Standard and Length of the Rail 3
1.1.3. Wheel- Rail contact 4
1.1.4. Railway Rail Fatigue 5
1.1.5. Rolling Contact Fatigue of railway rail 8
1.2. Statement of the Problem 11
1.2.1. General objective 11
1.2.2. Specific objective: 11
1.3. Research Methodology 12
1.4. Significance of the Research 12
1.5. Scope and Limit of the Thesis 12
1.6. Organization of the Paper 13
CHAPTER TWO 14
2. LITERATURE REVIEW 14
2.1. Wheel/rail Contact Mechanics 14
2.2. Rail failure mechanism 15
2.3. Rolling Contact Fatigue of railway rails 17
CHAPTER THREE 22
3. MODEL, ANALYTICAL METHODS AND CONDITIONS 22
3.1. Wheel/Rail material 22
3.2. Wheel /Rail dimension and specification 24
3.3. Wheel/ Rail Analysis Methods. 26
3.3.1. Analysis of Load Distribution and 3D Contact Point Shape 26

3.3.2. Wheel/ Rail Geometrical Model and Assembly 40
3.3.3. Wheel/Rail Analysis using ANSYS16 Work Bench 41
CHAPTER FOUR 48
4. RESULT AND DISCUSSION 48
4.1. Result 48
4.2. Discussion 113
CHAPTER FIVE 115
5. CONCLUSION, RECOMMENDATION AND FUTURE WORK. 122
5.1. Conclusion. 122
5.2. Recommendation. 123
5.3. Future work. 123
APPENDIX 124
REFERENCE 127

LIST OF TABLES

Table 3.1: Mechanical property of rail material for AALRT (19). 23
Table 3.2: Chemical composition of rail material for AALRT (19). 24
Table 3.3: Wheel dimension and specification of AALRT (20). 24
Table 3.4: Operating speed of train for AALRT [20]. 26
Table 3.5: Main parameters of line for AALRT [20]. 26
Table 3.6: Hertz coefficients m and n [8]. 30
Table 3.7: Passenger Loads at Stadium. 33
Table 3.8: Passenger Loads at Saint Lideta. 33
Table 3.9: Passenger Loads at Autobistera. 34
Table 3.10: Vehicle Weight and Passenger Loads. 35
Table 3.11: Vertical and lateral wheel Load. 36
Table 3.12: Vertical and Lateral Wheel Force. 37
Table 3.13: Normal force. 37
Table 3.14: The values of a and b. 37
Table 3.15: Maximum pressure. 38
Table 3.16: The values of a and b. 39
Table 3.17: Maximum pressure. 39
Table 3.18: The values of a and b. 40
Table 3.19: Maximum pressure. 40
Table 4.1: Result summary. 113
Table 4.2: Result summary for worn rail. 118

LIST OF FIGURES

Figure 1.1: Transverse section of rails [1]. 1
Figure 1.2: Rail Profile [3] 2
Figure 1.3:Contact forces at wheel- rail contact zone [4]. 3
Figure 1.4: Wheel rail contact zones [6]. 4
Figure 1.5: Fatigue failure types on rail [3, 4, 10]. 7
Figure 1.6: Spalling originated at head checks [4]. 8
Figure 1.7: Fracture of a rail with origin from a head check [4]. 9
Figure 1.8:Squat: damage of the running surface [4]. 9
Figure 1.9:“Kidney-shaped” crack in a rail head [4]. 10
Figure 2.1: Wheel rail contact [6]. 15
Figure 2.2: Material response to repeated loading [9]. 16
Figure 2.3: Head Checks of high rail. The traffic is in the x direction [12]. 18
Figure 2.4: (a) Severe Head Checks and (b) cross section of a severe single Head Check [12]. . 18
Figure 2.5: Three phases of life of a (rolling contact) fatigue crack initiated at the surface of a rail (8). 19
Figure 2.6. Crack and direction of horizontal load (a,b) [15]. 21
Figure 3.1: Geometrical wheel dimension [20]. 24
Figure 3.2: Geometrical dimension of P50 standard rail for AALRT (19). 25
Figure 3.3: Hertzian contact: the railway case (22). 27
Figure 3.4: The three location of R50 radius of curvature in AALRT [24]. 32
Figure 3.5: Wheel/rail constraint forces (23). 36
Figure 3.6: Wheel/Rail model. 41
Figure 3.7: Wheel/Rail Assembly. 41
Figure 3.8: Wheel/rail assembly imported to ANSYS 16 workbench. 42
Figure 3.9: Wheel/rail assembly mesh. 42
Figure 3.10: Stadium morning peak hour wheel/rail boundary condition and input data. 43
Figure 3.11: Stadium day flat hour boundary condition and input data. 43
Figure 3.12: Stadium afternoon pick hour wheel/rail boundary condition and input data. 44
Figure 3.13: Saint lideta morning peak hour boundary condition and input data. 44

Figure 3.14: Saint lideta during day flat hour boundary condition and input data. 45
Figure 3.15: Saint lideta afternoon peak hour boundary condition and input data. 45
Figure 3.16: Autobistera morning peak hour boundary condition and input data. 46
Figure 3.17: Autobistera day flat hour boundary condition and input data. 46
Figure 3.18: Autobistera afternoon peak hour boundary condition and input data. 47
Figure 4.1: Fatigue life at stadium during morning peak hour. 49
Figure 4.2: Damage at stadium during morning peak hour. 49
Figure 4.3: Safety factor at stadium morning peak hour. 50
Figure 4.4: Equivalent alternating stress at stadium during morning peak hour. 50
Figure 4.5: Fatigue sensitivity at stadium during morning peak hour. 51
Figure 4.6: Fatigue life at stadium during day flat hour. 52
Figure 4.7: Fatigue damage at stadium day flat hour. 52
Figure 4.8: Safety factor at stadium during day flat hour. 53
Figure 4.9: Equivalent alternating stress at stadium day flat hour. 53
Figure 4.10: Fatigue sensitivity at stadium day flat hour. 54
Figure 4.11: Fatigue life at stadium during afternoon peak hour. 55
Figure 4.12: Damage at stadium during afternoon peak hour. 55
Figure 4.13: Fatigue safety factor at stadium afternoon peak hour. 56
Figure 4.14: Equivalent alternating stress.at stadium afternoon pick hour. 56
Figure 4.15: Fatigue sensitivity at stadium during afternoon peak hour. 57
Figure 4.16: Fatigue life at saint lideta during morning peak hour. 58
Figure 4.17: Damage at saint lideta morning peak hour. 58
Figure 4.18: Safety factor at saint lideta morning peak hour. 59
Figure 4.19: Equivalent alternating stress at saint lideta during morning peak hour. 59
Figure 4.20: Fatigue sensitivity at saint lideta during morning peak hour. 60
Figure 4.21: Fatigue life at saint lideta during day flat hour. 61
Figure 4.22: Fatigue damage at saint lideta during day flat hour. 61
Figure 4.23: Safety factor at saint lideta during day flat hour. 62
Figure 4.24: Equivalent alternating stress at saint lideta during day flat hour. 62
Figure 4.25: Safety factor at saint lideta during day flat hour. 63
Figure 4.26: Fatigue life at saint lideta during afternoon peak hour. 64

Figure 4.27: Damage at saint lideta afternoon peak hour. 64
Figure 4.28: Safety factor at saint lideta during morning peak hour. 65
Figure 4.29: Equivalent alternating stress at saint lideta during afternoon peak hour. 65
Figure 4.30: Fatigue sensitivity at saint lideta during afternoon peak hour. 66
Figure 4.31: Fatigue life at autobistera during morning peak hour. 67
Figure 4.32: Fatigue damage at Autobistera during morning peak hour. 67
Figure 4.33: Safety factory at autobistera morning peak hour. 68
Figure 4.34: Equivalent alternating stress at autobistera during morning peak hour. 68
Figure 4.35: Fatigue sensitivity at autobistera during morning peak hour. 69
Figure 4.36: Fatigue life at autobistera during day flat hour. 70
Figure 4.37: Fatigue damage at autobistera during day flat hour. 70
Figure 4.38: Safety factor at autobistera during day flat hour. 71
Figure 4.39: Equivalent alternating stress at autobistera during day flat hour. 71
Figure 4.40: Fatigue sensitivity at autobistera during day flat hour. 72
Figure 4.41: Life at autobistera during afternoon peak hour. 73
Figure 4.42: Damage at autobistera afternoon peak hour. 73
Figure 4.43: Safety factor at autobistera during afternoon peak hour. 74
Figure 4.44: Equivalent alternating stress at autobistera during afternoon peak hour. 74
Figure 4.45: Fatigue sensitivity at autobistera during afternoon peak hour. 75
Figure 4.46: Pressure distribution at stadium during morning peak hour. 76
Figure 4.47: Pressure distribution at stadium during day flat hour. 76
Figure 4.48: Pressure distribution at stadium during afternoon peak hour. 77
Figure 4.49: Pressure distribution saint lideta morning peak hour. 77
Figure 4.50: Pressure distribution at saint lideta during day flat hour. 78
Figure 4.51: Pressure distribution at saint lideta during afternoon peak hour. 78
Figure 4.52: Pressure distribution at autobistera during morning peak hour. 79
Figure 4.53: Pressure distribution at autobistera during day flat hour. 79
Figure 4.54: Pressure distribution at autobistera during afternoon peak hour. 80
Figure 4.55: Fatigue life at stadium during morning peak hour for worn rail. 81
Figure 4.56: Damage at stadium during morning peak hour for worn rail. 81
Figure 4.57: Safety factor at stadium morning peak hour for worn rail. 82

Figure 4.58: Equivalent alternating stress at stadium during morning peak hour for worn rail.. 82
Figure 4.59: Fatigue sensitivity at stadium during morning peak hour for worn rail. 83
Figure 4.60: Fatigue life at stadium during day flat hour for worn rail. 84
Figure 4.61: Fatigue damage at stadium day flat hour for worn rail. 84
Figure 4.62: Safety factor at stadium during day flat hour for worn rail. 85
Figure 4.63: Equivalent alternating stress at stadium day flat hour for worn rail. 85
Figure 4.64: Fatigue sensitivity at stadium day flat hour for worn rail. 86
Figure 4.65: Fatigue life at stadium during afternoon peak hour for worn rail. 87
Figure 4.66: Damage at stadium during afternoon peak hour for worn rail. 87
Figure 4.67: Fatigue safety factor at stadium afternoon peak hour for worn rail. 88
Figure 4.68: Equivalent alternating stress.at stadium afternoon peak hour for worn rail. 88
Figure 4.69: Fatigue sensitivity at stadium during afternoon peak hour for worn rail. 89
Figure 4.70: Fatigue life at saint lideta during morning peak hour for worn rail. 90
Figure 4.71: Damage at saint lideta morning peak hour for worn rail. 90
Figure 4.72: Safety factor at saint lideta morning peak hour for worn rail. 91
Figure 4.73: Equivalent alternating stress at saint lideta during morning peak hour for worn rail. 91
Figure 4.74: Fatigue sensitivity at saint lideta during morning peak hour for worn rail. 92
Figure 4.75: Fatigue life at saint lideta during day flat hour for worn rail. 93
Figure 4.76: Fatigue damage at saint lideta during day flat hour for worn rail. 93
Figure 4.77: Safety factor at saint lideta during day flat hour for worn rail. 94
Figure 4.78: Equivalent alternating stress at saint lideta during day flat hour for worn rail. 94
Figure 4.79: Safety factor at saint lideta during day flat hour for worn rail. 95
Figure 4.80: Fatigue life at saint lideta during afternoon peak hour for worn rail. 96
Figure 4.81: Damage at saint lideta afternoon peak hour for worn rail. 96
Figure 4.82: Safety factor at saint lideta during morning peak hour for worn rail. 97
Figure 4.83: Equivalent alternating stress at saint lideta during afternoon peak hour for worn rail. 97
Figure 4.84: Fatigue sensitivity at saint lideta during afternoon peak hour for worn rail. 98
Figure 4.85: Fatigue life at autobistera during morning peak hour for worn rail. 99
Figure 4.86: Fatigue damage at Autobistera during morning peak hour for worn rail. 99

Figure 4.87: Safety factory at autobistera morning peak hour for worn rail. 100
Figure 4.88: Equivalent alternating stress at autobistera during morning peak hour for worn rail. 100
Figure 4.89: Fatigue sensitivity at autobistera during morning peak hour for worn rail. 101
Figure 4.90: Fatigue life at autobistera during day flat hour for worn rail. 102
Figure 4.91: Fatigue damage at autobistera during day flat hour for worn rail. 102
Figure 4.92: Safety factor at autobistera during day flat hour for worn rail. 103
Figure 4.93: Equivalent alternating stress at autobistera during day flat hour for worn rail. 103
Figure 4.94: Fatigue sensitivity at autobistera during day flat hour for worn rail. 104
Figure 4.95: Life at autobistera during afternoon peak hour for worn rail. 105
Figure 4.96: Damage at autobistera afternoon peak hour for worn rail. 105
Figure 4.97: Safety factor at autobistera during afternoon peak hour for worn rail. 106
Figure 4.98: Equivalent alternating stress at autobistera during afternoon peak hour for worn rail. 106
Figure 4.99: Fatigue sensitivity at autobistera during afternoon peak hour for worn rail. 107
Figure 4.100: Pressure distribution at stadium during morning peak hour for worn rail. 108
Figure 4.101: Pressure distribution at stadium during day flat hour for worn rail. 108
Figure 4.102: Pressure distribution at stadium during afternoon peak hour for worn rail..... 109
Figure 4.103: Pressure distribution saint lideta morning peak hour for worn rail. 109
Figure 4.104: Pressure distribution at saint lideta during day flat hour for worn rail. 110
Figure 4.105: Pressure distribution at saint lideta during afternoon peak hour for worn rail. 110
Figure 4.106: Pressure distribution at autobistera during morning peak hour for worn rail. 111
Figure 4.107: Pressure distribution at autobistera during day flat hour for worn rail. 111
Figure 4.108: Pressure distribution at autobistera during afternoon peak hour of worn rail. 112
Figure 4.109: Pressure distribution graph during morning peak hour. 115
Figure 4.110: Pressure distribution graph during day flat hour. 116
Figure 4.111: Pressure distribution graph during afternoon peak hour. 117
Figure 4.112: Pressure distribution graph during morning peak hour for worn rail. 119
Figure 4.113: Pressure distribution graph during day flat hour for worn rail. 120
Figure 4.114: Pressure distribution graph during afternoon peak hour for worn rail. 121

NOMENCLATURE

UIC: International union of railways.

AREA: American Railway Engineering Association

ASCE: American Society of Civil Engineers

ASTM: American Society for Testing and Materials

BS: British Standards

AOA: Angle of attack.

S: Stress

N: Number of cycles to failure.

KN: Kilo Newton.

Kg: kilogram.

m: Meter.

mm: Millimeter

RCF: Rolling contact fatigue

HC: Head check

WEL: white etching layer

HCT: Hertz contact theory

AALRT: Addis Ababa light Rail Transit.

R_1^w : The principal rolling radii of the wheel

R_2^w: The principal transverse radii of the wheel

R_1^r: The principal rolling radii of the rail

R_2^r : The principal transverse radii of the rail.

P: The contact pressure,

F_n: The vertical load on the contact patch

a: The longitudinal semi-axes of the contact ellipse

b: Lateral semi-axes of the contact ellipse

φ: The angle of the orientation difference of the principal axes of the two bodies.

θ: For a curved rail segment,

v: Poisson's ratio and railway wheel material

E^w: Young's modulus of the railway wheel material

v^r: Poisson's ratio of railway rail material.

E^r: Young's modulus of the railway rail material

CHAPTER ONE

1. INTRODUCTION

1.1. Background of the Study

The technology of rail tracks developed over a long period, starting with primitive timber rails in mines in the 16thcentury. The use of the iron rails goes back to the middle of 1700 together with the invention of the first steam machine [1]. During a crisis as a result of overproduction in the iron industry in England in 1760, the wooden rails were covered with cast iron plates which caused the running resistance to diminish to such an extent that the application of such plates soon proliferated. About 1800 the first free bearing rails were applied, which were supported at the ends by cast iron sockets on wooden sleepers [2].

The rails are the supporting parts with which the wheels are in contact. They are steel madeand must resist to the heavy vertical and lateral loads transmitted by the wheels. Figure: 1.1.Shows the transverse sections of three types of rails: the first, named *Vignola* (by its inventor *Charles Vignolas*) is the most used in the railroads while the second and third types are used in the urban transport; the last type is used in the curve [1].

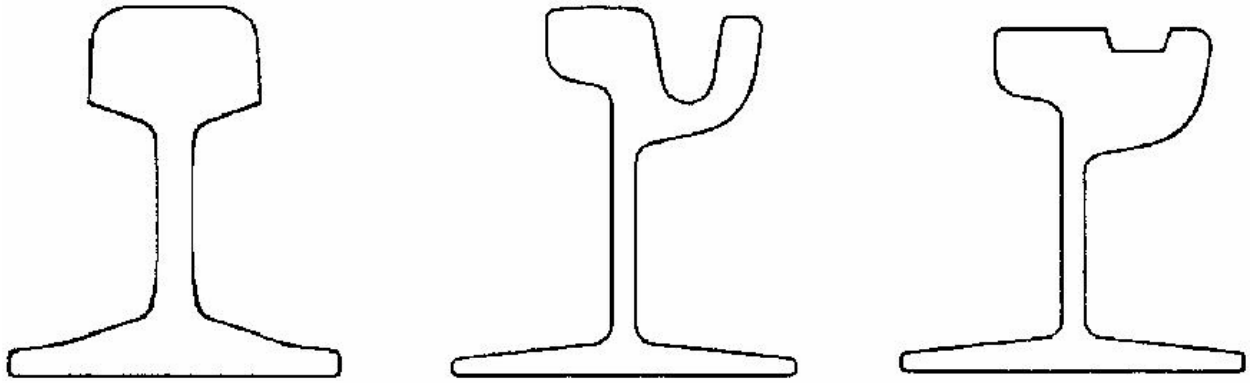

1. Vignola 2. Phoenix 3. Gola riempita

Figure 1.1: Transverse section of rails [1].

It took many decades to improve the quality of the rail materials, including the change from iron to steel. The heavier the rails and the rest of the track work the heavier and faster the trains the track can carry. Modern track typically uses Flat bottomed rail Hot rolled steel with a profile of

an asymmetrical rounded I-beam. Unlike some other uses of iron and steel, railway rails are subject to very high stresses and have to be made of very high-quality steel alloy

The rail is one of the most important components of the track structure. Usually a flat-bottom rail is used in conventional railway track, which can be divided into three parts: the *head* that is in contact with the wheels, the *foot* that is connected with the sleepers and the *web* that connects together the head and the foot [3].

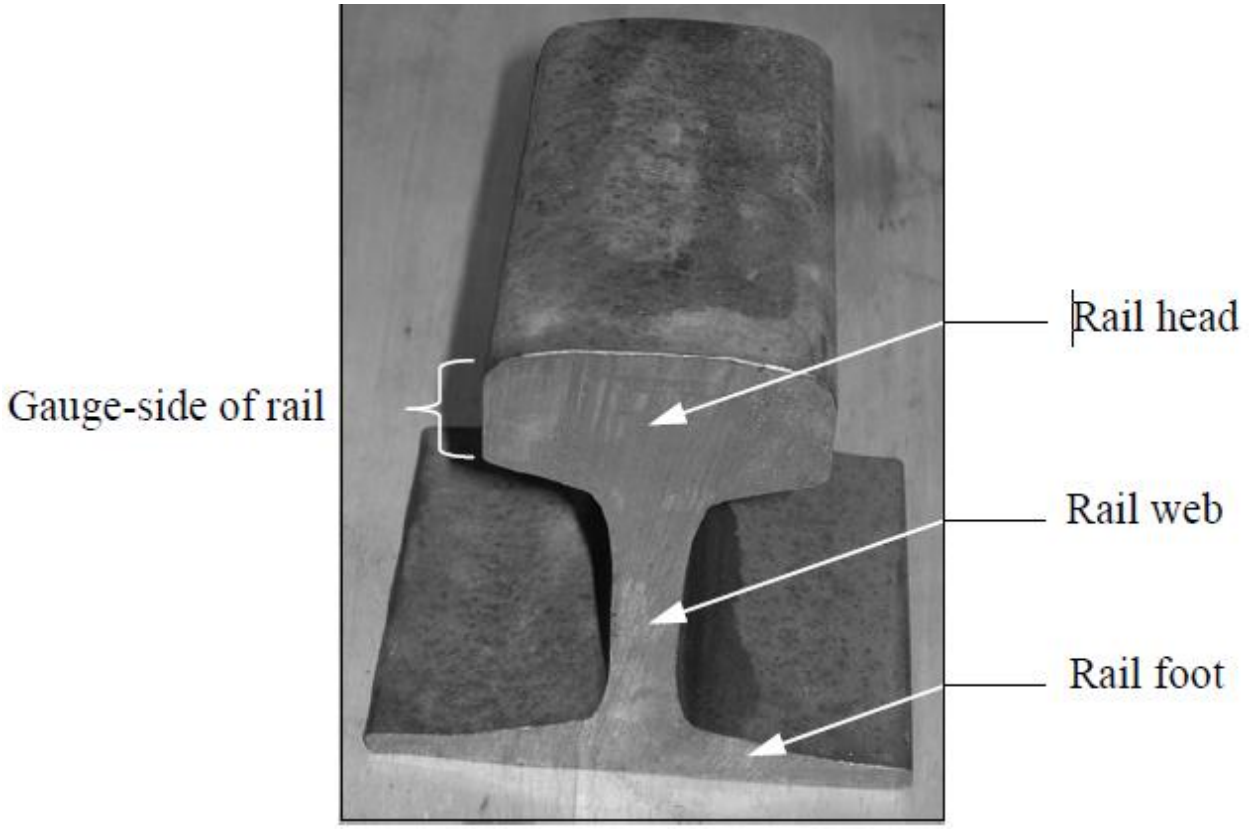

Figure 1.2: Rail Profile [3]

1.1.1. Loads on the track system

The wheel loads acting rail can be divided into three components, which are Vertical, longitudinal and lateral forces. The vertical force results from the weight of the wheel and the car bodies. The lateral force is generated due to the movement of the wheel set on the rail, and is especially high on the curved track. The longitudinal force is a traction force which is produced by the locomotive. In general the magnitude of the forces acting between the wheel and the rail must be set to a limit by railway organization. For instance, to decrease any initiation of the

surface damages on the rail surface such as crack or plastic deformation the international union of railways (UIC) sets the vertical and lateral wheel load as per wheel for static load. When a train running on the small radius curved track (less than 600m) ,the force is set to a limit of 145 KN for the static vertical force and 60 KN for the static lateral force (4).

The three elements of the contact forces are illustrated in a figure1.3.

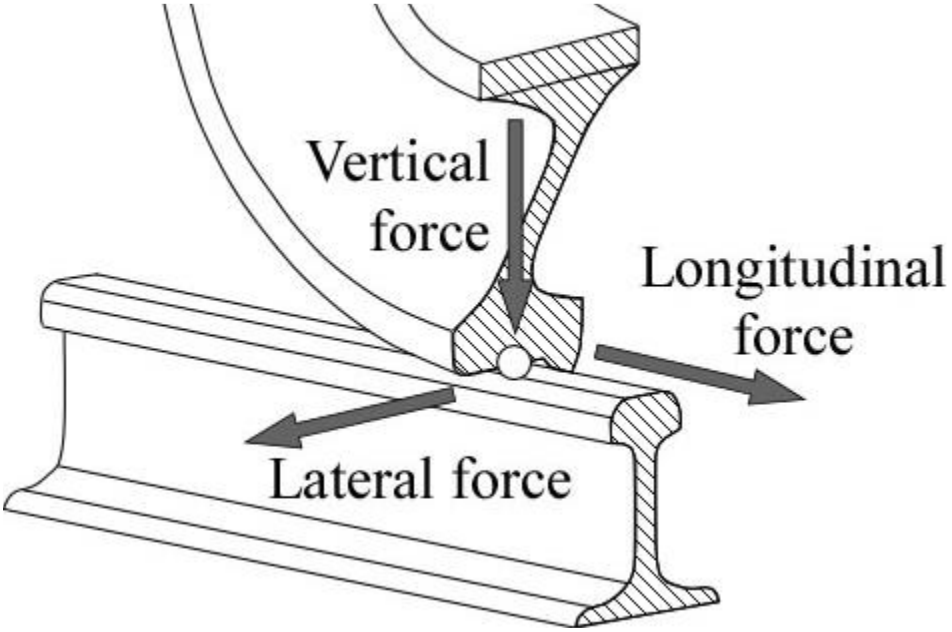

Figure 1.3: Contact forces at wheel- rail contact zone [4].

1.1.2. Standard and Length of the Rail

Many standards are used for rail profiles, which are classified into UIC, ASCE, AREA and BS and other profiles are used in other countries as well. UIC 54 and UIC 60are widely used rail profile. Rail is graded by weight over a standard length (in kg/m) and the usual range is 40 to 60 kg/m. However, Ethiopia uses P50 kg/m rail for Addis Ababa Light Rail Transit (AALRT).

Rail is manufactured as per the country requirements. Different country uses different rail length manufactured. Rail length increases from 11.8 meter to 25 meter long. Some country manufactures 122meters length. Most country uses 25 meter length of rail commonly including Ethiopia.

1.1.3. Wheel- Rail contact

The real steel-to-steel contact area between a wheel of a train and a rail is very small in relation to the wheel and rail dimensions. The size of the contact area is important with respect to the running behavior of the train in general and in curves in particular. Because of the heavy loads and the small wheel/rail contact area, high stresses will occur in wheel and rail. Every cycle of a wheel/axle results in a stress cycle in the material of wheel and rail. This cyclic stressing of the material means fatigue during lifetime. This problem is exacerbated in the wheel/rail contact due to friction [5]. When two bodies (wheel and rail) are in contact, stresses and strains appear. A large force from the first body (wheel) is transferred to the second body (rail) through a small contact region [6].

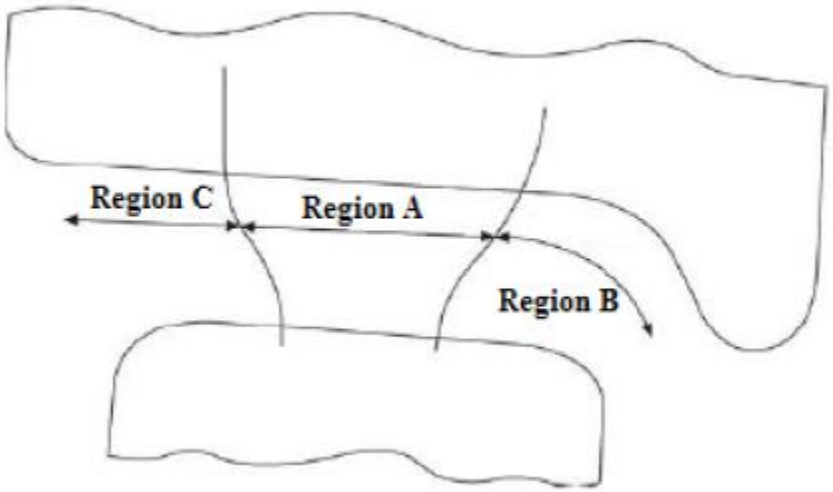

Figure 1.4: Wheel rail contact zones [6].

a) Region A [6]- wheel tread rail head contact:

- most common contact region;
- lower contact stress.

b) Region B [6] – wheel flange rail gauge corner:

-much smaller contact area and more severe;

-higher contact stresses.

c) Region C [6] - wheel and rail field sides contact:

-least likely contact region;

-high contact stress.

As the train travels on the curved track, the vehicle and any passengers inside are influenced by centrifugal force which is proportional to the square of the train velocity and inversely proportional to the radius of the track curvature. To neutralize the effects of centrifugal force on passengers, super elevation is usually applied to a curve by lowering the inside rail and raising the outside rail by an equal amount. Since a significant discrepancy of height is created between the inner and outer rail (the so called low and high rail respectively), the contact position and stress on this two rails are different. In wheel/rail contact, rolling phenomena on the curved track can be much more complicated than that on straight track, especially sharp curved track. Due the influences of super elevation (also called track cant) angle of attack (AOA) and rail cant, stress states on the high rail are significantly different from that on the low rail. Therefore the appearances of damages on the low and high rails are different as well. This damage can result in rail failures, subsequently leading to the vehicle derailment [4].

1.1.4. Railway Rail Fatigue.

The majority of component intentions involve parts subjected to fluctuating or cyclic loads. Such loading induces fluctuating or cyclic stresses that often result in failure by fatigue. About 90% of all structural failures occur through a fatigue mechanism [7]. It was well-known that wood or metal could be made to break by repeatedly bending it back and forth with large amplitude. But, it was then discovered that repeated stressing can produce fracture even when the stress amplitude is apparently well within the elastic range of the material. When fatigue failures of railway axles became a widespread problem in the middle of the Nineteenth century, this drew attention to cyclic loading effects. This was the first time that many similar components had been subjected to millions of cycles at stress levels well below the monotonic tensile yield stress. Between 1852 and 1870 the German railway engineer August Wohler set up and conducted the first systematic fatigue investigation. Some of Wohler's data are for Krupp axle steel and are plotted, in terms of nominal stress (S) vs. Number of cycles to failure (N), on what has become known as the S-N diagram[5,7,25].

The mechanism of fatigue has been unraveled during the 20th century, particularly in the last fifty years. It is now known that fatigue is caused by the initiation and growth of cracks. The quantification of crack growth has become possible through the use of fracture mechanics, although the quantification of the initiation stage remains rather tentative. It is well established

that fatigue initiation usually occurs at a free surface, aided by some kind of stress concentration feature. Circumstances can arise which produce non-propagating cracks [5].

Fatigue failures occur due to the application of fluctuating stresses that are much lower than the stress required to cause failure during a single application of stress. There are three basic factors necessary to cause fatigue: ((1) a maximum tensile stress of sufficiently high value, 2) a large enough variation or fluctuation in the applied stress, and (3) a sufficiently large number of cycles of the applied stress. High-cycle fatigue involves a large number of cycles ($N>10^5$ cycles) and an elastically applied stress. The fatigue life is the number of cycles to failure at a specified stress level, while the fatigue strength (also referred to as the endurance limit) is the stress below which failure does not occur. Normally, the fatigue strength increases as the static tensile strength increases. Low cycle fatigue possess during cyclic loading within the elastic regime, stress and strain are directly related through the elastic modulus. However, for cyclic loading that produces plastic strains, the responses are more complex and form a hysteresis loop [7]. Fatigue failure in rails can be initiated at the rail head, at the web and at the foot. Failures in the web are usually caused by poor manufacturing. One example is the longitudinal Vertical crack. Rail foot failures are usually initiated from galling due to wear and/or corrosion at the rail support and poor manufacturing. Rolling contact fatigue will lead to surface and subsurface failures on the rail head. Their growth can cause spalling of material fragments which will affect the travelling comfort. If not detected in due time the fatigue cracks can also lead to fracture of the rail which in some cases may cause derailment [8]. Based on the nature and location of the failures, they are classified as follows, figure 1.5.

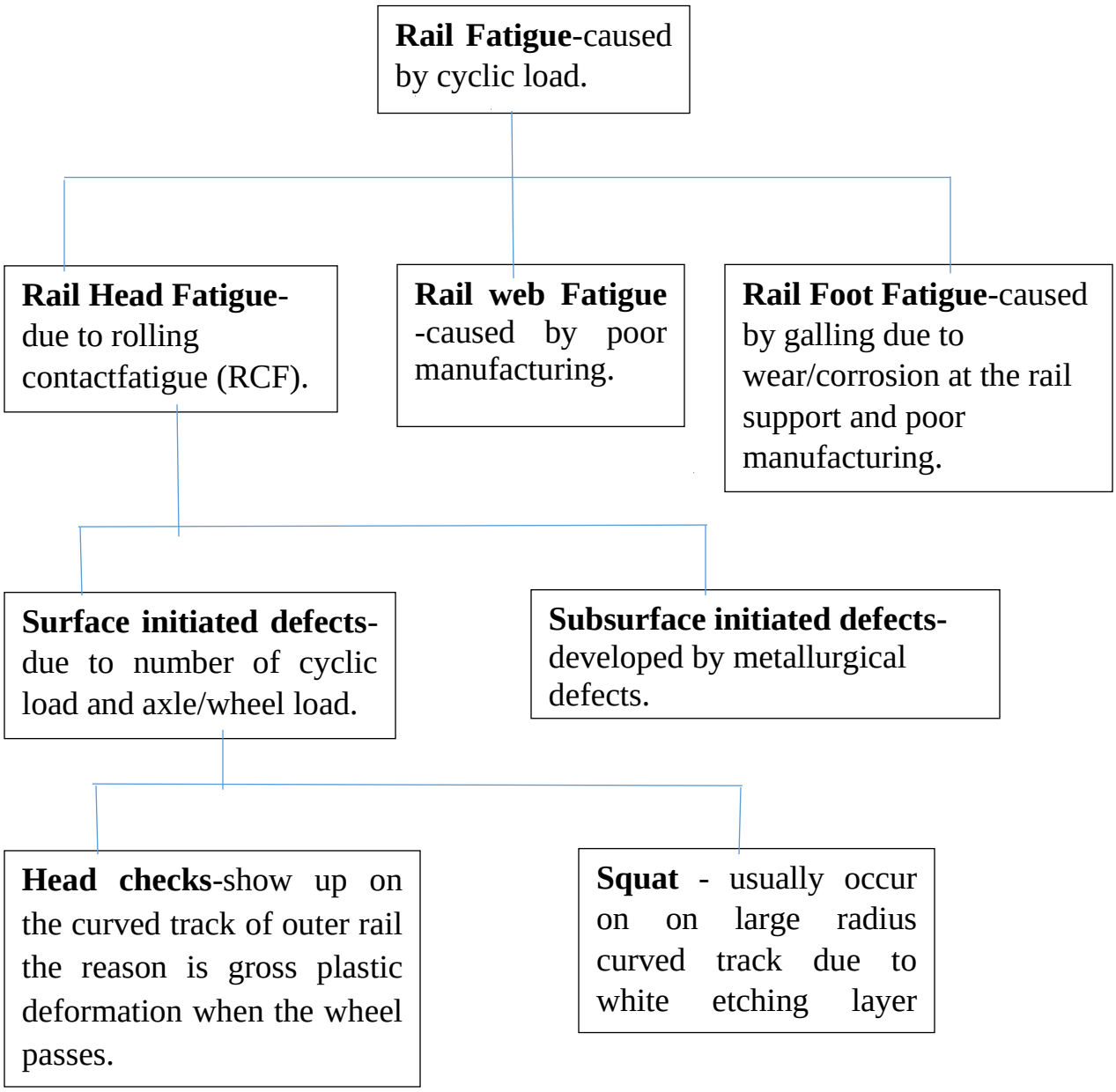

Figure 1.5: Fatigue failure types on rail [3, 4, 10].

1.1.5. Rolling Contact Fatigue of railway rail

Rolling contact fatigue (RCF) is one of the major current limitations of railway infrastructure productivity. It is a family of damage phenomena that appear on and in rails due to overstressing of the rail material.

Due to economic pressure there is a world-wide trend to increase axle loads, traffic density and speed to reduce operating costs and increase the efficiency of railways. Axle loads around the world have increased in general. This has led to an increased rate of rail defect formation. Rail defects occur due to a number of causes, which have been used as a basis for rail defect classification by many researchers. Rail defects which occur due to RCF classified into surface initiated and subsurface-initiated defects [3].

I. Surface-initiated defects

Surface-initiated defects are formed mostly due to an increase in traffic density or number of cycle loads and axle load (for example: head checks and squats) [3].

(a) Head Checks

Head checks are groups of fine surface cracks at the running gauge of the rails with a typical interspacing of 0.5 to 10 mm. Head checking preferentially occurs at the outer rail in curved tracks but is also found at switch or crossing rails. The reason is gross plastic deformation due to friction when the wheel passes. They can cause spalling of pieces of material between the cracks but also - after deviating at some millimeters of growth – cause transverse cracks leading to the eventual fracture of the rail [4].

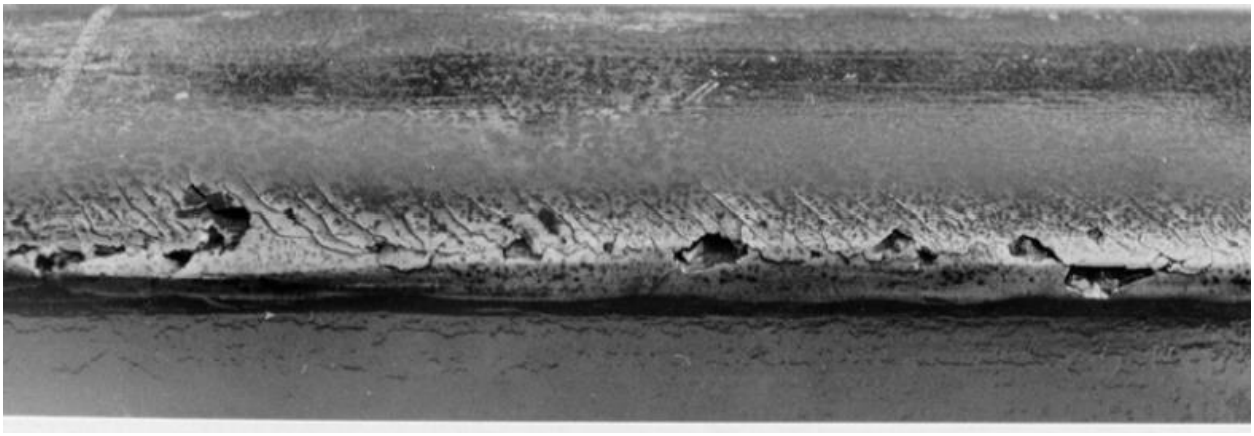

Figure 1.6: Spalling originated at head checks [4].

Figure 1.7: Fracture of a rail with origin from a head check [4].

(b) Squats

Like head checks squats are rolling contact induced defects. They occur in slightly curved cracks, at the running surface. In contrast to head checks they occur randomly at isolated sites. Squats and head checks have in common that their existence is not associated with any metallurgical fault but are caused by gross plasticity.

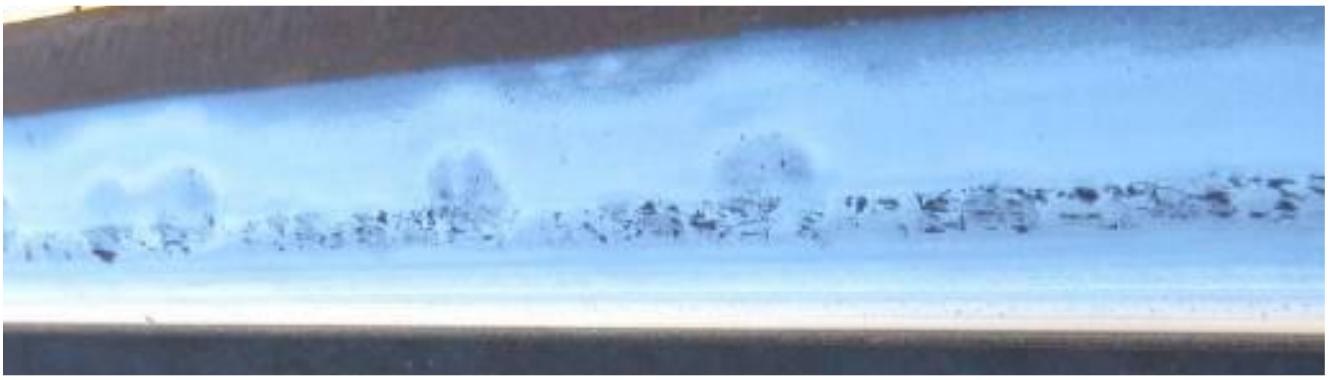

Figure 1.8: Squat: damage of the running surface [4].

II. Sub-Surface initiated

On the other hand, subsurface defects are often caused by metallurgical faults (for example: shelling, tache ovale and longitudinal vertical crack) [3].

Shattering Defects - These defects which develop around 10 to 15 mm below the rail head from longitudinal cavities caused by the presence of Hydrogen. These cavities develop under the influence of thermal and residual stresses from roller straightening and cooling processes in the normal rail section during the manufacturing process [3].

(a) kidney-shaped cracks.

In former times rail cracks with internal origin rather than surface induced cracks, were dominating the failure statistics. This type of cracks usually initiates from manufacturing defects, e.g. hydrogen shatter cracks, so-called “flakes”. The pre-existent flaw is the nucleus for a so-called “kidney-shaped” crack or “tache ovale”. Note, however, that sub-surface cracks can also initiate in virtually defect-free material [4].

Figure 1.9:“Kidney-shaped” crack in a rail head [4].

1.2. Statement of the Problem

Rails, as the heart of the railway system, are subjected to very high service loads and harsh environmental conditions. Due to heavy vertical and lateral cyclic wheel load, Fatigue failure may occurs at the rail head, web and foot. Wheel/rail contact may occur at the top of the rail surface or at the gauge corner, and is responsible for rolling contact fatigue usually happened on the rail head surface because rail fatigue depend mainly on the repeating contact loads to which the rail surface is subjected. Failure by fatigue mostly occurs in three stages: the initiation of a crack (caused by millions of repeated wheel loads), the growth of crack (no perceptible change in shape or dimension of rail) and final fracture (Sudden brittle failure occurs due to a severe loading). Therefore, fatigue failure analysis in the curved rail remains an important issue with respect to fatigue life and fatigue damage. The primary concern for this research is fatigue failures analysis at the rail head surface depending on current applied loads and operating condition, on minimum curved rail profile of Addis Ababa Light Rail Transit (AALRT) that assist toward knowing fatigue life of rail and taking measurements for safe functioning of rails.

Objective of the Study.

1.2.1. General objective

The main objective of the study is analyzing fatigue on curved rail head due to cyclic wheel load that causes failures and determining fatigue life of rail.

1.2.2. Specific objective:

- Analyzing fatigue failure of rail on curve condition.
- Determine fatigue life of curved rail.
- Comparing the fatigue life predicted on minimum curve radius located at: Stadium, Saintlideta and Autobistera.

1.3. Research Methodology

To fulfill the objectives of the study there are procedures that should be followed. The main procedures are:

- Use Hertzian contact theory for determinations of elliptical contact.
- Data collection through travelling with master train's from load sensor of a train.
- 3D contact and Load distribution analysis.
- The 3D model of wheel and rail has done on modeling package of CATIAV5.
- The developed 3D model of wheel and rail is assembled on CATIAV5
- The 3D assembled on CATIAV5 is imported to the ANSYS v16work bench for analysis.
- Finite element analysis of curved rail using the ANSYS software is carried out.
- Comparing the fatigue life predicted on curve (stadium, saint lideta and autobistera).
- Based on the analysis, recommendation to reduce the problem is put forward.

All the above methods are conducted at a specified conditions and stated constraints with appropriate methodologies.

1.4. Significance of the Research

This research has a role for predicting fatigue life and damage on curved rail and uses of rail. In the future, it will add new knowledge about existing one with curved rail life, damage and equivalent alternating stress of rail rolling contact fatigue under vertical and lateral wheel load based on morning peak hour, day flat hour and afternoon peak hour, which cause fracture, deterioration and failure of the rail. This paper try to figure out those problems related to the rail due to the wheel load at curved rail track location of Addis Ababa Light Rail Transit based on engineering mechanics.

1.5. Scope and Limit of the Thesis

There are many problems that are related to the analysis of rolling contact fatigue and fatigue life of rail. The research project is intended to study fatigue failure analysis and fatigue life on the curved rail head surface. The rail joint and experimental works are not considered, due to complexity and vastness of the research area. However, detailed analysis of fatigue failure

caused due to cyclic axle load on the rail and the fatigue life on the curved rail position for Addis Ababa light rail transit is conducted.

1.6. Organization of the Paper

The body of this study is divided into five main chapters. The first chapter discusses background, objectives and methodology of the study. In addition, the details of the fatigue failure type and rail rolling contact fatigue used for analyze. The second chapter covers the review of some of the books, journal articles, conference papers and publications which were referred during the study. Also, in relation and comparison with previous works, what is done in this study will be stated. The wheel/rail contact mechanics and rail fatigue failure mechanisms is reviewed. Also the analysis of RCF failure and prediction of fatigue life of the rail is seen. Analytical methods, material type used for the analysis, dimensions and conditions of operation discussed in the third chapter. This chapter also describes the Model on CATIAv5 and finite element analysis by ANSYS 16 workbench software of rolling contact fatigue failure on curved track. It covers 3D wheel/ rail contact analysis using hertz an contact theory, and load condition. The results obtained from the ANSYS 16 workbench for wheel/rail contact and discussions based on these results are included in the fourth chapter. Finally, the fifth chapter cover conclusions drawn based on the results of the analysis, recommendations and future work.

CHAPTER TWO

2. LITERATURE REVIEW

This part of the paper reviews the related literatures that support and guides the current work. The related literatures are directly and indirectly related to the current paper. The main attitude used to express previous studies are, the methods and approaches they used to develop and explain their study. There are thesis, books, conference papers, and journals revised that assist the current paper discussed as follows.

2.1. Wheel/rail Contact Mechanics

From elementary mechanics, it is known that two contact surfaces under load will deform. Depending on the magnitude of the load applied and the materials' hardness, the deformation may be either plastic or elastic. For many engineering applications, the contact surfaces are non-conformal. The resulting contact areas are very small and the resulting pressures very high. The stresses on those contact surfaces can be determined from analytical formulas.

As the wheel travels on rail, the appearance of contact zone depends on property of the track (straight track or curved track). There are two types of computational approaches to estimate the wheel- rail contact problems, namely numerical and theoretical methods. To save time and cost the investigations for the simple wheel- rail contact related problems are usually based on some classical theories. One of the popular theories to examine the normal contact problem is the one written by Heinrich Hertz.

Pioneer researcher, Henrich Hertz, famously formulated a theory of contact mechanics between two elastic solids many years earlier than 1882. When two elastic solids are brought into contact and are subjected to normal load, they deform elastically to form an elliptical contact area. A classic description of the Hertz contact theory (HCT) is given. HCT is based on some important assumptions, as given below [9].

1. The contacting surfaces are smooth, frictionless and only normal pressure is transmitted between them.
2. The contacting surfaces are continuous and non-conforming

3. Each solid can be considered as an elastic half space. The contact area is small compared to the radii of curvature of the contacting surface.
4. The contacting surfaces are linear elastic, and the strains are small and within elastic limits.

In a 3D wheel-rail contact problem, the more generic shape of a contact area on the centre of the railhead surface is elliptical, having major and minor-semi axes [9].

When two bodies (wheel and rail) are in contact, stresses and strains appear. A large force from the first body (wheel) is transferred to the second body (rail) through a small contact region about 1 cm2 [6].

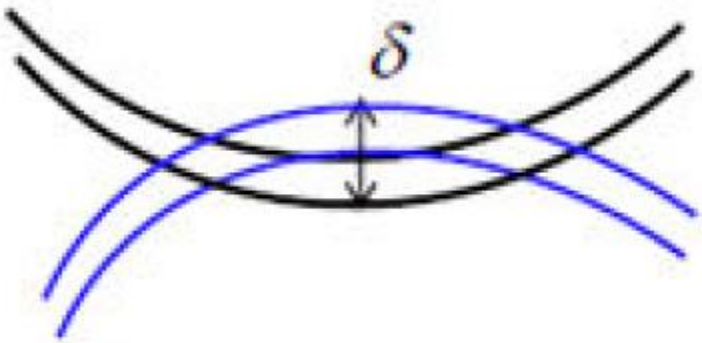

Figure 2.1: Wheel rail contact [6].

2.2. Rail failure mechanism

Different regions of the rail are affected differently due to induced stresses and deformations as a result of rail operations. In the region close to the contact zone, the plastic deformation due to the repeated rolling contact between the wheels and the rail is of great significance. This plastic deformation causes wear, crack initiation and propagation leading to rail defects such as head checks, gauge corner cracking and squats if the contact loads are sufficiently high compared to the strength of the rail material(s). In wheel-rail contact the Rail material is repeatedly loaded by train wheels as the train passes over the rail track. How a material responds to repeated loading depends on the magnitude of applied load. Several models exist to predict the initiation and propagation phases of crack development and this can be used to explain the concept of a shakedown limit [9].The maximum contact pressure that the rail material withstands under elastic deformation is called the shakedown limit [10]. The behavior of material under cyclic loading during rolling can take four different forms, as shown in the figure 2.2,below.

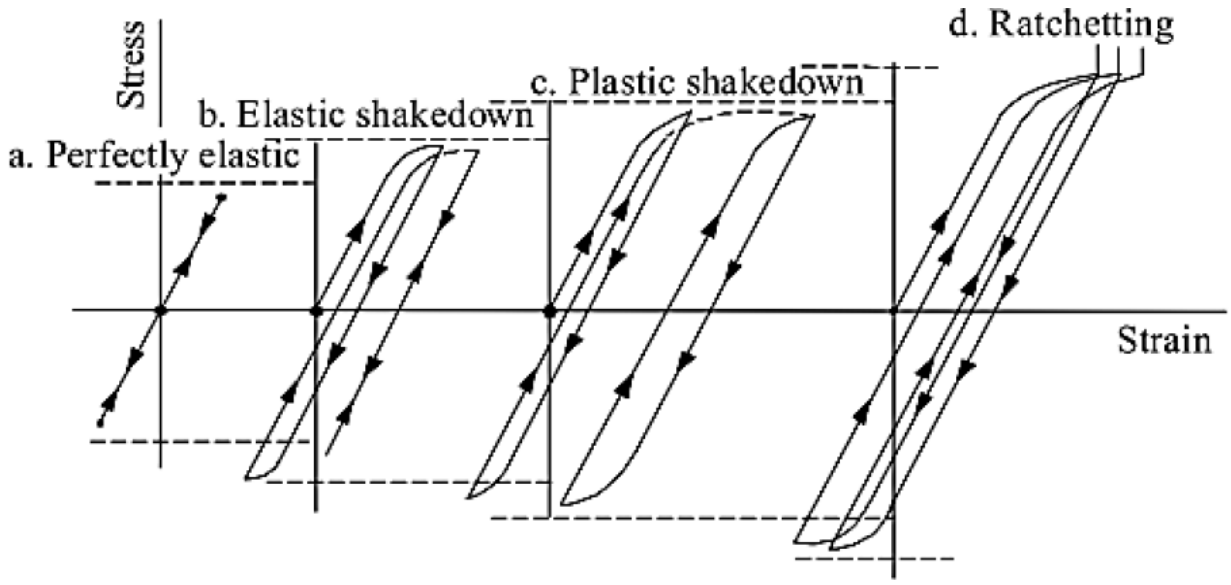

Figure 2.2: Material response to repeated loading [9].

1. Elastic response. If the yield stress of the material is not exceeded the (global) behavior will be elastic.
2. Elastic shakedown. An elastic response is obtained after the yield stress is exceeded in the initial load cycle(s).
3. Plastic shakedown. A closed plastic stress–strain loop is formed with no net accumulation of (unidirectional) plastic strain.
4. Ratcheting. Incremental (unidirectional) strain accumulation with each load cycle.

The first item in the above list requires the most number of load cycles to initiate a crack whereas the last item requires the fewest number of load cycles. If the material in a rolling contact deforms plastically at the initial load cycle, an elastic response may occur in subsequent load cycles due to [11]:

- Protective residual stresses created by the initial plastic deformation that suppresses subsequent yielding;
- strain hardening which raises the yield stress of the material, and

- geometric changes of the surfaces in contact that may result in a more conform contact and thereby lowering the intensity of the contacting stress – so-called wear-in.

2.3. Rolling Contact Fatigue of railway rails

The real steel-to-steel contact area between a wheel of a train and a rail is very small in relation to the wheel and rail dimensions. The size of the contact area is important with respect to the running behavior of the train in general and in curves in particular. Because of the heavy loads and the small wheel/rail contact area, high stresses will occur in wheel and rail. Every cycle of a wheel/axle results in a stress cycle in the material of wheel and rail. This cyclic stressing of the material means fatigue during lifetime. This problem is exacerbated in the wheel/rail contact due to friction. It results in cracks in wheel and rail and occurs in a very early stage of the lifetime cycle nowadays in railways. This is better known as Rolling Contact Fatigue (RCF) and RCF is a worldwide problem for Rail. There are two types of rolling contact fatigue: surface-initiated RCF and subsurface-initiated RCF. Subsurface RCF may initiate in the rails at metallurgical defects. The current surface-initiated RCF manifests itself in two types: Squats and Head Checks (HC). A mature Squat has typically a “two-lung” shape with widened running band and with U, V or Y shaped cracks. The cracks may branch down when they have a depth of 3 – 5 mm. Squats are usually found on tangent tracks and in curves of large radius. Squats usually initiate from rail surface geometry defects such as indentations and wheel burns. Head Checking (HC) is a major type of Rolling Contact Fatigue (RCF) in railway rails across the globe. It mainly occurs on curved tracks in the rail shoulder of the gauge side and at the gauge corner of the outer (high) rail, usually with many of them clustered at uniform intervals because of the large lateral force. It initiates from the surface due to high surface shear stresses arising at wheel-rail contact. The surface cracks take an orientation angle α with respect to the lateral direction y. (see Figure 2.3). In the initial stage, the short cracks grow at a shallow angle with the rail surface. At a later stage these cracks can sometimes grow at a steeper angle. This crack growing tends to occur when cracks reach 30 mm in visual (surface) length, and at this stage the probability of rail fracture becomes very high. Severe HC particularly threaten the safety of traffic due to the multiple cracks which, when a fracture occurs, will result in disintegration of the rail and, in turn, to derailment [12].

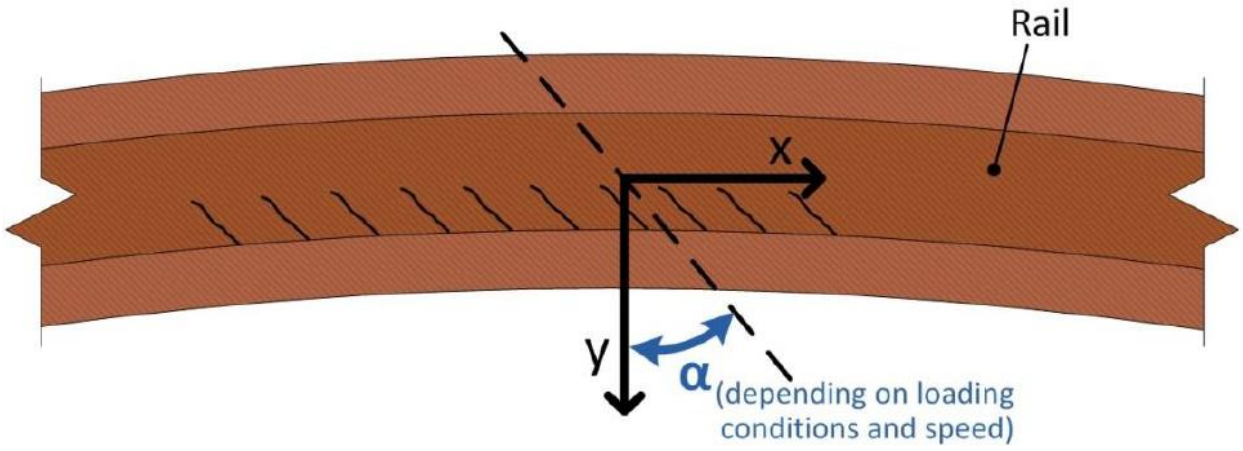

Figure 2.3: Head Checks of high rail. The traffic is in the x direction [12].

(a) (b)

Figure 2.4: (a) Severe Head Checks and (b) cross section of a severe single Head Check [12].

Ir. R.P.B.J. Dollevoet [12]: Deals with the design of an anti-HC profile of rails, based on a fundamental understanding of the mechanical mechanism of HC initiation. An investigation has been carried out on the quantitative relationship between HC occurrences, contact geometry, stresses and micro-slip. HC initiation has been reproduced under controlled laboratory conditions on a full-scale wheel-rail test rig. At the same time, HC initiation has been monitored in the field under service conditions. Using a non-Hertzian rolling contact solution method, it is found that HC initiation location tends to be at a distance 7 – 12 mm from the gauge face, where the surface shear stress is the highest as a result of the large geometrical spin in the wheel-rail contact. Conclusions from analyses of rolling contact in a controlled full scale lab test and of rolling contact under operational loading conditions that:

- The HC initiates in surface ratcheting layer.
- The HC initiation at the gauge corner is caused by the large surface shear stress, which is a result of the large geometrical spin due to the profile.
- The cracks initiate along the direction of the sheared texture.
- The orientation of the initial HC crack is perpendicular to the direction of the maximal surface shear stress.
- Wear plays an important role in HC initiation.
- At gauge face it is wear which dominates so that any initiating HC cracks are removed by wear. This is because at gauge face micro-slip is very large owing to the geometrical spin.

Khoa Duy Vo [8]: Considered introduction to the damage tolerance behaviour of railway rails. Repeated rolling contacts cause RCF and wear on the railhead. High tangential forces together with surface roughness induce uniaxial plastic deformations in a thin surface layer. Surface breaking cracks are then initiated on the top of the rail (squat & rail fracture). Once a crack has been initiated (with a length of, say, 0.1 mm) it will grow at a shallow angle (10-25^{o}) from the surface in the direction of the plastically deformed anisotropic material until it reaches a critical length (of, say, 1-2 mm), see Figure 2.5. At this critical length the stresses and strains at the crack tip will govern the continued growth which can be upwards (spall) or downwards (squat).

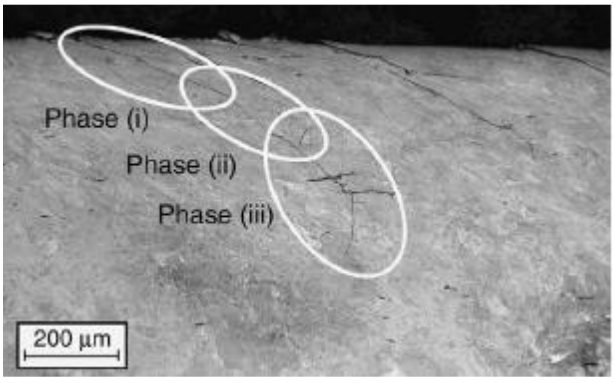

Figure 2.5: Three phases of life of a (rolling contact) fatigue crack initiated at the surface of a rail (8).

Jungwon Seo, Seokjin Kwon, Deonghyeong Lee [13]: studied Effects of surface defects on rolling contact fatigue of rail. In this paper, the contact fatigue test and the Finite Element analysis were performed to investigate the effect of ballast imprints on rolling contact fatigue

damage. This form of damage is associated with ballast particles becoming trapped between the wheel and the surface of rail. In this study, they have investigated whether the ballast imprint is an initiator of head check type cracks. In order to investigate the size effect of dent, four types of artificial defect were manufactured on the rail specimen. The finite element analysis was used to investigate stresses and strains around dents during the rolling contact. Based on loading cycles obtained from FE analysis, fatigue life analysis on each point was carried out. The test results show that cracks initiate and propagate in dents larger than a certain size.

Mark C. Burstow [14]: Carried out Improving track geometry alignment to reduce rolling contact fatigue (RCF). The research was undertaken through application of vehicle dynamics simulations of a range of vehicle types interacting with different track alignment faults on a range of curves. The results showed that the risk of RCF depends on the combination of track alignment, curve radius and cant deficiency. On the whole, it has been found that two different mechanisms are responsible for generating RCF: quasi-static forces generated during curving are generally responsible for RCF on moderate radius curves and dynamic forces resulting from lateral track misalignments tend to be responsible for RCF on shallow radius curves and tangent track. This can lead to the formation of RCF cracks in regular groups or 'clusters'. These studies used the Vampire vehicle dynamics simulation software.

Jungwon Seo [15] Studied Fatigue crack growth behavior of surface crack in rails by two-dimensional computational model used to simulate the fatigue crack growth behavior at the surface of rail. The model considers the moving contact pressure and tangential force. The growth behavior of the crack on rail surface was analyzed with F.E. analysis. the crack was simulated with an inclined angle from 30° to 45° from 8 mm deep and was impacted by three separated load cases represented for pure rolling ($\mu = 0$), tractive force ($\mu = 0.4$) and braking force ($\mu = -0.4$). In the Mode I, the value of the KI is zero while the crack is closed. In the Mode II, KII increases as the contact load approaches the crack, and the sign of the stress intensity factor (K) is reversed when the load has passed over the crack, because the direction of the relative slip of the crack faces is reversed. Comparing the K values in the Mode I and Mode II, that of the Mode II is greater than that of the Mode I, which means that the crack grows in Mode II.

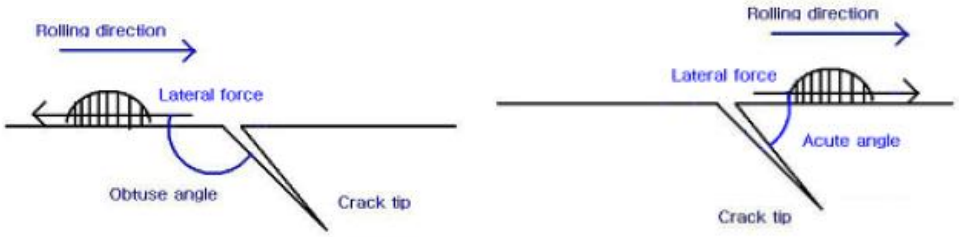

a) Under traction force b) Under braking force

Figure 2.6. Crack and direction of horizontal load (a,b) [15].

The results of the F.E. analysis showed that the behavior of the crack generated on rail surface varies by the load condition and crack length. The crack growth rate increased down to a certain depth from the surface, then decreased [15].

Xiangyun Deng*[16]: Conducted Residual fatigue life evaluation of rail at squats seeds using 3D explicit finite element analysis**.** A modeling procedure to predict the residual fatigue life of rail at squats seeds is developed this article. Two models are involved: a 3D explicit Finite Element (FE) model to compute the stress and strain at squats in rail, and the J-S fatigue damage model to determine the residual fatigue life on the basis of the computed stress and strain. In the FE model dynamic effects of wheel-rail system under rolling contact is taken into account. Bilinear isotropic elastic-plastic material properties are adopted to represent the hardening of wheel and rail. Squats are subject to multiple loading cycles. The geometry of the squat is varied in the simulation corresponding to a growing squat at different ages. It is found that small squats lead to fatigue failure while severe ones lead to ratcheting failure.

As it is mentioned on the above review, this part (fatigue failure analysis on curved rail or root) needed more research to identify the fatigue life, damage and failure of the rail by ANSYS16 Workbench to increase the comfort, safety of the passenger and minimize maintenance cost. This research contributes additional concept on the previous research. The focus of this research therefore is fatigue failure analysis due to cyclic vertical and lateral wheel load on minimum curved rail located at Stadium, Saint lideta and Autobistera of Addis Ababa Light Rail Transit based on morning peak hour, day flat hour and afternoon peak hour.

CHAPTER THREE

3. MODEL, ANALYTICAL METHODS AND CONDITIONS

The railways formed a new means of transportation with increasing capacity, speed, and reliability. Large areas of railway transportation were opened which could be developed for efficient service. The railways formed an enormous stimulus to the political, economical and social development. The rails are the supporting parts with which the wheels are in contact. Surfaces of rails are consistently subjected to contact, thermal and others loading due to these large stresses applied over localized area. The material in and around the contact area is therefore highly stressed. High rates of wear might be expected for such a contact but, in addition, because the load is applied and removed many times during the passage of each train, there is the possibility of fatigue of the rail surface. Many researchers studied different parameters and their influence to improve the failurities of the different component of the contact area. Since the adoption of steel rather than iron as the material of choice for rails, the wheel/rail system has remained virtually unchanged.

3.1. Wheel/Rail material

The resistance of a train to rolling has several components, including grade and acceleration resistance, aerodynamic and wind drag, bearing resistance, and wheel/rail contact resistance. Only this last resistance is influenced by the choice of wheel and rail materials. Several factors contribute to wheel/rail contact resistance. First, during rolling, the wheel and rail surfaces are elastically deflected such that relative motion can occur. Second, energy can be dissipated by plastic deformation. Third, surface adhesion phenomena can dissipate energy. To a first approximation, contact resistance is proportional to the length of the contact patch and, hence, resistance is minimized if, for a given geometry, the contact area is kept small by choosing materials with a high elastic modulus.

Of the common and inexpensive metals, steel has one of the highest values of elastic modulus. For this reason and because steel is relatively inexpensive and offers a very attractive combination of strength, ductility, and wear resistance almost all wheels and rails worldwide are made from plain carbon-manganese pearlitic steel, which has a lamellar structure of iron and iron

carbide. In general, passenger vehicle wheels tend to have lower carbon content and hardness than heavy axle load freight vehicles. Steel of about 300 Brinell hardness is typically used for rail in straight track, while rail in the hardness range 340 to 390 Brinell tends to be used for curved track where thestress environment is more severe. Although numerous studies have examined the use of higher hardness materials, such as bainitic and martensitic steels, for wheel and rail materials few materials can compete on wear resistance with pearlitic steel, first used for wheels and rails last century [17]. Rolling Contact Fatigue is a damage phenomenon that appears on and in rails and railway wheels due to overstressing of the materials. Fatigue of railway rails is an extremely important problem and become an important issue with respect to failure. Two processes govern Rolling Contact Fatigue: the crack initiation and the crack propagation influenced by a number of factors like environmental conditions, rail and wheel profiles, track geometry, vehicle characteristics [18]. The railway tracks are mostly steel material. Steel is the most common and widely used metallic material in modern society. Steel contains 50% iron and one or more alloying element. These elements generally include carbon, manganese, silicon, chromium, phosphorus, Sulphur etc. wheel has approximately similar material property to rail.

For Addis Ababa light rail transit (AA LRT), the rail standard used is China National Railways standard of P50U71MN14 (50 kg/m). Wheel and rail materials are quite similar in composition, differing slightly in the amounts of chemical composition in the steels used. Table 3.1 shows mechanical property of rail material and Table 3.2 presents the chemical compositions.

Table 3.1: Mechanical property of rail material for AALRT (19).

Item No	1	2	3	4	5	6
Mechanical property	Poison's Ratio	Young's Modulus (GPa)	Ultimate tensile strength (MPa)	Yield strength(MPa)	Density (kg/m^3)	Elongation
value	0.3	207 GPa	880 MPa	460 MPa	7850	9

Table 3.2: Chemical composition of rail material for AALRT (19).

Item No	1	2	3	4	5
Chemical element	C	Si	Mn	P	S
Composition	0.65-0.77	0.15-0.35	1.10-1.50	0.04	0.04

3.2. Wheel /Rail dimension and specification.

Table 3.3: Wheel dimension and specification of AALRT(20).

Item No	Description	Dimension
1	The principal rolling radii of the wheel(R_1^w)	330mm
2	The principal transverse radii of the wheel(R_2^w)	∞
3	The principal rolling radii of the rail(R_1^r)	∞
4	The principal transverse radii of the rail(R_2^r)	300mm

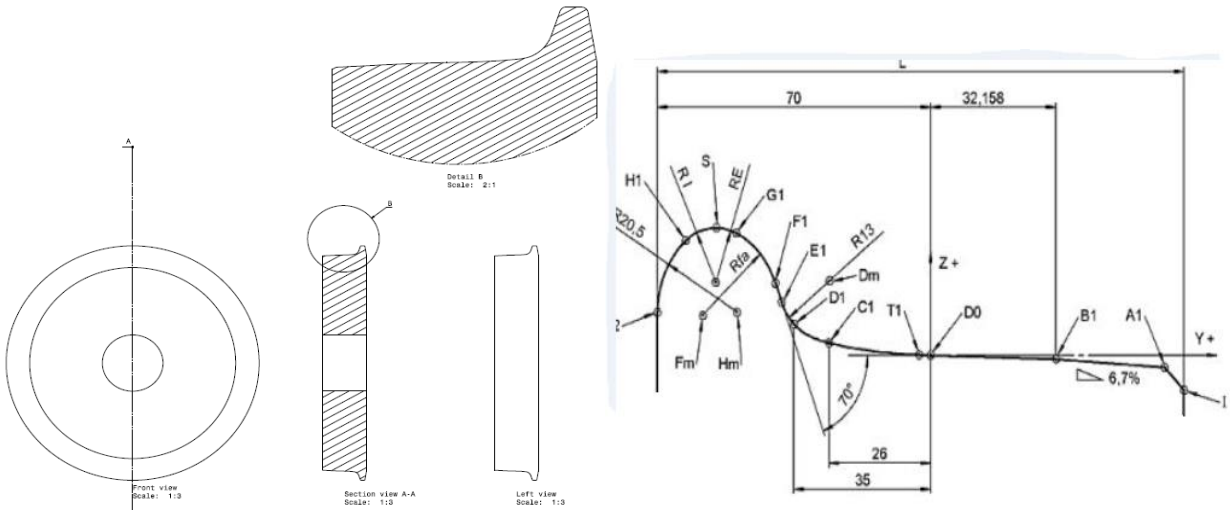

Figure 3.1: Geometrical wheel dimension [20].

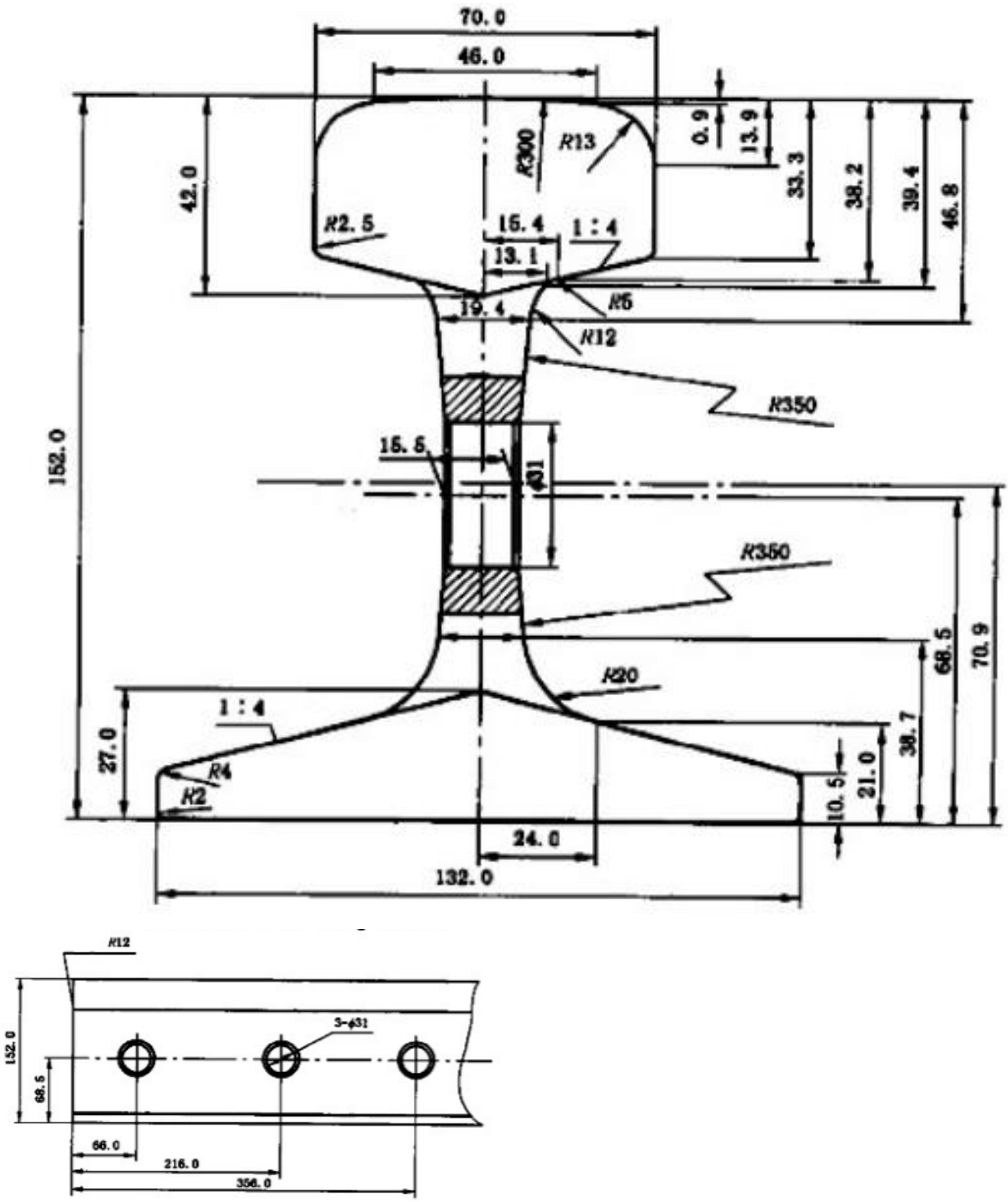

Figure*3.2*:Geometrical dimension of P50 standard rail for AALRT (19).

Table 3.4: Operating speed of train for AALRT [20].

Item No	Parameter	Speed
1	Maximum operation speed	70km/h
2	Travelling speed on minimum curve radius	≥12km/h
3	Operation speed during car wash	3~4 km/h

Table 3.5: Main parameters of line for AALRT [20].

Item no	Description	Dimension
1	Track gauge	1435mm
2	Maximum gradient	55%
3	Minimum radius of horizontal curve for main lines	50m
4	Minimum radius of horizontal curve for depot	30m
5	Minimum radius of vertical curve	1000m
6	Type of rails for main lines and depot	50kg/m
7	Maximum super elevation	120mm
8	Inclination at rail bottom	1/40

3.3. Wheel/ Rail Analysis Methods.

3.3.1. Analysis of Load Distribution and 3D Contact Point Shape.

Rail vehicles rely on the track to guide the wheels along straight and curved tracks. This demands a certain amount of force to be exerted by the wheel onto the rail. The load that is observed depends on the exact design of the rail vehicle, the wheel profile, the degree of curvature of the track.

3.3.1.1. Analysis of 3D Contact Shape.

When considering two elastic bodies in contact, as shown in Figure 3.4, they will meet at a single point *O*, where the normal distance between them is zero. Near this contact point, without load, the body surface shapes may be represented by two second-order polynomials:

$Z_1 = A_1x^2 + B_1y^2$ Eq. 3.1

$Z_2 = A_2x^2 + B_2y^2$.Eq. 3.2

The coefficients *A*1, *A*2 and *B*1, *B*2are assumed to be constant.

In the case of a railway, the four main curvatures can be considered to be in perpendicular planes. Their directions correspond to the main axes of the frame: *O-xy*.

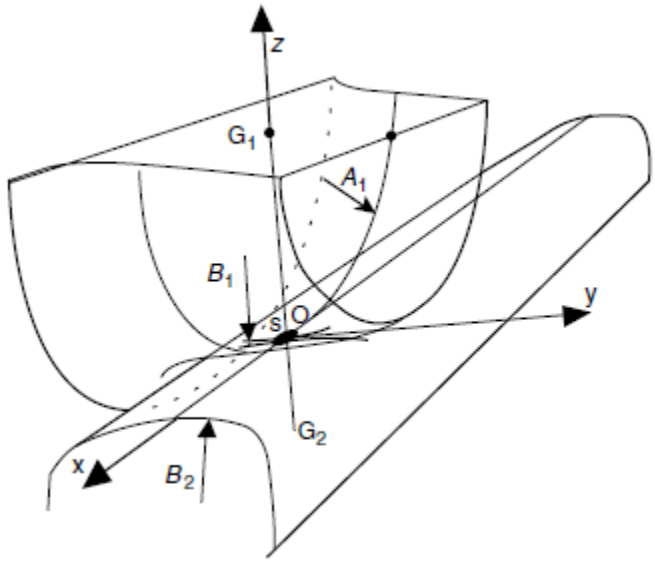

Figure 3.3: Hertzian contact: the railway case (22).

In the 3D railway case, the above-mentioned curvatures and radii will be:

Wheel: $\frac{d^2z_1}{dx^2} = 2A1 = R_1^W$ Eq. 3.3

Wheel: $\frac{d^2z_1}{dy^2} = 2B1 = R_2^W$ Eq. 3.4

Rail: $\frac{d^2z2}{dy^2} = 2B2 = R_2^r$ Eq. 3.5

Where$R_1^W$the longitudinal radius of the wheel at the contact point,$R_2^r$is the transversal radius of the rail profile and$R_2^w$is the transversal radius of the wheel profile. Before being loaded, the vertical relative distance $d(x,y)$ between the two bodies can be written as

$z_1+ z_2=d\ (x,\ y) =Ax^2+ By^2$Eq. 3.6

$A=\frac{1}{2R_1^W}$ and B= $\frac{1}{2}\left(\frac{1}{R_2^w}+\ \ \frac{1}{R_2^r}\right)$Eq. 3.7

And A and B being strictly positive.

For elliptical Hertzian contact, the contact pressure is given by,

$P\ (x,\ y) =$ $\frac{3F_n}{2\pi ab}\sqrt{1-\ \frac{x^2}{a2}\ -\ \frac{y2}{b2}}$, Eq. 3.8

Where$P\ (x,\ y)$ is the contact pressure, F_n is the vertical load on the contact patch, while$a$and b are the longitudinal and lateral semi-axes of the contact ellipse, respectively. In order to calculate a and b, the following formulations are defined.

$a=m\left[\frac{3\pi Fn\ (Kw+Kr)}{4K3}\right]^{\frac{1}{3}}$ Eq.3.9

$b=n\left[\frac{3\pi Fn\ (Kw+Kr)}{4K3}\right]^{\frac{1}{3}}$ Eq.3.10

According to these assumptions and by using equation (3.8) the maximum contact pressure, P_0 (Hertz stress) occur at x=0 and y=0.

$P=P_0=\frac{3Fn}{2\pi ab}$Eq.3.11

To calculate a and b, first let's find the values of K_w, K_r and K_3. K_w and K_r are constants that depend on the material properties of railway wheel and rail respectively. Where

$K_w=\frac{1-(V^w)\ 2}{\pi E^w}$Eq.3.12

$K_r=\frac{1-(V^r)\ 2}{\pi E^r}$ Eq.3.13

Where v^w and E^w are Poisson's ratio and young's modulus of the railway wheel material and v^r, and E^r are Poisson's ratio and young's modulus of railway rail material.

$K_w=\frac{1-(0.3)2}{\pi\times207\times10^9\mathrm{N/mm2}}$,$K_w$=$1.4\times10^{-12}\ \frac{m^2}{N}$

$K_r=\frac{1-(vr)^2}{\pi Er}$,$K_r=\frac{1-(0.3)2}{\pi\times207\times10^9\mathrm{N/mm2}}$ = $1.4\times10^{-12}\ \frac{m^2}{N}$

$K_3$is a constant and depends on the geometric properties of the two bodies and is defined as follows,

$K_3=A+B=\frac{1}{2}\left[\frac{1}{R_1^w}+\frac{1}{R_2^w}+\frac{1}{R_1^r}+\frac{1}{R_2^r}\right]$3.14

R_1^{w} and R_1^{r}, are the principal rolling radii of the wheel and the rail respectively and R_2^{w} and R_2^{r}, are the principal transverse radii of curvature of the wheel and rail respectively.

$K_3=\frac{1}{2}\left[\frac{1}{330}\ mm+\frac{1}{\infty}+\frac{1}{\infty}+\frac{1}{300}\ mm\right]$, K3=0.0032/mm

The coefficients m and n are Hertz coefficients and they are given as a function of the angle θ ($0-90^0$) where θ is defined as [8]:

$\theta=\cos^{-1}\left(\frac{K_4}{K_3}\right)$3.15

And

$K4=B-A=\frac{1}{2}\sqrt{\left(\frac{1}{R_1^w}-\frac{1}{R_2^w}\right)^2+\left(\frac{1}{R_1^r}-\frac{1}{R_2^r}\right)^2+2\left(\frac{1}{R_1^w}-\frac{1}{R_2^w}\right)\left(\frac{1}{R_1^r}-\frac{1}{R_2^r}\right)\cos 2\varphi}$

φ is the angle of the orientation difference of the principle axes of the two bodies; also called yaw rotation.

$K4=B-A=\frac{1}{2}\sqrt{\left(\frac{1}{330}-\frac{1}{\infty}\right)^2+\left(\frac{1}{\infty}-\frac{1}{300}\right)^2+2\left(\frac{1}{330}-\frac{1}{\infty}\right)\left(\frac{1}{\infty}-\frac{1}{300}\right)\cos 2\varphi}$

$K4=B-A=\frac{1}{2}\left[\left(\frac{1}{300}+\frac{1}{\infty}\right)-\left(\frac{1}{\infty}+\frac{1}{330}\right)\right]$ = 0.00015/mm

$\theta=\cos^{-1}\left(\frac{K_4}{K_3}\right)$

$\theta=\cos^{-1}\left(\frac{0.00015}{0.0032}\right),\ \theta=87.3^{\circ}$

By using the Hertz coefficient table and linear interpolation method the value of m and n for the selected rail can be easily obtained.

Where$E$ is the Young's modulus, ν is the Poisson's ratio (assuming the same material for the rail and the wheel), m and n are non-dimensional coefficients and their relationships with the angle θ is shown in Table 3.6 below.

Table 3.6: Hertz coefficients m and n [8].

θ (deg)	m	n	θ (deg)	m	n	θ (deg)	m	n
0.5	61.4	0.1018	10	6.604	0.3112	60	1.4186	0.717
1	36.89	0.1314	20	3.813	0.4125	65	1.378	0.759
1.5	27.48	0.1522	30	2.731	0.493	70	1.284	0.802
2	22.26	0.1691	35	2.397	0.530	75	1.202	0.846
3	16.5	0.1964	40	2.136	0.567	80	1.128	0.893
4	13.31	0.2188	45	1.926	0.604	85	1.061	0.944
6	9.79	0.2552	50	1.754	0.641	90	1.0	1.0
8	7.86	0.285	55	1.611	0.678			

(Source: Damage analysis of wheel/rail contact associated to high adhesion condition, 2015).

By interpolation method, we can calculate m and n

$\theta_1=85^0$, $m_1=1.06$, $n_1= 0.94$, $\theta_2=90^0$ $m_2= 1.0$, $n_2= 1.0$

$m=m_1+\left(\frac{m_2-m_1}{\theta_2-\theta_1}\right)(\theta-\theta_1)$

$m=1.06+\left(\frac{1-1.06}{90-85}\right)(87.3-85)$

$m=1.0324$

$n=n_1+\left(\frac{n_2-n_1}{\theta_2-\theta_1}\right)(\theta-\theta_1)$

$n=0.94+\left(\frac{1-0.94}{90-85}\right)(87.3-85)$

$n=0.9676$

Assumption: The radius from the top of the rail decreases continuously due to wear. The decreasing rate due to wear is high on minimum curve radius than the other rail part. Therefore the paper assumed that the height of the rail decreases by five millimeter radius from the top of the rail and the radius of the wheel assumed to be constant.

The principal transverse radii of the rail(R_2^r)= 300mm-5mm = 295mm

$K_w=\frac{1-(0.3)2}{\pi\times207\times10^9\mathrm{N/mm2}}$, $K_w=1.4\times10^{-12}\frac{m^2}{N}$

$K_r=\frac{1-(vr)^2}{\pi\mathrm{Er}}$, $K_r=\frac{1-(0.3)2}{\pi\times207\times10^9\mathrm{N/mm2}}=1.4\times10^{-12}\frac{m^2}{N}$

K_3= A+B=$\frac{1}{2}\left[\frac{1}{330}\ mm+\frac{1}{\infty}+\frac{1}{\infty}+\frac{1}{295}\ mm\right]$, K3=0.00321/mm

K4=B-A= $\frac{1}{2}\left[\left(\frac{1}{295}+\frac{1}{\infty}\right)-\left(\frac{1}{\infty}+\frac{1}{330}\right)\right]$ = 0.000179/mm.

θ= $\cos^{-1}\left(\frac{K_4}{K_3}\right)$

θ= $\cos^{-1}\left(\frac{0.000179}{0.00321}\right)$, $\theta = 86.8^{\circ}$

By using hertz coefficient table 3.6 above, the value of m and n are calculated using interpolation method.

θ_1=85^0, m_1=1.061, n_1= 0.944, θ_2=90^0 m_2= 1.0, n_2= 1.0

m=m_1+$\left(\frac{m_2-m_1}{\theta_2-\theta_1}\right)(\theta-\theta_1)$

m=1.061+$\left(\frac{1-1.06}{90-85}\right)(86.8-85)$

m=1.039

n=n_1+ $\left(\frac{n_2-n_1}{\theta_2-\theta_1}\right)(\theta-\theta_1)$

n=0.944+$\left(\frac{1-0.94}{90-85}\right)(86.8-85)$

n=0.964.

Again for the second reduction from the top of the rail due to wear.

The principal transverse radii of the rail(R_2^r)= 295mm-5mm = 290mm

K_w =$\frac{1-(0.3)2}{\pi\times207\times10^9\mathrm{N/mm2}}$, K_w=$1.4\times10^{-12}\frac{m^2}{N}$

K_r=$\frac{1-(vr)^2}{\pi\mathrm{Er}}$, K_r =$\frac{1-(0.3)2}{\pi\times207\times10^9\mathrm{N/mm2}}$ = $1.4\times10^{-12}\frac{m^2}{N}$

K_3= A+B =$\frac{1}{2}\left[\frac{1}{330}\ mm+\frac{1}{\infty}+\frac{1}{\infty}+\frac{1}{290}\ mm\right]$, K3=0.003239/mm

K4=B-A= $\frac{1}{2}\left[\left(\frac{1}{295}+\frac{1}{\infty}\right)-\left(\frac{1}{\infty}+\frac{1}{330}\right)\right]$ = 0.000208/mm.

θ= $\cos^{-1}\left(\frac{K_4}{K_3}\right)$

θ= $\cos^{-1}\left(\frac{0.000208}{0.003239}\right)$, $\theta = 86.3^{\circ}$

By using hertz coefficient table 3.6 above, the value of m and n are calculated using interpolation method.

θ_1=85^0, m_1=1.061, n_1= 0.944, θ_2=90^0 m_2= 1.0, n_2= 1.0

m=m_1+$\left(\frac{m_2-m_1}{\theta_2-\theta_1}\right)(\theta-\theta_1)$

m=1.061+$\left(\frac{1-1.06}{90-85}\right)(86.3-85)$

m=1.045

n=n_1+ $\left(\frac{n_2-n_1}{\theta_2-\theta_1}\right)(\theta-\theta_1)$

n=0.944+$\left(\frac{1-0.94}{90-85}\right)(86.8-85)$

n=0.9585.

3.3.1.2. Load Distribution Analysis and Site Selection.

There are two minimum radius of curved rail profile in AALRT. The first minimum radius of curved rail profile is thirty meter (30m), located in Kality depot and Ayat depot. The second minimum radius of curvature fifty meter (50m) is located in three places namely: at stadium, saint lideta and Autobustera. The minimum radius of curvature located in the depot is not considered due to passenger load is not available in the depot. However, detailed analysis of curved rail profile with fifty meter radius located at three places will be done.

Stadium, Saint Lideta and Autobistera

Figure 3.4: The three location of R50 radius of curvature in AALRT [24].

The paper considers the morning pick hour loads, day flat hour loads and afternoon pick hour loads based on three curved roots located at stadium, saint lideta and autobistera. The primary data of passenger loads at three curved roots are collected from load sensor of train's passenger load. Among train's passenger loads, the paper takes three different train's passenger loads at three curved rail locations (stadium, saintlideta and autobustera)with three different time or working period (morning peak hour(7am-9am), day flat hour(9am-5pm) and afternoon peak hour(5pm-7pm)).On each every single train the passenger loads are displayed in to passenger loads on motor one and passenger loads on motor two. From this two loads the average loads

will be taken for one train passenger loads. Taking three different train's passenger load helps to take the average loads that will be applied on rail for analysis. The data collected from train's load sensor below on three tables: table 3.7, 3.8 and 3.9 shows, passenger loads at three locations (stadium, saintlideta and autobistera) with three different time working period (morning peak hour, day flat hour and afternoon peak hour).

The primary data in three tables below 3.7, 3.8, and 3.9 are collected through traveling with master trains.

Table 3.7: Passenger Loads at Stadium.

Travelling time	Trains	Passenger loads in tons		
		Motor one	motor two	average
Morning peak hour (7am-9am)	Vehicle no. 205	18.5	18.5	18.5
	Vehicle no.206	18.6	18.5	18.55
	Vehicle no.207	18.4	18.3	18.35
	Average mean			18.46
Day flat hour(9am-5pm)	Vehicle no.210	16.7	16.5	16.6
	Vehicle no.209	16.9	16.6	16.75
	Vehicle no.211	16.5	16.4	16.45
	Average mean			16.6
Afternoon peak hour(5pm-7pm)	Vehicle no.205	19.1	19.0	19.05
	Vehicle no.208	19.3	18.9	19.1
	Vehicle no.212	19.2	19.1	19.15
	Average mean			19.1

Table 3.8:Passenger Loads at SaintLideta.

Travelling time	Trains	Passenger loads in tons		
		Motor one	motor two	average
Morning peak hour(7am-	Vehicle no. 205	18.1	18.2	18.15

9am)	Vehicle no.206	18.1	17.9	18.0
	Vehicle no.207	18.2	17.6	17.9
	Average mean			18.0
Day flat hour(9am-5pm)	Vehicle no.210	16.2	16.1	16.15
	Vehicle no.209	16.1	16.3	16.2
	Vehicle no.211	16.4	16.3	16.35
	Average mean			16.23
Afternoon peak hour(5pm-7pm)	Vehicle no.205	18.7	18.6	18.65
	Vehicle no.208	18.8	18.8	18.8
	Vehicle no.212	18.6	18.5	18.55
	Average mean			18.66

Table 3.9: Passenger Loads at Autobistera.

Travelling time	Trains	Passenger loads in tons		
		Motor one	motor two	average
Morning peak hour(7am-9am)	Vehicle no.205	17.2	16.9	17.05
	Vehicle no.206	17.8	17.5	17.65
	Vehicle no.207	17.9	18.1	18.0
	Average mean			17.56
Day flat hour(9am-5pm)	Vehicle no.210	15.8	15.7	15.75
	Vehicle no.209	15.8	16.0	15.9
	Vehicle no.211	15.3	15.2	15.25
	Average mean			15.63
Afternoon peak hour(5pm-7pm)	Vehicle no.205	18.3	18.3	18.3
	Vehicle no.208	18.4	18.3	18.35
	Vehicle no.212	18.4	18.2	18.3
	Average mean			18.3

The table 3.10 below shows average passenger loads taken from three tables 3.7,3.8,3.9 above and vehicle loads together that gives total vertical loads applied on rail.

Table 3.10: Vehicle Weight and Passenger Loads.

No	Working time/period	Location								
		Stadium			Saint lideta			Autobistera		
		Car body weight in tone	Passenger weight in tone	Total weight in tone	Car body weight in tone	Passenger weight in tone	Total weight in tone	Car body weight In tone	Passenger weight in tone	Total weight in tone
	Empty vehicle	44	0	44	44	0	44	44	0	44
	Morning peak hour	44	18.46	**62.46**	44	18	**62**	44	17.56	**61.56**
	Day flat hour	44	16.6	**60.6**	44	16.23	**60.23**	44	15.63	**59.63**
	Afternoon peak hour	44	19.1	**63.1**	44	18.66	**62.66**	44	18.3	**62.3**

Addis Ababa Light Rail Transit (AALRT) uses:

Number of bogies= 3

Number of axles on one bogie= 2

Total number of axle: number of bogies× number of axles on bogie= 3×2: 6

Number of wheels on one axle= 2

Total number of wheels= total number of axle× number of wheels on axle= 6×2:12

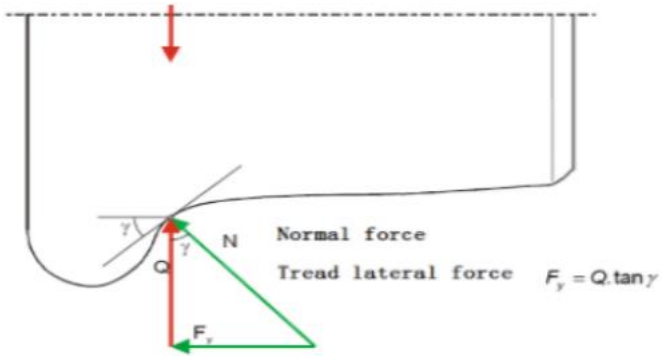

Figure 3.5:Wheel/rail constraint forces (23).

Assumption: There are tangential and normal force constraints, when wheel/rail contact forces are considered. For simplicity of the analysis the paper considers normal constraints (Q = wheel/rail vertical force N = wheel/rail normal forces, and F_y = wheel/rail lateral forces).

Flange angle used in Addis Ababa Light Rail Transit (AALRT) is seventy degree (70°). For seventy degree flange angle $\tan\gamma$ is $1/40$ or 0.025.

Vertical load on wheel= (vehicle weight+ passenger loads) ÷total number of wheels

Lateral load on wheel=vertical wheel load×$\tan\gamma$.

Table 3.11: Vertical and lateral wheel Load.

No	Working time/period	Location					
		Stadium		Saint lideta		Autobistera	
		Vertical Wheel load (Q) in kg	Lateral Wheel load (F_y) in kg	Vertical wheel load (Q) in kg	Lateral wheel load (F_y) in kg	Vertical wheel load (Q) in kg	Lateral Wheel load (F_y) in kg
	Morning peak hour	5205	130.125	5166.67	126.167	5130	128.25
	Day flat hour	5050	126.25	5019.167	125.479	4969.167	124.229
	Afternoon peak hour	5258.33	131.458	5221.67	130.54	5191.67	129.79

The above table 3.11 shows the vertical and lateral wheel load at three locations with different time.

Vertical wheel force in N = vertical wheel load in kg×earth gravity in m/s^2.

Lateral wheel force in N =lateral wheel load in kg × earth gravity in m/s^2.

Table 3.12: Vertical and Lateral Wheel Force.

No	Working time/period	Location					
		Stadium		Saint lideta		Autobistera	
		Vertical Wheel force (Q) in N	Lateral Wheel force (F_y) in N	Vertical wheel force (Q) in N	Lateral wheel force (F_y) in N	Vertical wheel force (Q) in N	Lateral Wheel force (F_y) in N
	Morning peak hour	51061.05	1276.53	50685	1237.7	50325.3	1258
	Day flat hour	49540.5	1238.5	49238	1230.95	48747.5	1218.7
	After noon peak hour	51584.22	1289.6	51224.6	1280.6	50930.3	1273

The above table 3.12 shows the vertical and lateral wheel force at three locations with different time applied on rail for analysis.

Normal force in N=$\sqrt{(\text{vertical wheel force})^2 \times (\text{lateral wheel force})^2}$

Table 3.13: Normal force.

No.	Working time/period	Location		
		Stadium	Saint lideta	Autobistera
		Normal force (F_n) in N	Normal force (F_n) in N	Normal force (F_n) in N
	Morning peak hour	51077	50700	50341
	Day flat hour	49555.98	49253	48762.7
	Afternoon peak hour	51600	51240.6	50946

Now the value of a and b are calculated as follows:

$$a=m\left[\frac{3\pi Fn\,(Kw+Kr)}{4K3}\right]^{\frac{1}{3}}$$

$$b=n\left[\frac{3\pi Fn\,(Kw+Kr)}{4K3}\right]^{\frac{1}{3}}$$

Table 3.14: The values of a and b.

No	Working time/period	Location					
		Stadium		Saint lideta		Autobistera	
		a in meter (m)	b in meter (m)	a in meter (m)	b in meter (m)	a in meter (m)	b in meter (m)
	Morning peak hour	0.00697	0.004569	0.00695	0.004558	0.006937	0.004547
	Day flat hour	0.0069	0.004523	0.006886	0.00451	0.006864	0.004499
	Afternoon peak hour	0.00699	0.00458	0.006978	0.004574	0.006964	0.004565

Using the values of a, b, and normal force, the maximum contact pressure will be calculated as follows:

$$P = P_O = \frac{3Fn}{2\pi ab}$$

Table 3.15: Maximum pressure.

No.	Working time/period	Location		
		Stadium	Saint lideta	Autobistera
		Maximum pressure (P_O) in MPa	Maximum pressure (P_O) in MPa	Maximum pressure (P_O) in MPa
	Morning peak hour	765.79	764.17	762.02
	Day flat hour	758.16	757.23	753.94
	Afternoon peak hour	769.57	766.52	765.16

The all maximum contact pressure is less than the ultimate tensile strength of rail, so the rail can resist the pressure applied at the contact area. The angular velocity of the wheel with minimum operating speed of the vehicle is:$\omega = v/R_{1w}$

The minimum operating speed of a train on minimum curved rail in AALRT is less than or equal to twelve (12) kilometer per hour. The paper takes the maximum value twelve (12) kilometer per hour.

Where $v$is the minimum operation speed of the vehicle, 12km/hr = 3.33 m/s and
R_{1w} is the principal rolling radius of the wheel, 330mm = 0.33m.

ω=3.33 / 0.33=10.1rad/s.

The value of a and b for the principal transverse radii of the rail (R_2^r) = 295mm are calculated as follows:

$$a=m\left[\frac{3\pi Fn\ (Kw+Kr)}{4K3}\right]^{\frac{1}{3}}$$

$$b=n\left[\frac{3\pi Fn\ (Kw+Kr)}{4K3}\right]^{\frac{1}{3}}$$

Table 3.16: The values of a and b.

No	Working time/period	Location					
		Stadium		Saint lideta		Autobistera	
		a in meter (m)	b in meter (m)	a in meter (m)	b in meter (m)	a in meter (m)	b in meter (m)
	Morning peak hour	0.007	0.00454	0.00699	0.0045	0.00697	0.00452
	Day flat hour	0.0069	0.0045	0.0069	0.00449	0.0069	0.00446
	Afternoon peak hour	0.007	0.00456	0.007	0.00455	0.007	0.00453

The maximum contact pressure is calculated as follows:

$$P = P_O = \frac{3Fn}{2\pi ab}$$

Table 3.17: Maximum pressure.

No.	Working time/period	Location		
		Stadium	Saint lideta	Autobistera
		Maximum pressure (P_O) in MPa	Maximum pressure (P_O) in MPa	Maximum pressure (P_O) in MPa
	Morning peak hour	767.4	766.18	766
	Day flat hour	762	759	756.56
	Afternoon peak hour	771.84	768.15	767.1

The angular velocity of the wheel with minimum operating speed of the vehicle is: $\omega=v/R_{1w}$

Where v is the minimum operation speed of the vehicle, 12km/hr = 3.33 m/s and
R_{1w} is the principal rolling radius of the wheel, 330mm = 0.33m.ω=3.33 / 0.33=10.1rad/s.

The analysis for the principal transverse radii of the rail (R_2^r) = 295mmis done.

The value of a and b for the principal transverse radii of the rail (R_2^r) = 290mm are calculated as follows:

$$a=m\left[\frac{3\pi Fn\,(Kw+Kr)}{4K3}\right]^{\frac{1}{3}}$$

$$b=n\left[\frac{3\pi Fn\,(Kw+Kr)}{4K3}\right]^{\frac{1}{3}}$$

Table 3.18: The values of a and b.

No	Working time/period	Location					
		Stadium		Saint lideta		Autobistera	
		a in meter (m)	b in meter (m)	a in meter (m)	b in meter (m)	a in meter (m)	b in meter (m)
	Morning peak hour	0.007027	0.004508	0.007009	0.004497	0.00699	0.004486
	Day flat hour	0.006957	0.00446	0.00694	0.00445	0.00692	0.004438
	Afternoon peak hour	0.007051	0.004523	0.007034	0.00451	0.007021	0.004504

The maximum contact pressure is calculated as follows:

$$P = P_O = \frac{3Fn}{2\pi ab}$$

Table 3.19: Maximum pressure.

No.	Working time/period	Location		
		Stadium	Saint lideta	Autobistera
		Maximum pressure (P_O) in MPa	Maximum pressure (P_O) in MPa	Maximum pressure (P_O) in MPa
	Morning peak hour	769.86	767.92	766.52
	Day flat hour	762.57	761.47	758.1
	Afternoon peak hour	772.5	771.2	769.23

3.3.2. Wheel/ Rail Geometrical Model and Assembly

Wheel and rail are modeled separately and assembled on CATIAV5 software.

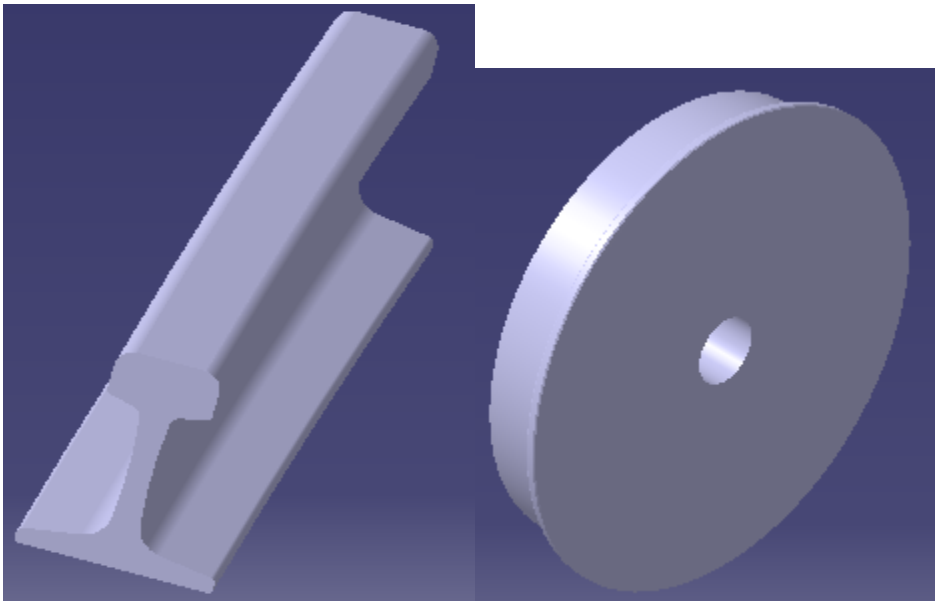

a) Rail Model b) Wheel model.

Figure 3.6: Wheel/Rail model.

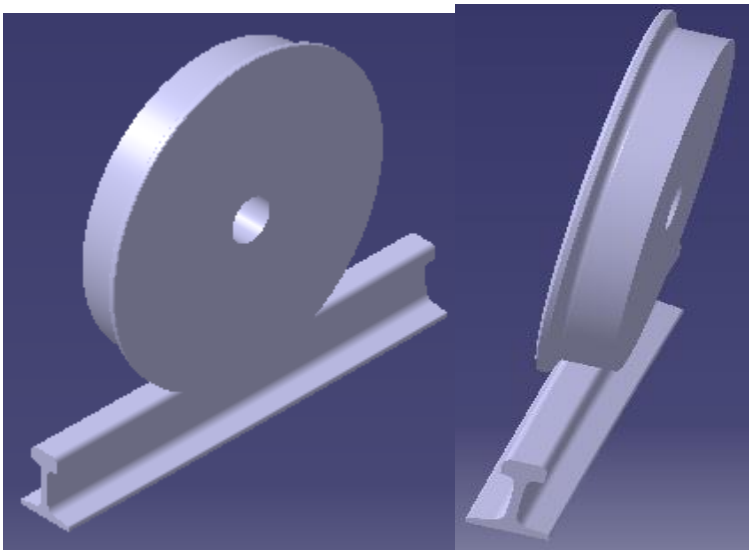

Figure 3.7: Wheel/Rail Assembly.

3.3.3. Wheel/Rail Analysis using ANSYS16 Work Bench

Wheel/rail assembly made on CATIA V5software is imported to ANSYS16 workbench for analysis.

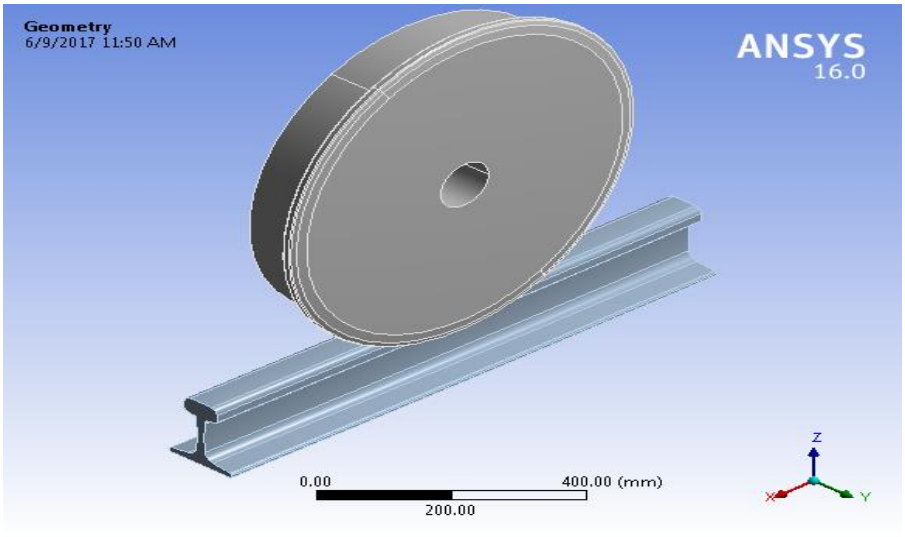

Figure 3.8: Wheel/rail assembly imported to ANSYS16 workbench.

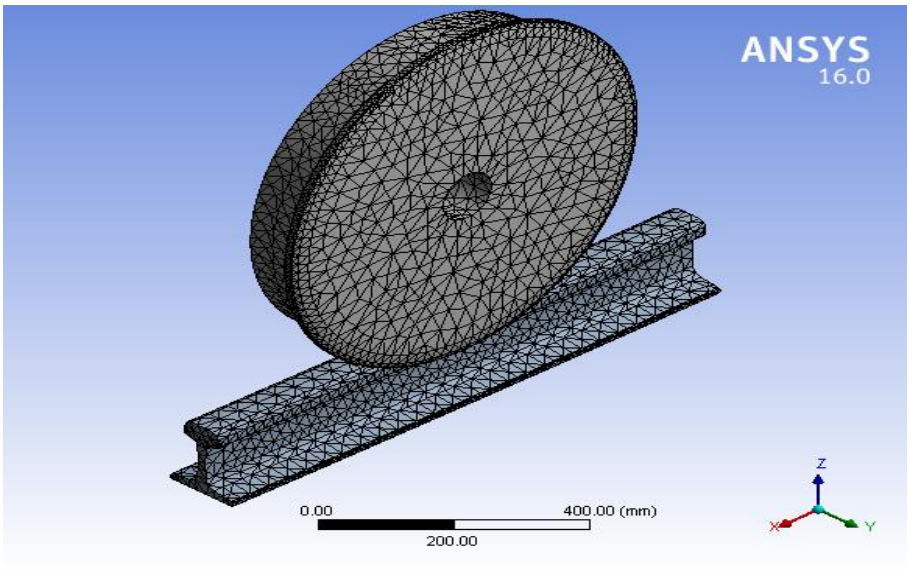

Figure 3.9: Wheel/rail assembly mesh.

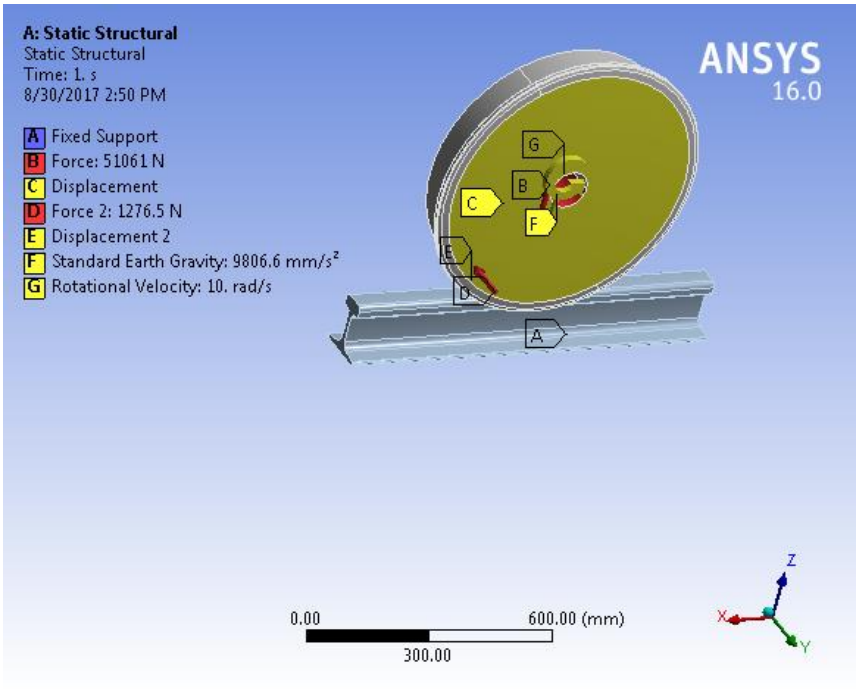

Figure 3.10: Stadium morning peak hour wheel/rail boundary condition and input data.

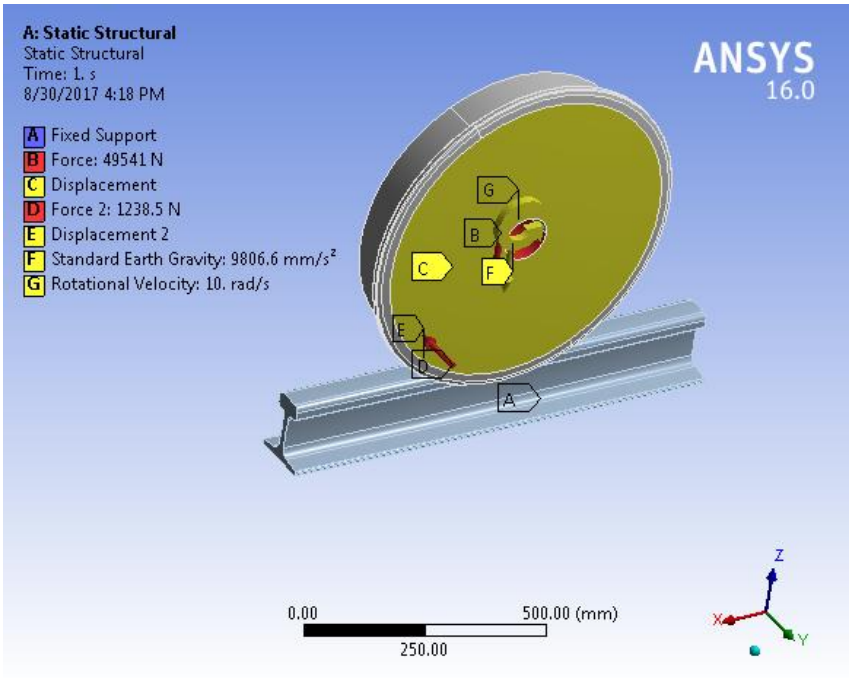

Figure 3.11: Stadium day flat hour boundary condition and input data.

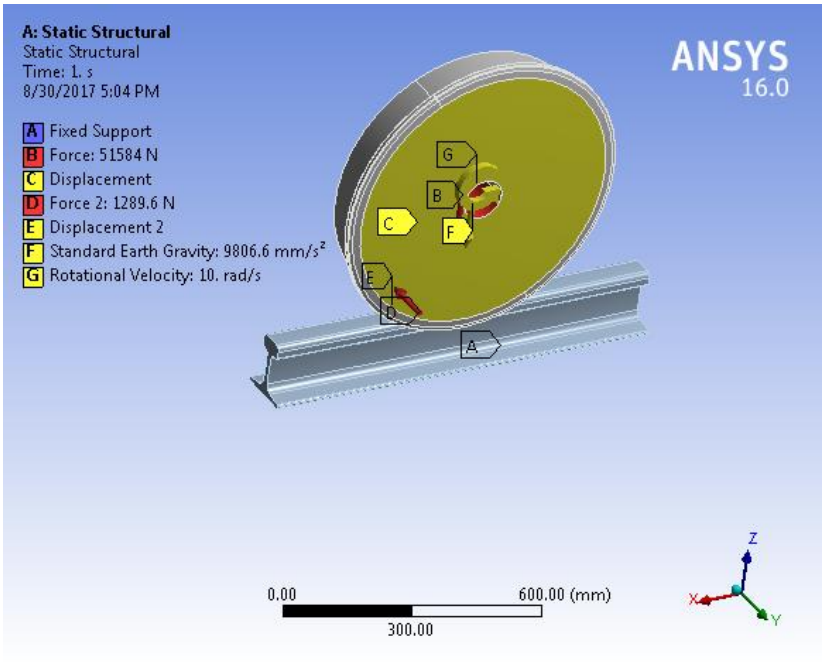

Figure 3.12: Stadium afternoon pick hour wheel/rail boundary condition and input data.

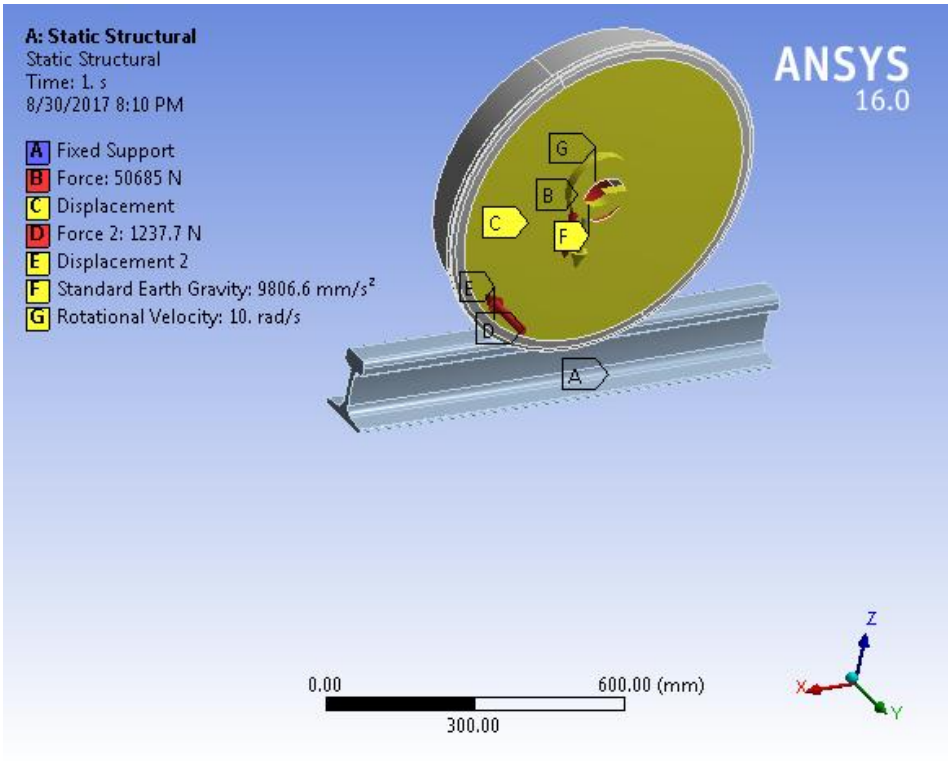

Figure 3.13: Saint lideta morning peak hour boundary condition and input data.

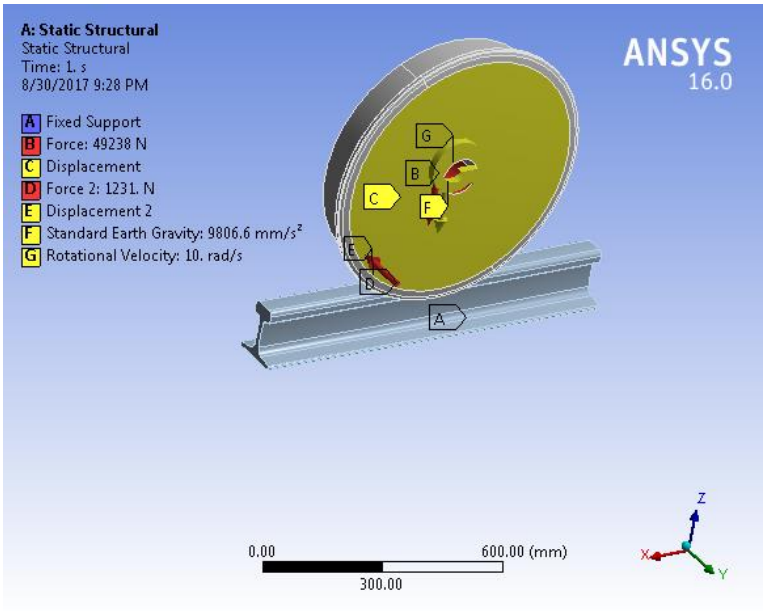

Figure 3.14: Saint lideta during day flat hour boundary condition and input data.

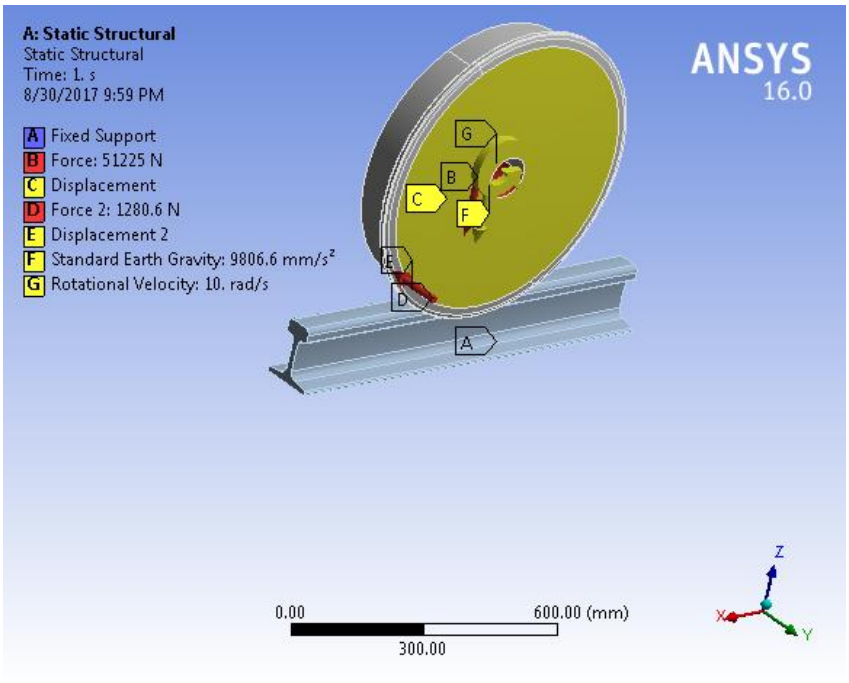

Figure 3.15:Saint lideta afternoon peak hour boundary condition and input data.

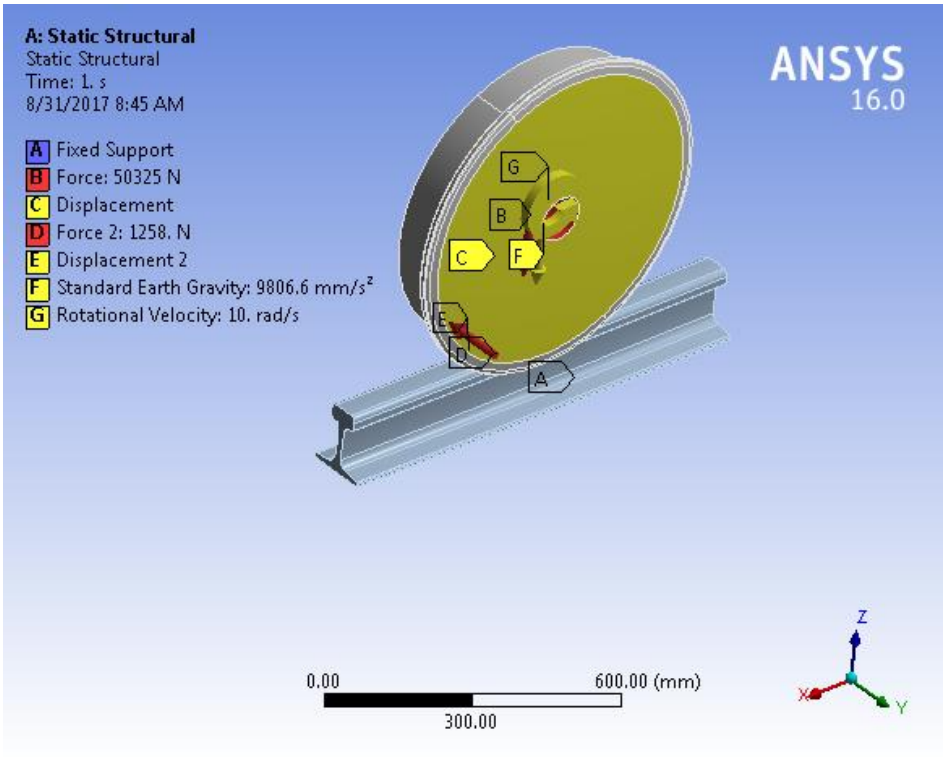

Figure 3.16: Autobistera morning peak hour boundary condition and input data.

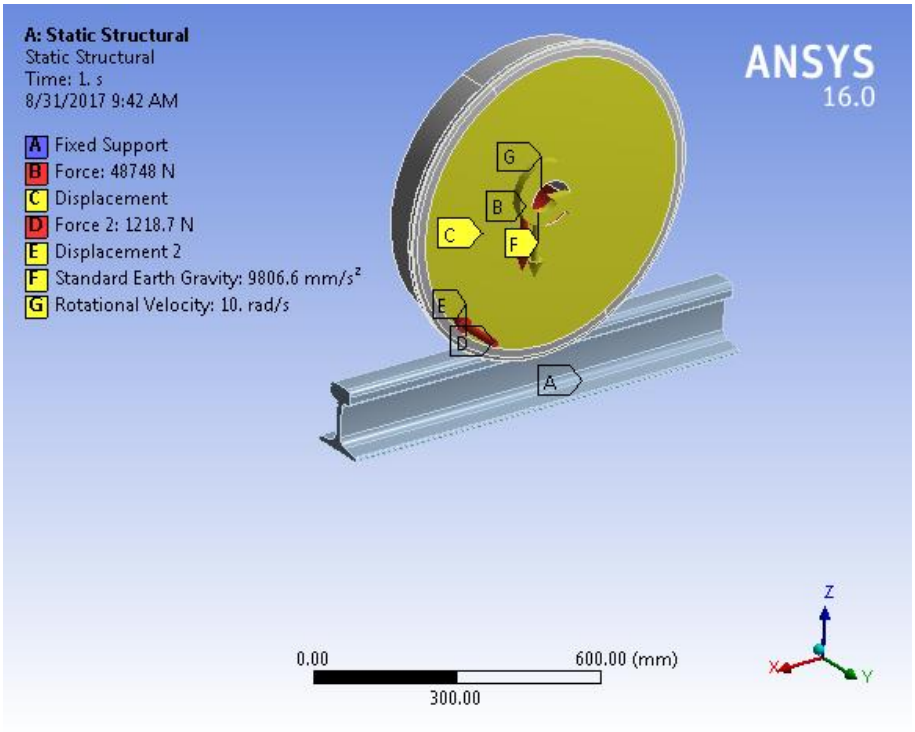

Figure 3.17: Autobisteraday flat hour boundary condition and input data.

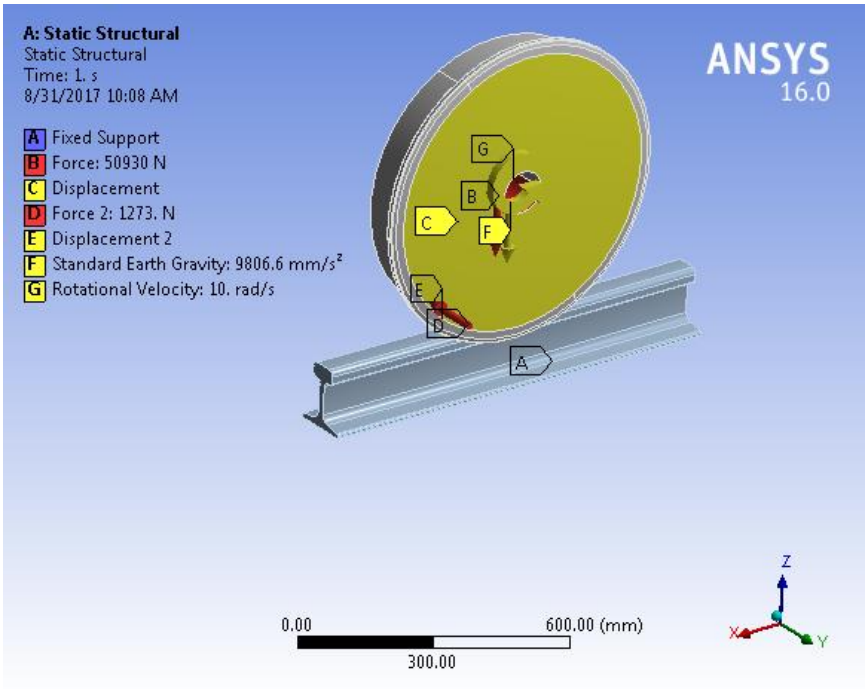

Figure 3.18: Autobistera afternoon peak hour boundary condition and input data.

CHAPTER FOUR

4. RESULT AND DISCUSSION

4.1. Result

The static fatigue failure analysis on minimum curved rail of AALRT(stadium, saint lideta and autobistera) are accomplished by using finite element model consists of static analysis and fatigue analysis to determine the impact of wheel load on curved rail of Addis Ababa light rail transit. The same geometry and different loads as per theworking period (morning peak hour, day flat hour and afternoon peak hour) are used for finite element analysis.In addition the five millimeter worn rail is analyzed. The paper deals with static structural analysis.

A static structural analysis determines pressure distribution, fatigue life, damage, safety factor, equivalent alternating stress, and fatigue sensitivity.

The types of loads applied on static structural analysis contains:

- Vertical wheel load (force).
- Lateral wheel load (force)
- Standard earth gravity
- Rotational velocity
- Displacement

I. Fatigue.

Fatigue Life: is available life for the given fatigue analysis.

Fatigue Damage: is defined as design life /available life.

Fatigue safety factor: is a factor of safety at with respect to a fatigue failure at a given design life.

Fatigue sensitivity: shows how the fatigue result changes as a function of loading the loading at the critical location on the model.

1.1. Stadium during morning peak hour.

1.1.1. Fatigue Life.

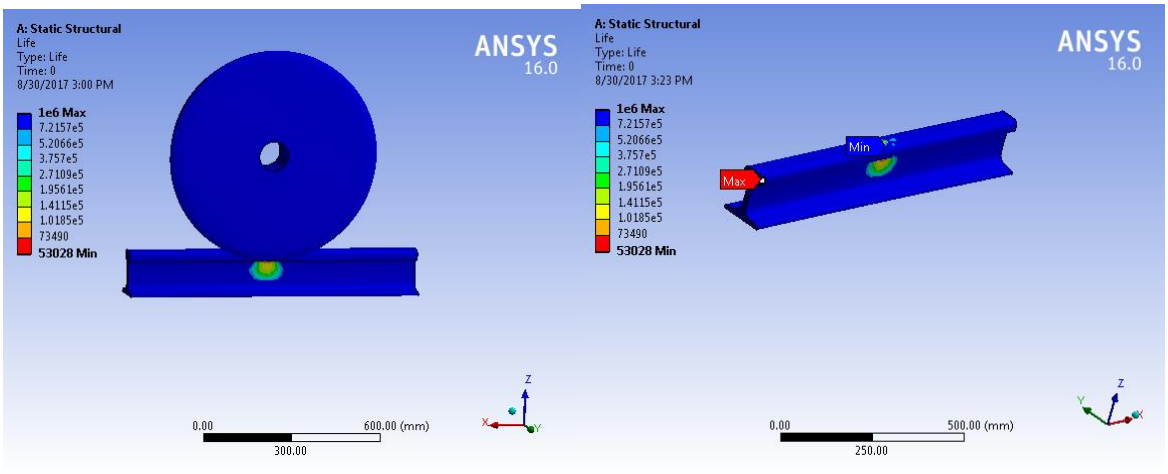

Figure 4.1: Fatigue life at stadium during morning peak hour.

As shown in above figure 4.1 the maximum fatigue life is $1e^6$cycles and the minimum fatigue life is 53028 cycles at stadium during morning peak hour.

1.1.2. Fatigue Damage

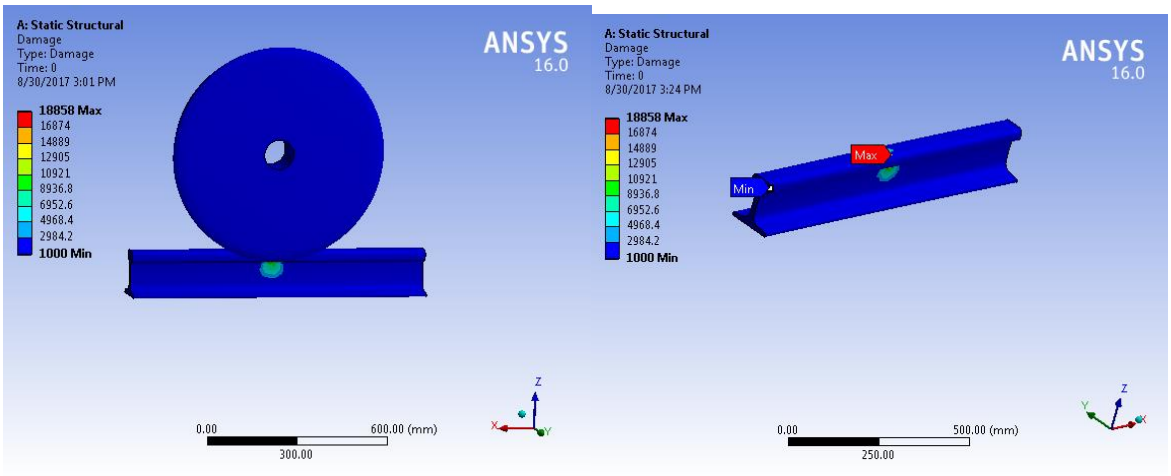

Figure 4.2: Damage at stadium during morning peak hour.

As shown in the figure 4.2 above the maximum fatigue damage is 18858and minimum fatigue damage is 1000 at stadium during morning peak hour.

1.1.3. Fatigue Safety factor.

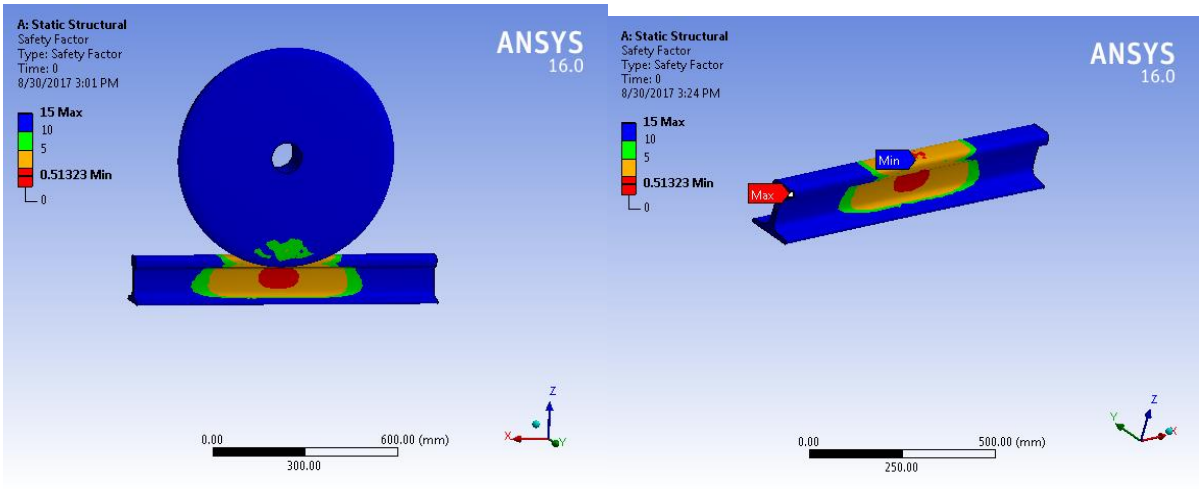

Figure 4.3: Safety factor at stadium morning peak hour.

As shown in the figure 4.3 above the maximum fatigue safety factor is 15 and minimum fatigue safety factor is 0.51323 at stadium during morning peak hour.

1.1.4. Equivalent alternating stress.

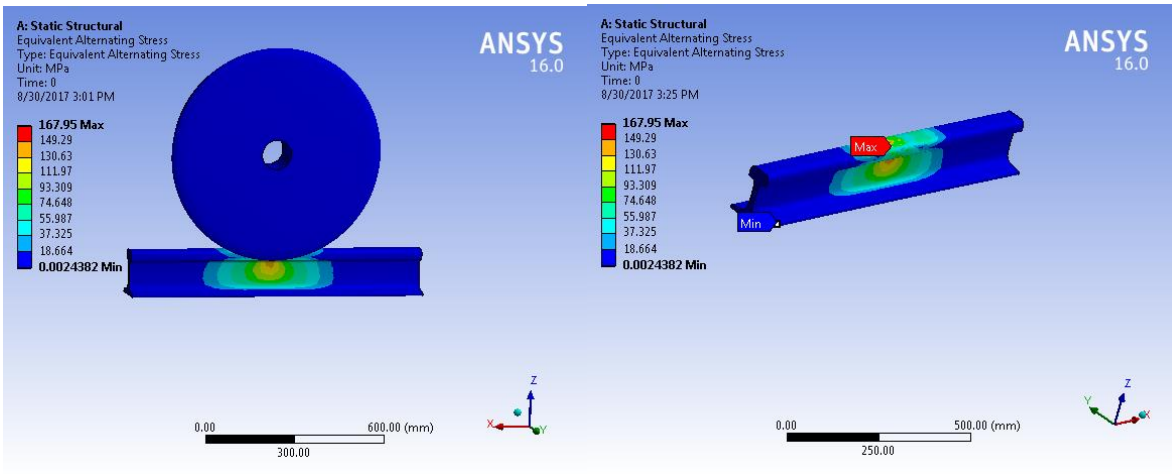

Figure 4.4: Equivalent alternating stress at stadium during morning peak hour.

As shown in the figure 4.4 above the maximum equivalent alternating stress is 167.95 MPa and minimum equivalent alternating stress is 0.0024382MPa at stadium during morning peak hour.

1.1.5. Fatigue sensitivity

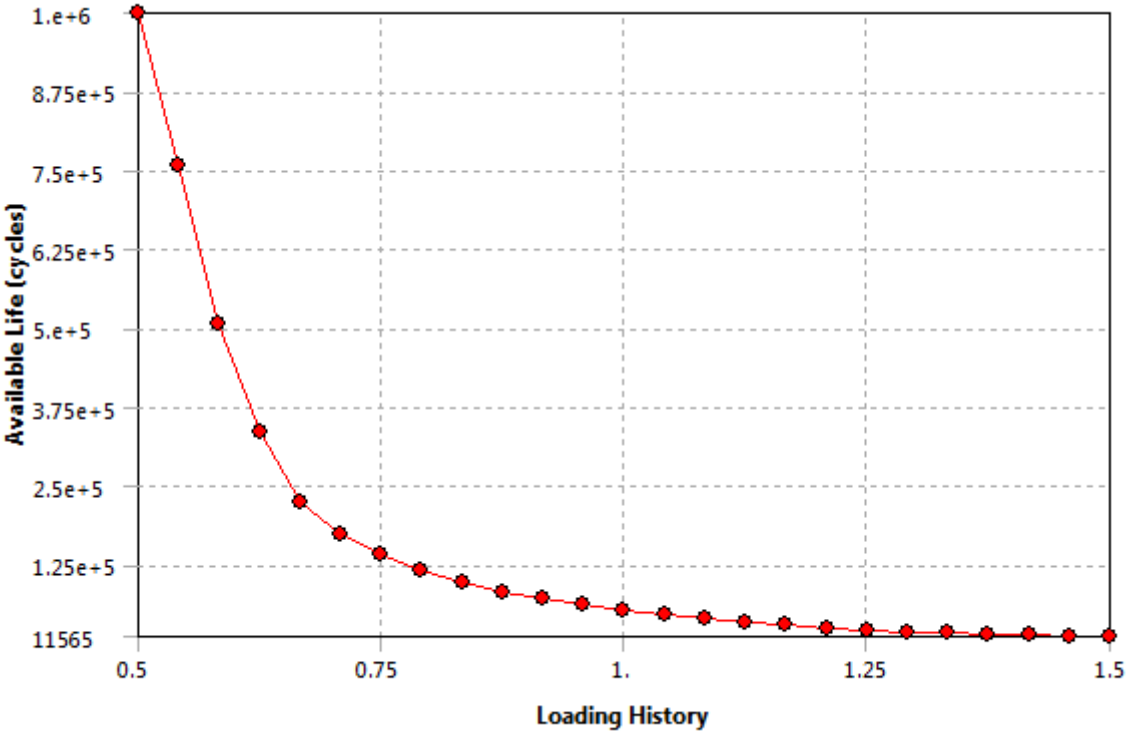

Figure 4.5: Fatigue sensitivity at stadium during morning peak hour.

As shown in the figure 4.5 above the maximum fatigue sensitivity is$1e^6$cycles and minimum fatigue sensitivity is 11565 cycles at stadium during morning peak hour.

1.2. Stadium during day flat hour.

1.2.1. Fatigue life.

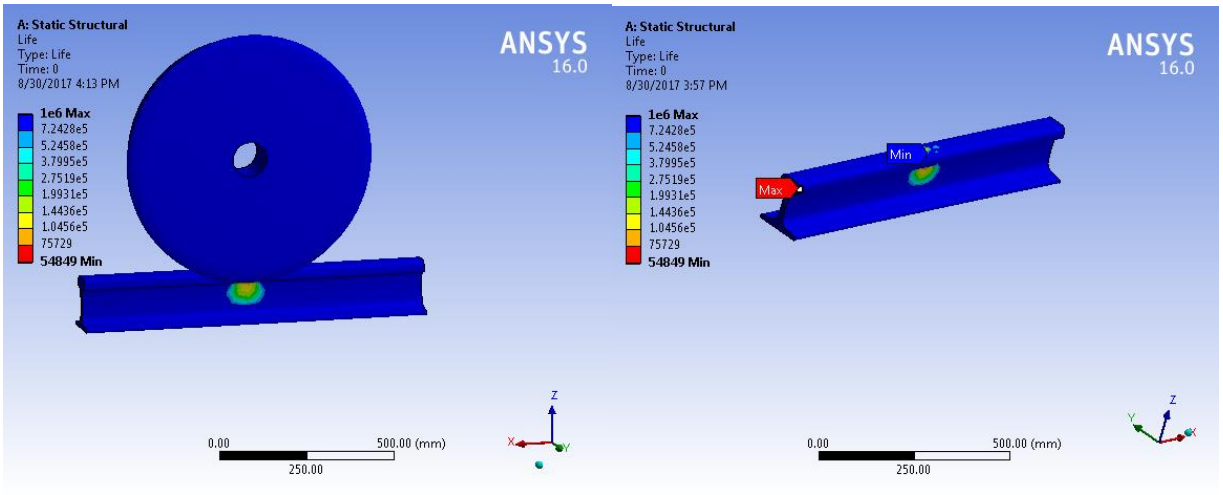

Figure 4.6: Fatigue life at stadium during day flat hour.

As shown in the figure 4.6 above the maximum fatigue life is $1e^6$cycle and minimum fatigue life is54849cycle at stadium during day flat hour.

1.2.2. Fatigue Damage.

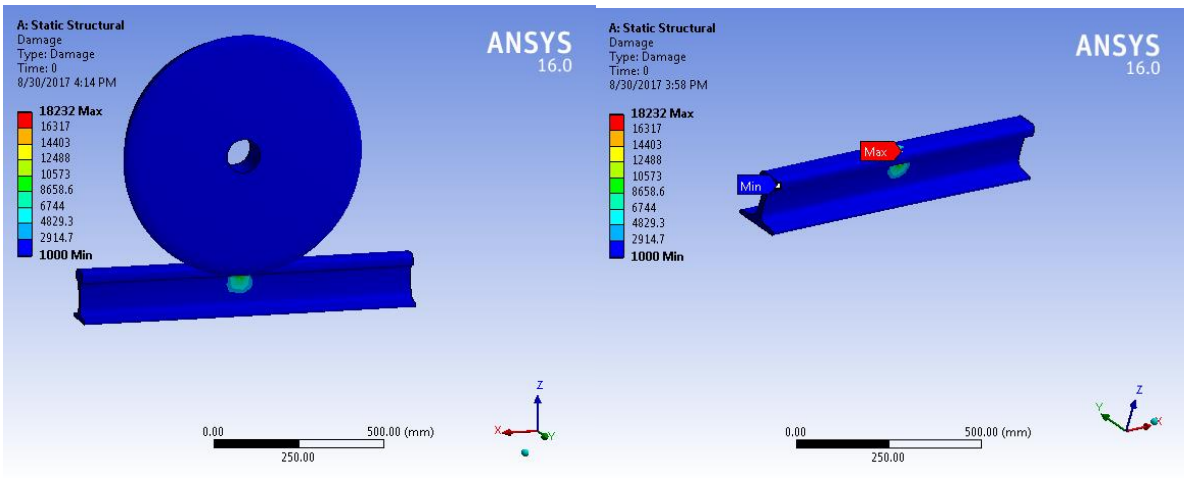

Figure 4.7: Fatigue damage at stadium day flat hour.

As shown in the figure 4.7 above the maximum fatigue damage is 18232 and minimum fatigue damage is 1000 at stadium during day flat hour.

1.2.3. Fatigue Safety factor.

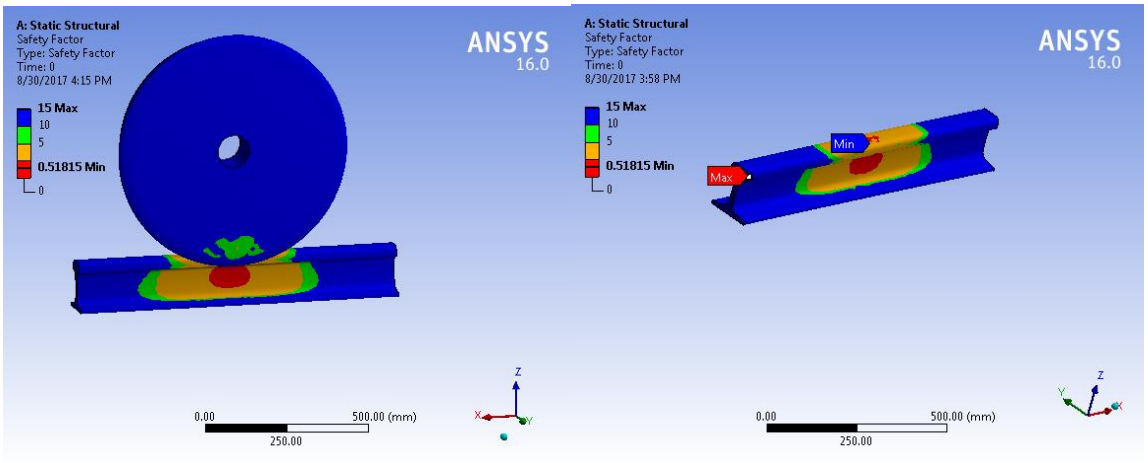

Figure 4.8: Safety factor at stadium during day flat hour.

As shown in the figure 4.8 above the maximum fatigue safety factor is 15 and minimum fatigue safety factor is0.51815at stadium during day flat hour.

1.2.4. Equivalent alternating stress.

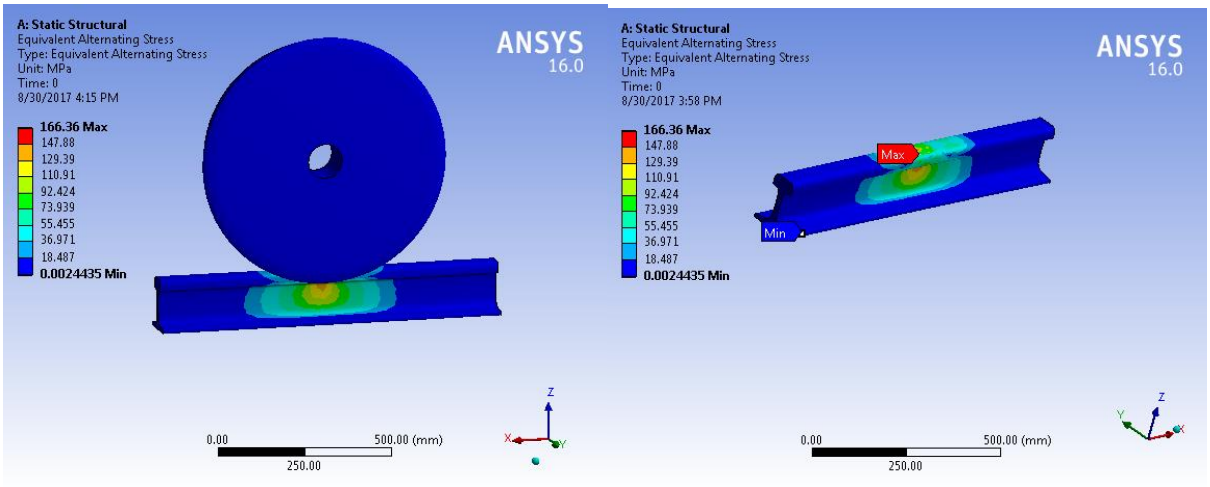

Figure 4.9: Equivalent alternating stress at stadium day flat hour.

As shown in the figure 4.9 above the maximum equivalent alternating stress is166.36 MPa and minimum equivalent alternating stress is 0.0024435 MPa at stadium during day flat hour.

1.2.5. Fatigue sensitivity.

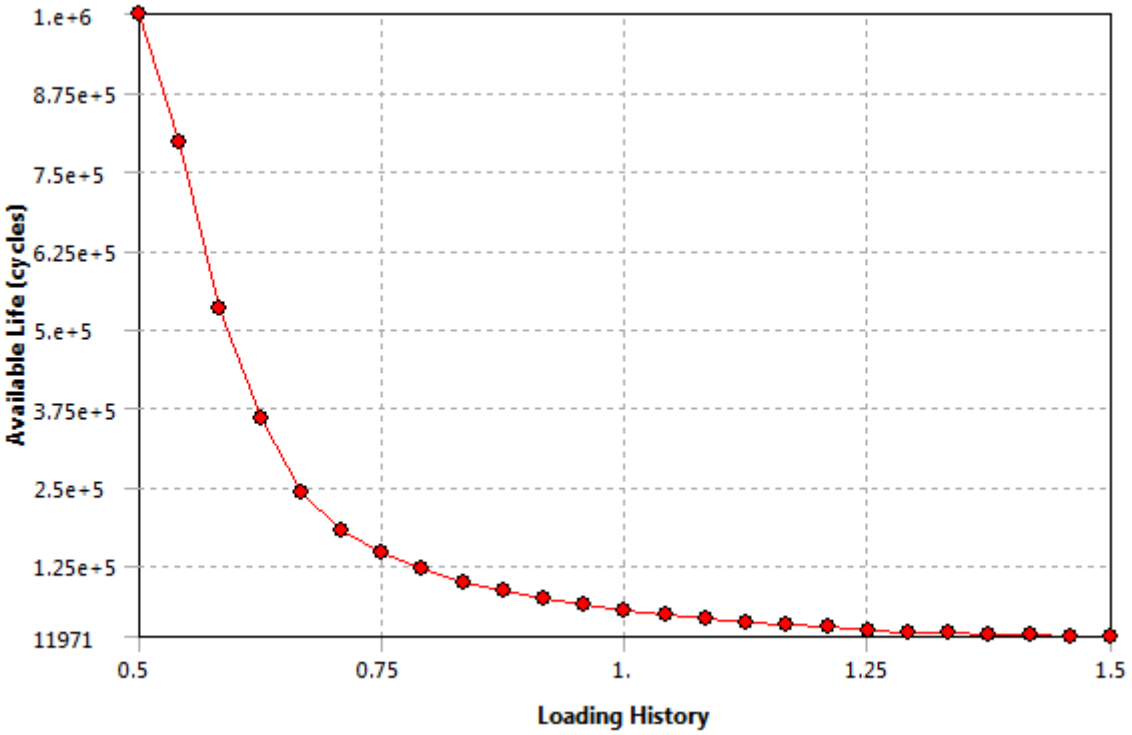

Figure 4.10: Fatigue sensitivity at stadium day flat hour.

As shown in the figure 4.10 above the maximum fatigue sensitivityis1e^{6}cycleand minimum fatigue sensitivity is 11971 at stadium during day flat hour.

1.3. Stadium during afternoon peak hour

1.3.1. Fatigue life

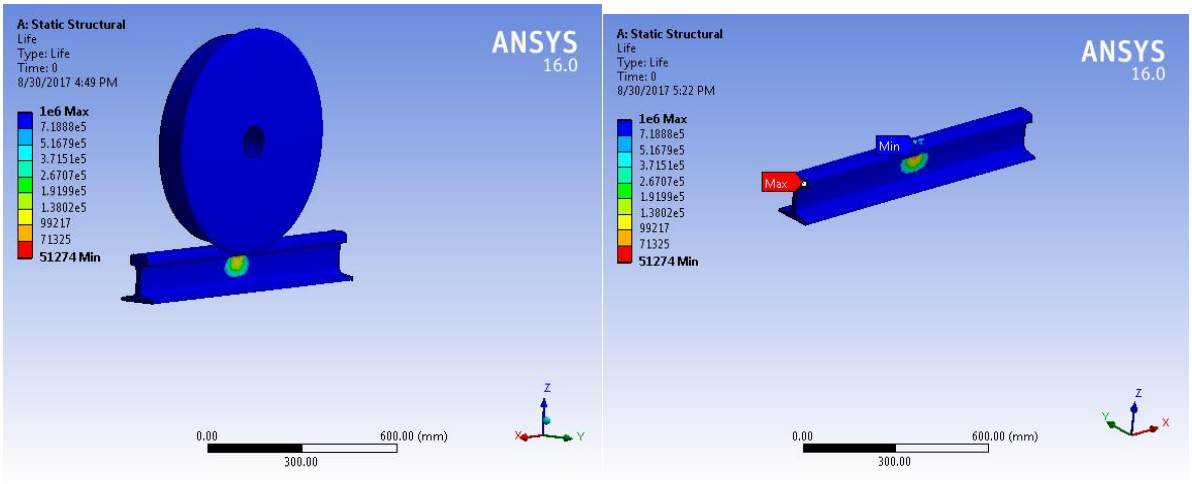

Figure 4.11:Fatigue life at stadium during afternoon peak hour.

As shown in the figure 4.11 above the maximum fatigue life is $1e^6$cycle and minimum fatigue life is 51274cycle at stadium during afternoon peak hour.

1.3.2.Fatigue damage.

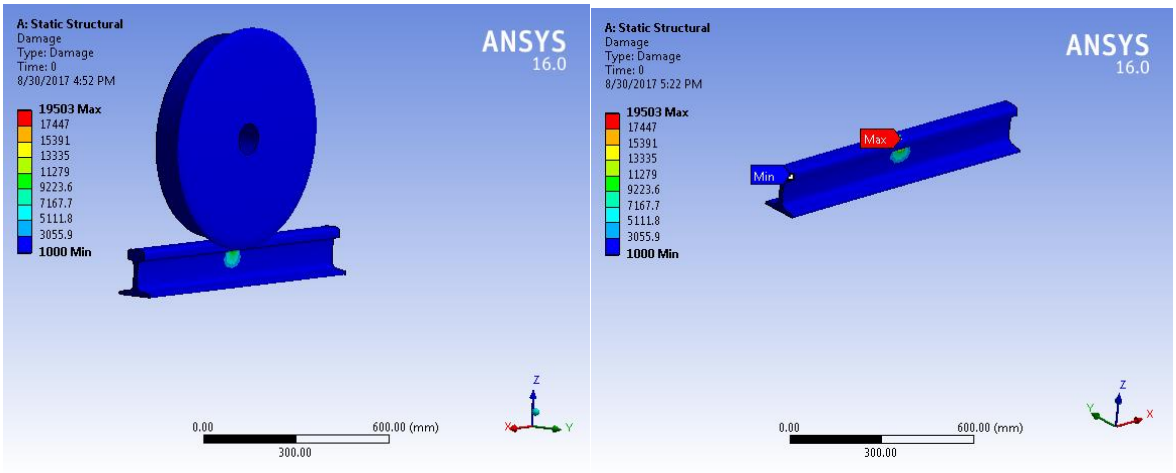

Figure 4.12: Damage at stadium during afternoon peak hour.

As shown in the figure 4.12 above the maximum fatigue damage is 19503and minimum fatigue damage is1000 at stadium during afternoon peak hour.

1.3.3. Fatigue safety factor

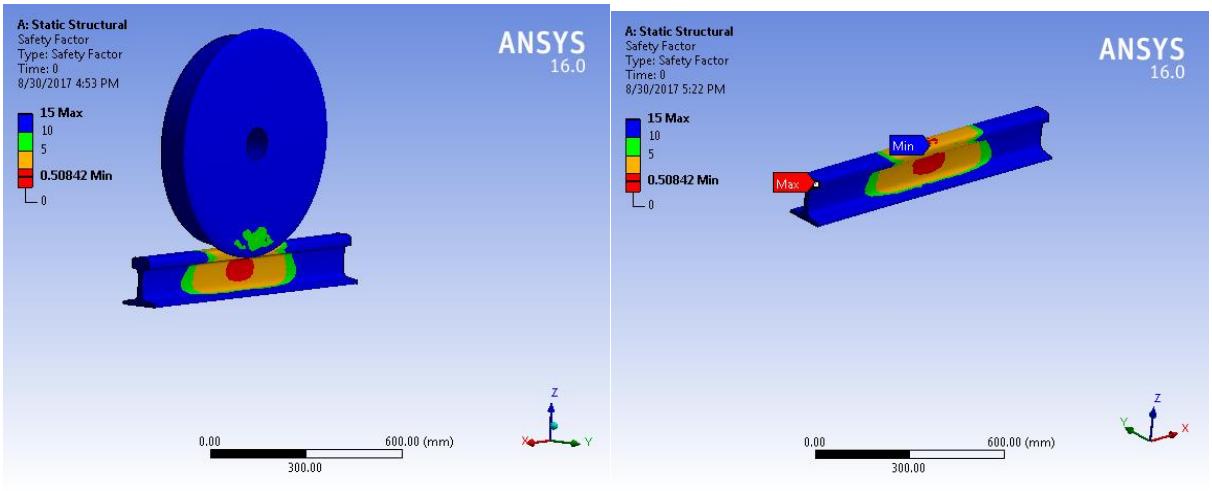

Figure 4.13:Fatigue safety factor at stadium afternoon peak hour.

As shown in the figure 4.13 above the maximum fatigue safety factor is 15and minimum fatigue safety factor is 0.50842 at stadium during afternoon peak hour.

1.3.4. Equivalent alternating stress.

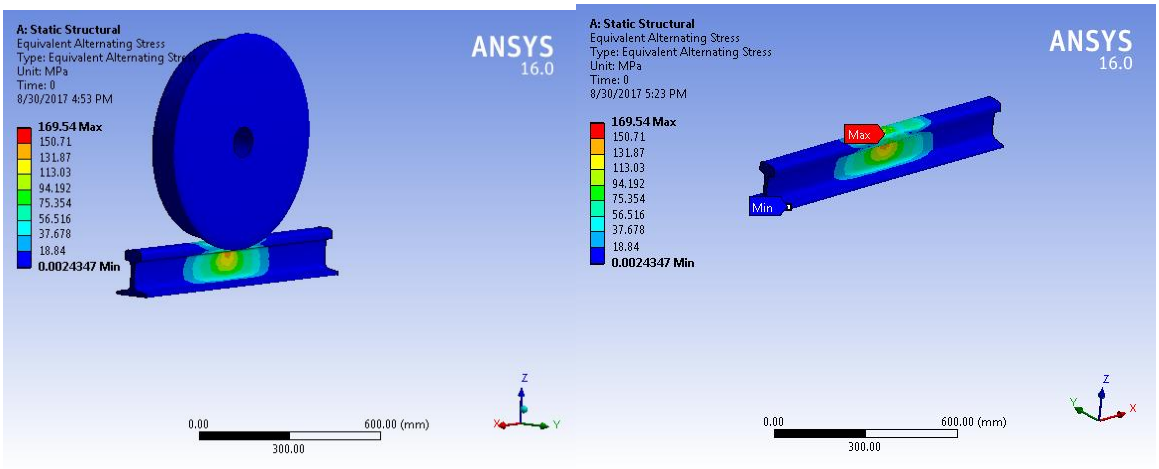

Figure 4.14: Equivalent alternating stress. at stadium afternoon peak hour.

As shown in the figure 4.14 above the maximum equivalent alternating stress is 169.54 MPa and minimum equivalent alternating stress is 0.0024347 MPa at stadium during afternoon pick hour.

1.3.5. Fatigue sensitivity.

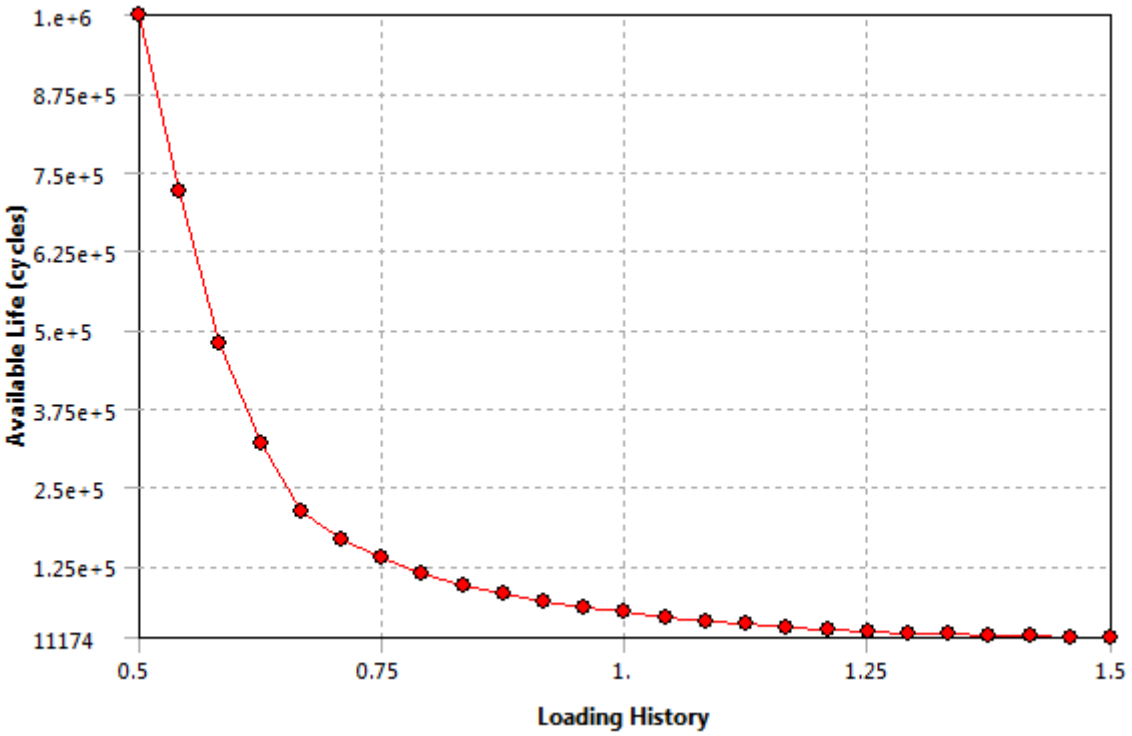

Figure 4.15: Fatigue sensitivity at stadium during afternoon peak hour.

As shown in the figure 4.15 above the maximum fatigue sensitivity is $1e^6$cyclesand minimum fatigue sensitivity is 11174cycles at stadium during afternoon peak hour.

Case 2: Saint Lideta.

2.1. Saint Lideta during morning peak hour.

2.1.1. Fatigue life.

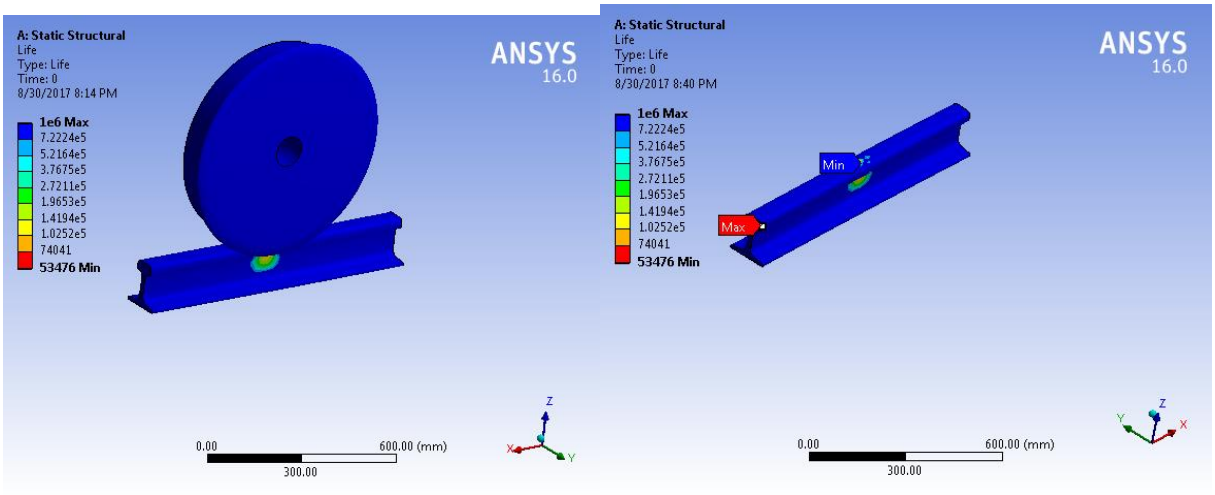

Figure 4.16: Fatigue life at saint lideta during morning peak hour.

As shown in the figure 4.16 above the maximum fatigue life is $1e^6$cycle and minimum fatigue life is 53476 cycle at saint lideta during morning peak hour.

2.1.2. Fatigue damage

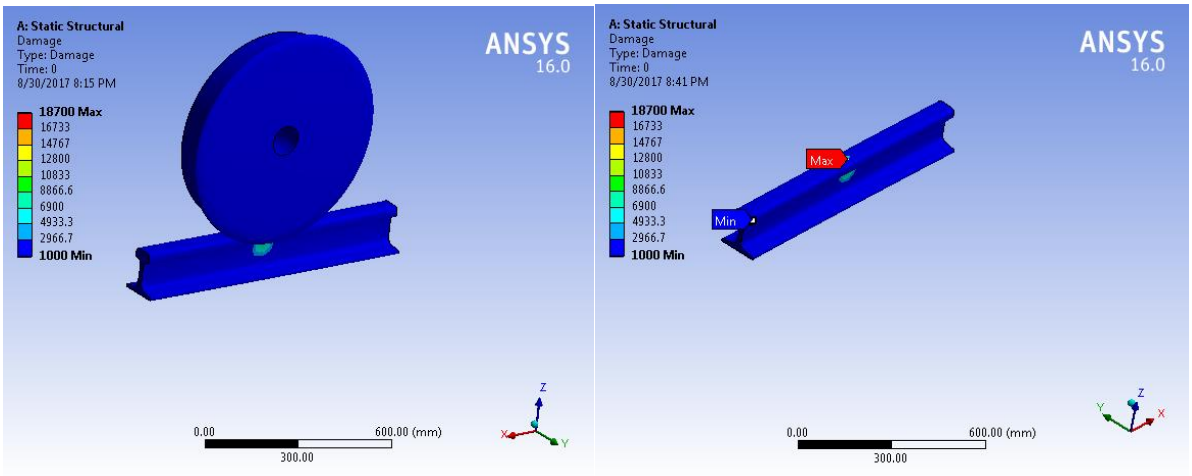

Figure 4.17: Damage at saint lideta morning peak hour.

As shown in the figure 4.17 above the maximum fatigue damage is 18700and minimum fatigue damage is 1000 at saint lideta during morning peak hour.

2.1.3. Safety factor.

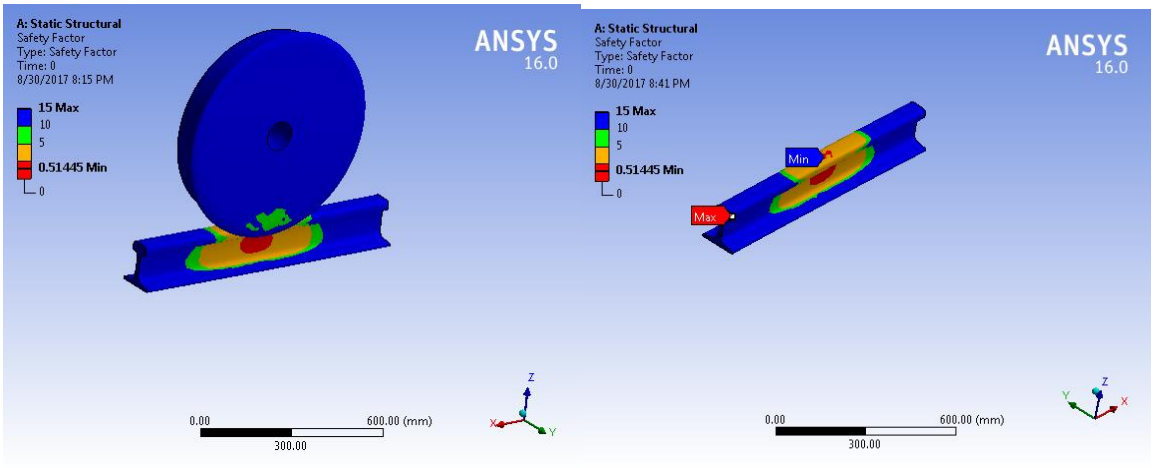

Figure 4.18: Safety factor at saint lideta morning peak hour.

As shown in the figure 4.18 above the maximum fatigue safety factor is 15and minimum fatigue safety factor is 0.51445 at saint lideta during morning peak hour.

2.1.4. Equivalent alternating stress.

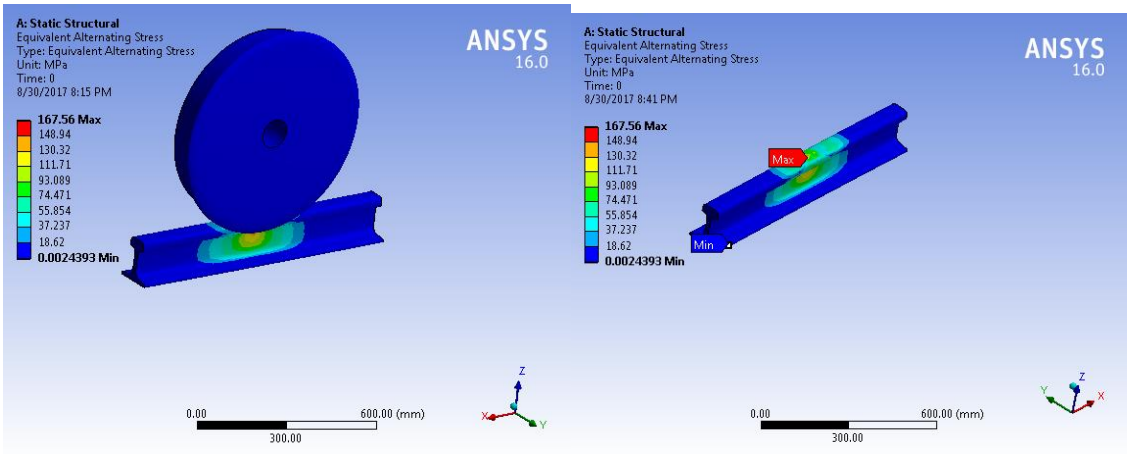

Figure 4.19: Equivalent alternating stress at saint lideta during morning peak hour.

As shown in the figure 4.19 above the maximum equivalent alternating stress is 167.56 MPaand minimum equivalent alternating stress is 0.0024393 MPa at saint lideta during morning peak hour.

2.1.5. Fatigue sensitivity.

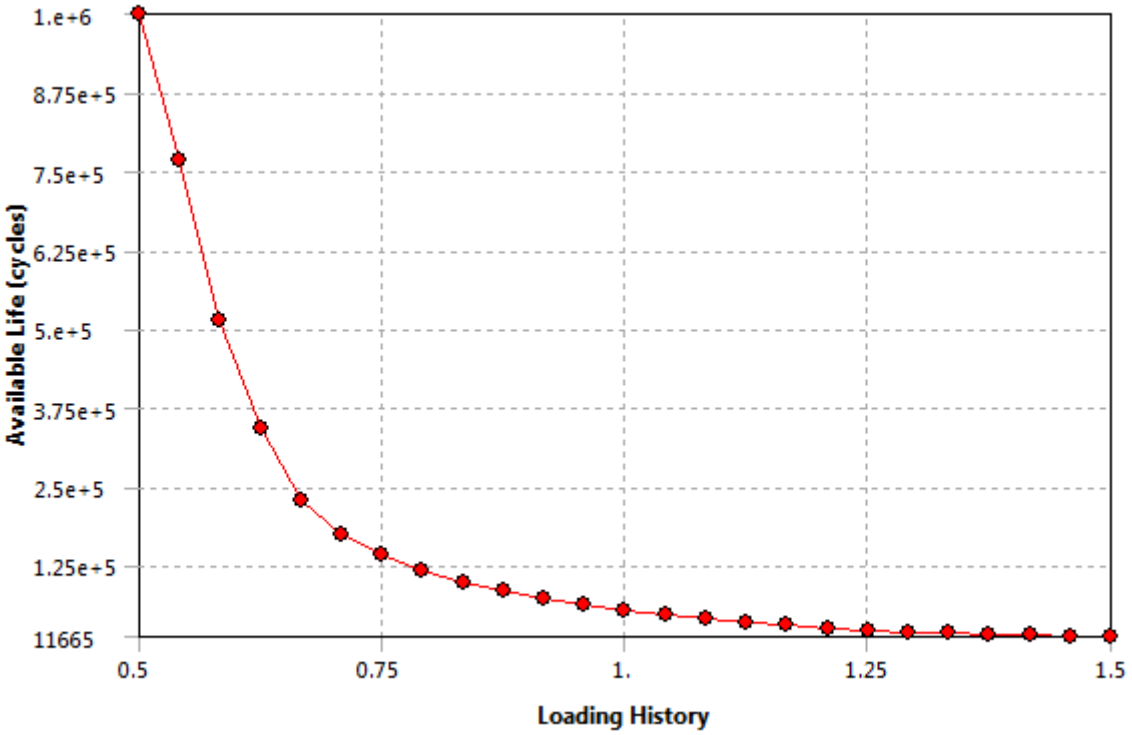

Figure 4.20: Fatigue sensitivity at saint lideta during morning peak hour.

As shown in the figure 4.20 above the maximum fatigue sensitivityis1e^{6}cycleand minimum fatigue sensitivity is 11665cycle at saint lideta during morning peak hour.

2.2. Saint Lideta during day flat hour day flat hour.

2.2.1. Fatigue life.

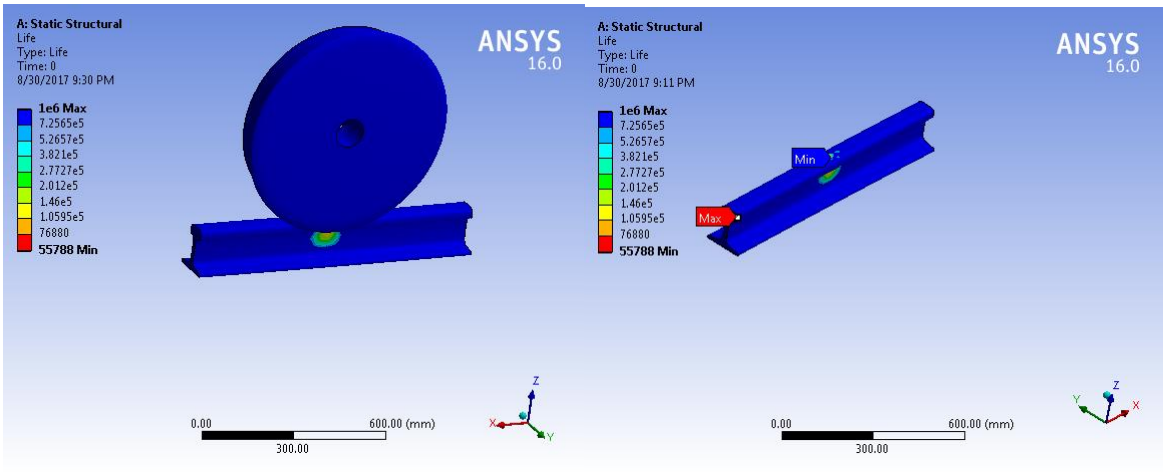

Figure 4.21: Fatigue life at saint lideta during day flat hour.

As shown in the figure 4.21 above the maximum fatigue life is $1e^6$cycles and minimum fatigue life is 55788 cycle at saint lideta during day flat hour.

2.2.2.Fatigue damage.

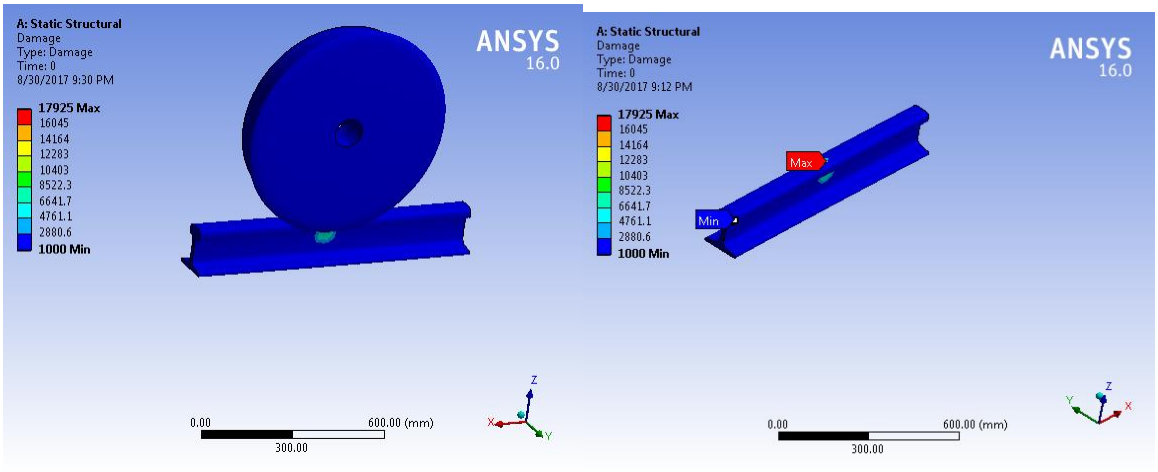

Figure 4.22: Fatigue damage at saint lideta during day flat hour.

As shown in the figure 4.22 above the maximum fatigue damage is 17925 and minimum fatigue damage is 1000 at saint lideta during day flat hour.

2.2.3. Safety factor.

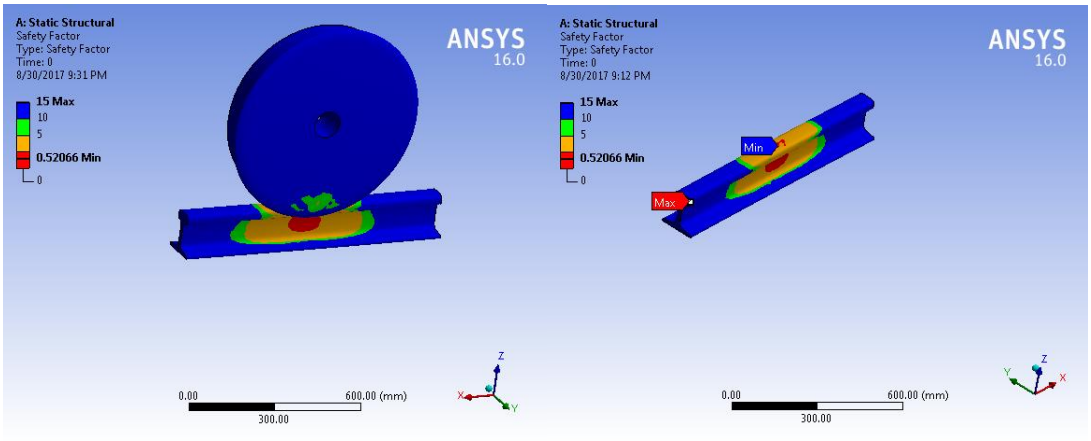

Figure 4.23: Safety factor at saint lideta during day flat hour.

As shown in the figure 4.23 above the maximum fatigue safety factor is 15and minimum fatigue safety factor is 0.52066 at sait lideta during day flat hour.

2.2.4. Equivalent alternating stress.

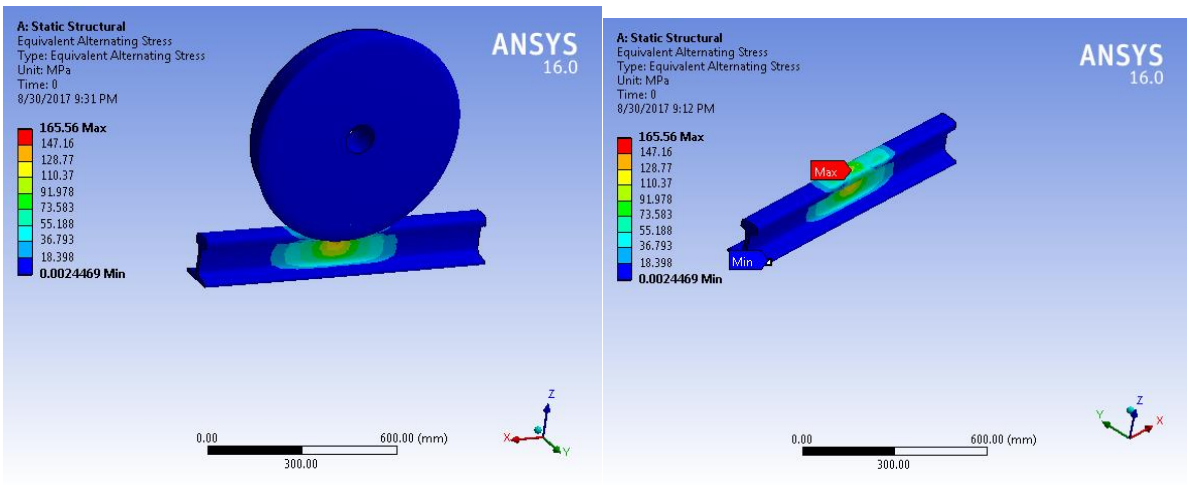

Figure 4.24: Equivalent alternating stress at saint lideta during day flat hour.

As shown in the figure 4.24 above the maximum equivalent alternating stress is 165.56 MPaand minimum equivalent alternating stress is 0.0024469 MPa at saint lideta during day flat hour.

2.2.5. Fatigue sensitivity.

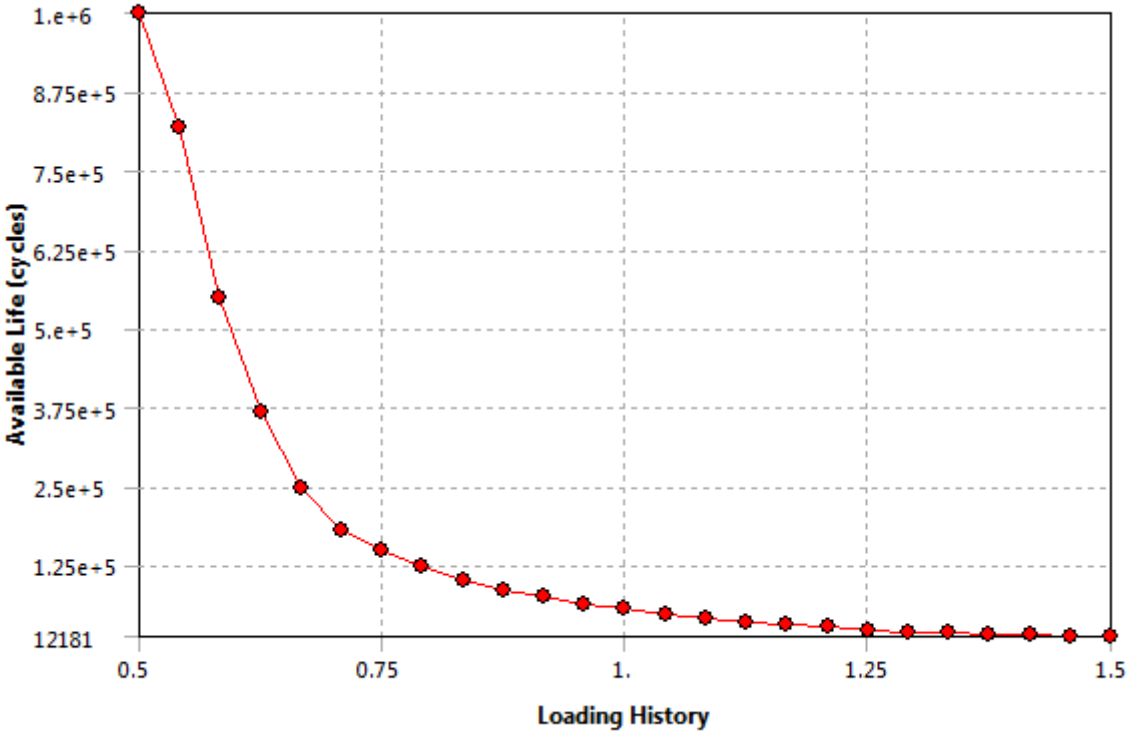

Figure 4.25: Safety factor at saint lideta during day flat hour.

As shown in the figure 4.25 above the maximum fatigue safety factor is $1e^{6}$cyclesand minimum fatigue safety factor is 12181 at saint lideta during day flat hour.

2.3. Saint Lideta during afternoon peak hour.

3.3.1. Fatigue life.

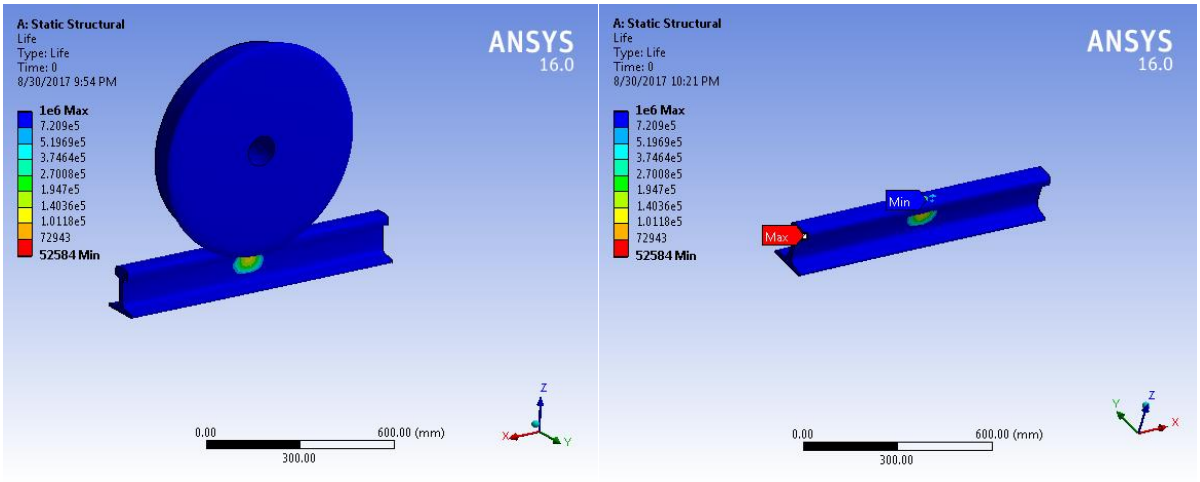

Figure 4.26: Fatigue life at saint lideta during afternoon peak hour.

As shown in the figure 4.26 above the maximum fatigue life is $1e^6$cycle and minimum fatigue life is52584cycle at saint lideta during afternoon peak hour.

3.3.2. Fatigue damage.

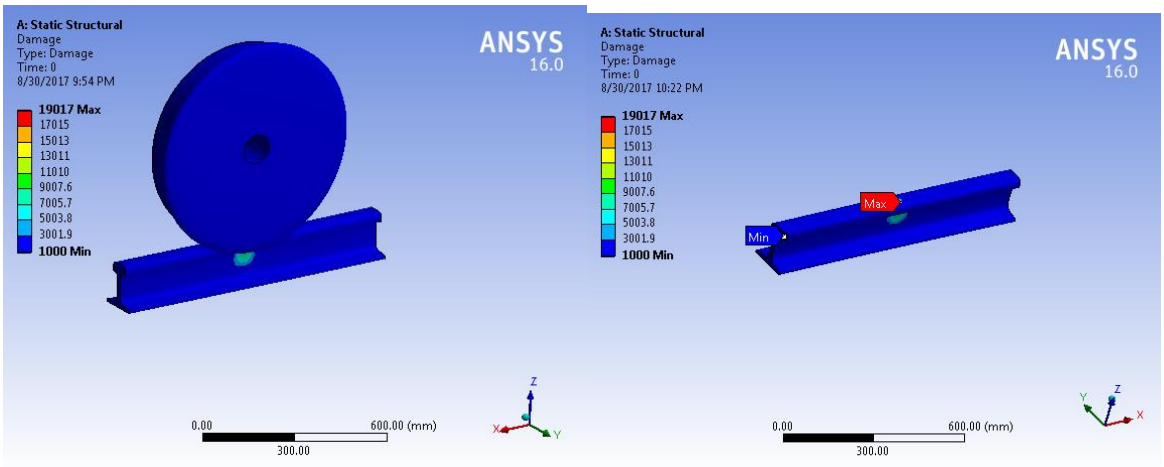

Figure 4.27: Damage at saint lideta afternoon peak hour.

As shown in the figure 4.27 above the maximum fatigue damage is 19017 and minimum fatigue damage is 1000 at saint lideta during afternoon peak hour.

3.3.3. Safety factor.

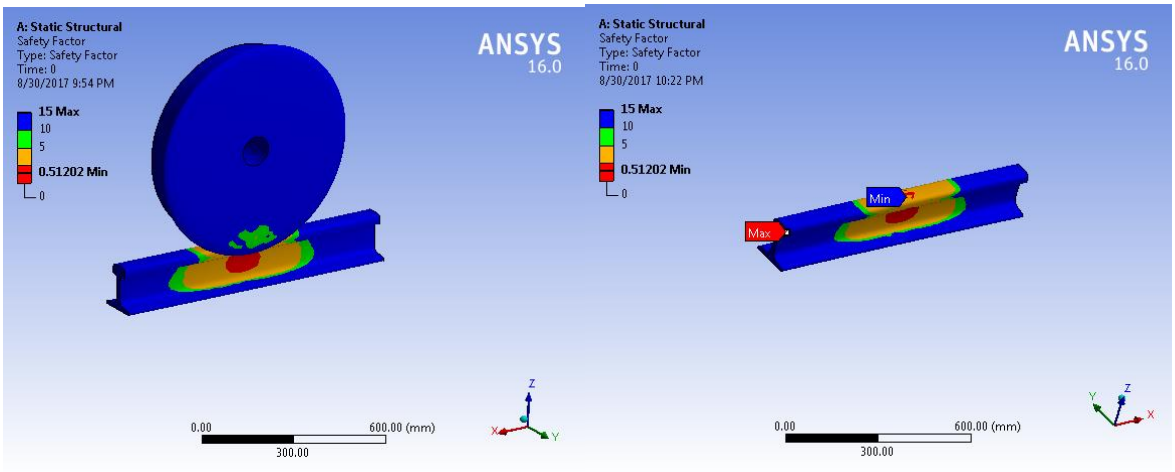

Figure 4.28: Safety factor at saint lideta during morning peak hour.

As shown in the figure 4.28 above the maximum safety factor is 15and minimum safety factor is 0.51202 at saint lideta during afternoon peak hour.

3.3.4. Equivalent alternating stress.

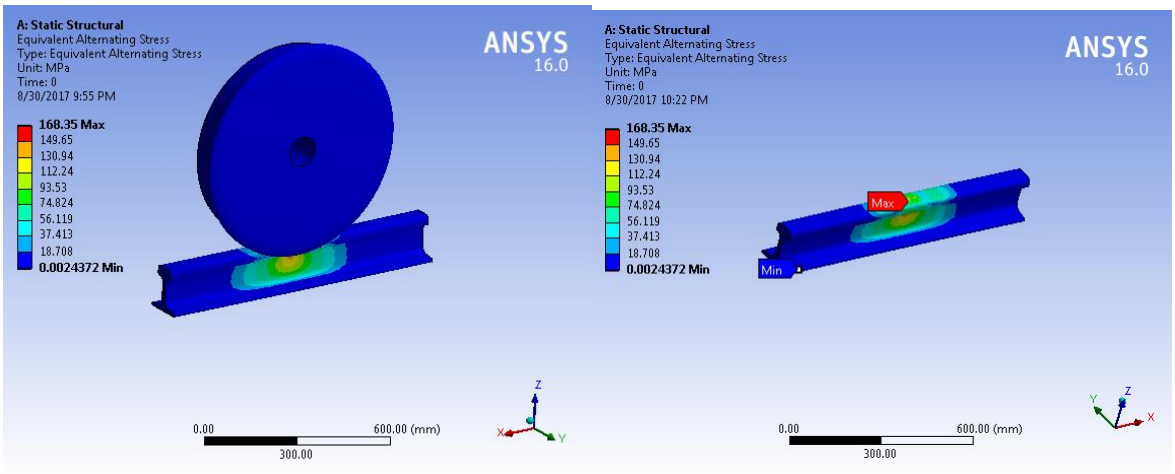

Figure 4.29: Equivalent alternating stress at saint lideta during afternoon peak hour.

As shown in the figure 4.29 above the maximum equivalent alternating stress is 168.35 MPa and minimum equivalent alternating stress is0.0024372 MPa at saint lideta during afternoon peak hour.

3.3.5. Fatigue sensitivity.

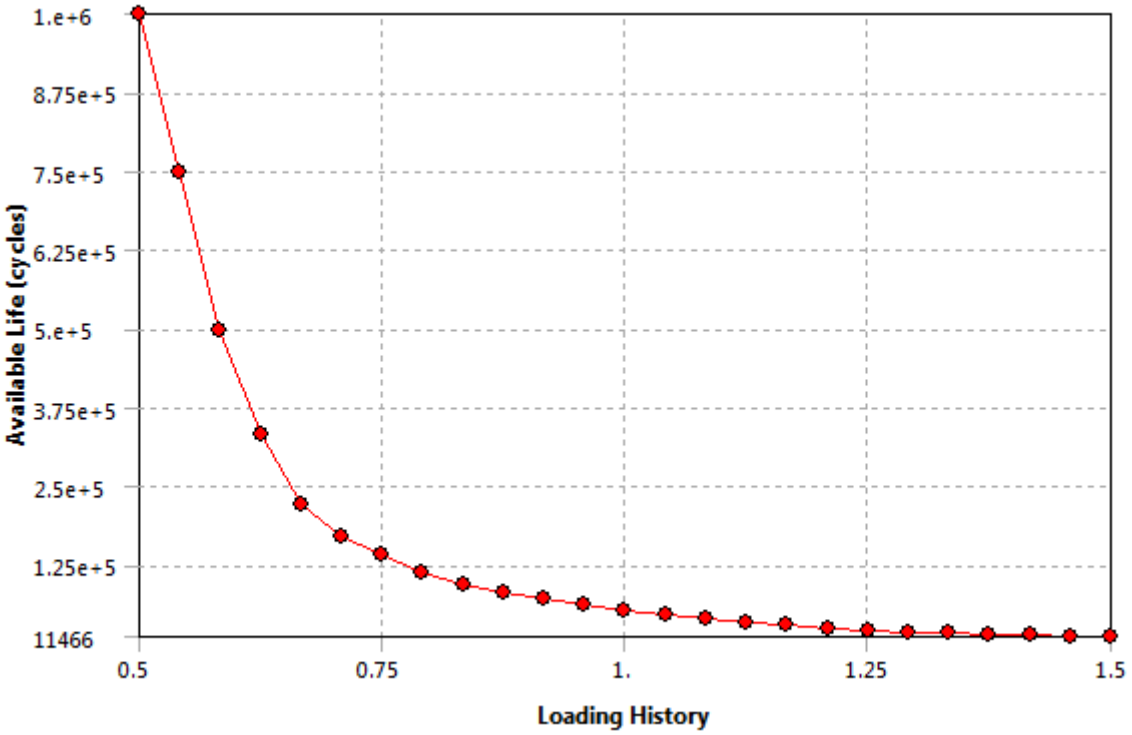

Figure 4.30: Fatigue sensitivity at saint lideta during afternoon peak hour.

As shown in the figure 4.30 above the maximum fatigue sensitivity is $1e^6$cycle and minimum fatigue sensitivity is 11466cycle at saint lideta during afternoon peak hour.

Case 3: Autobistera.

3.1. Autobistera during morning peak hour.

3.1.1. Fatigue life.

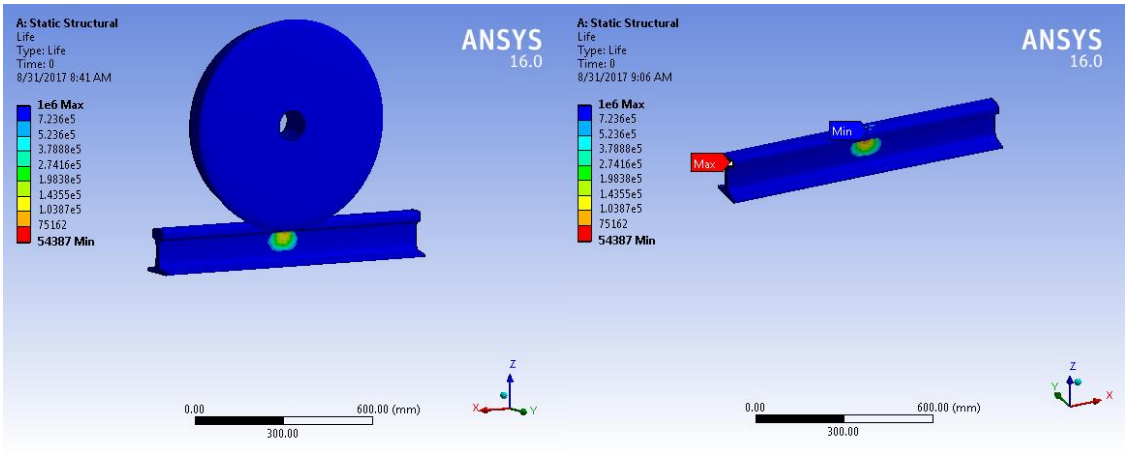

Figure 4.31: Fatigue life at autobistera during morning peak hour.

As shown in the figure 4.31 above the maximum fatigue life is $1e^6$cycle and minimum fatigue life is 54387 cycle at autobistera during morning peak hour.

3.1.2. Fatigue damage.

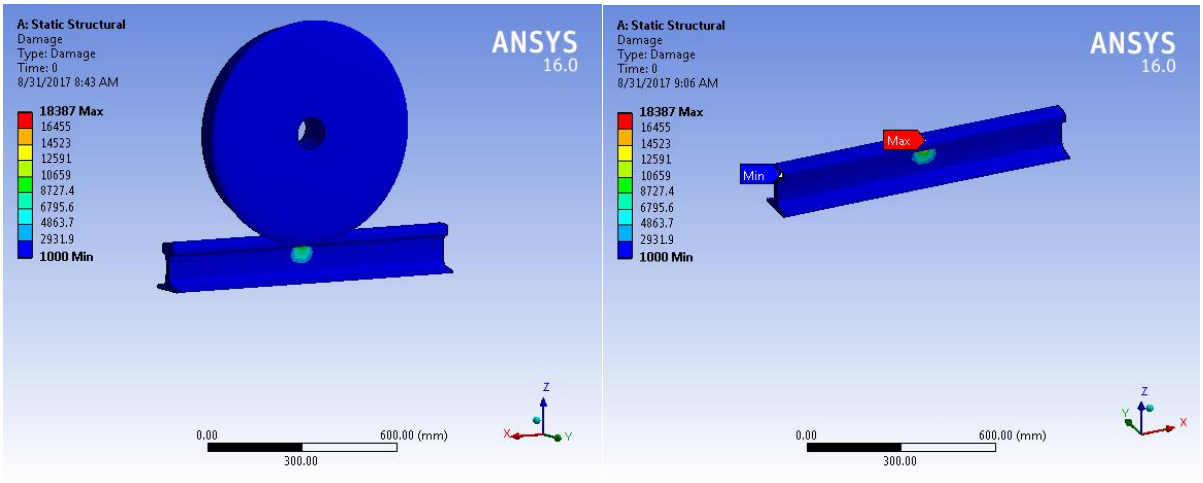

Figure 4.32: Fatigue damage at Autobistera during morning peak hour.

As shown in the figure 4.32 above the maximum fatigue damage is 18387 and minimum fatigue damage is 1000 at autobistera during morning peak hour.

3.1.3. Safety Factor.

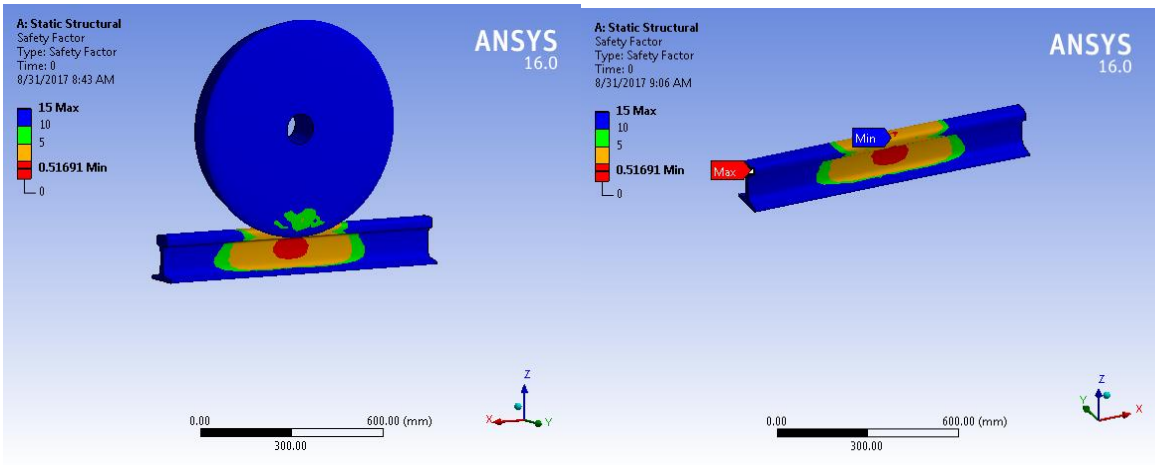

Figure 4.33: Safety factory at autobistera morning peak hour.

As shown in the figure 4.33 above the maximum fatigue safety factor is 15 and minimum fatigue safety factor is 0.51691 at autobistera during morning peak hour.

3.1.4. Equivalent Alternating Stress.

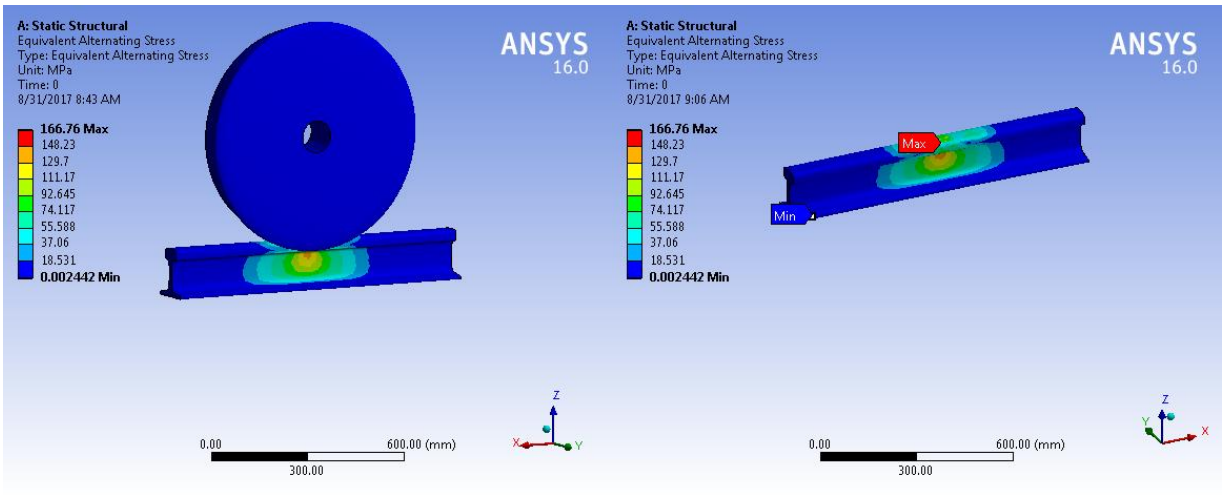

Figure 4.34: Equivalent alternating stress at autobistera during morning peak hour.

As shown in the figure 4.34 above the maximum equivalent alternating stress is 166.76 MPa and minimum equivalent alternating stress is 0.002442 MPa at autobistera during morning peak hour.

3.1.5. Fatigue Sensitivity.

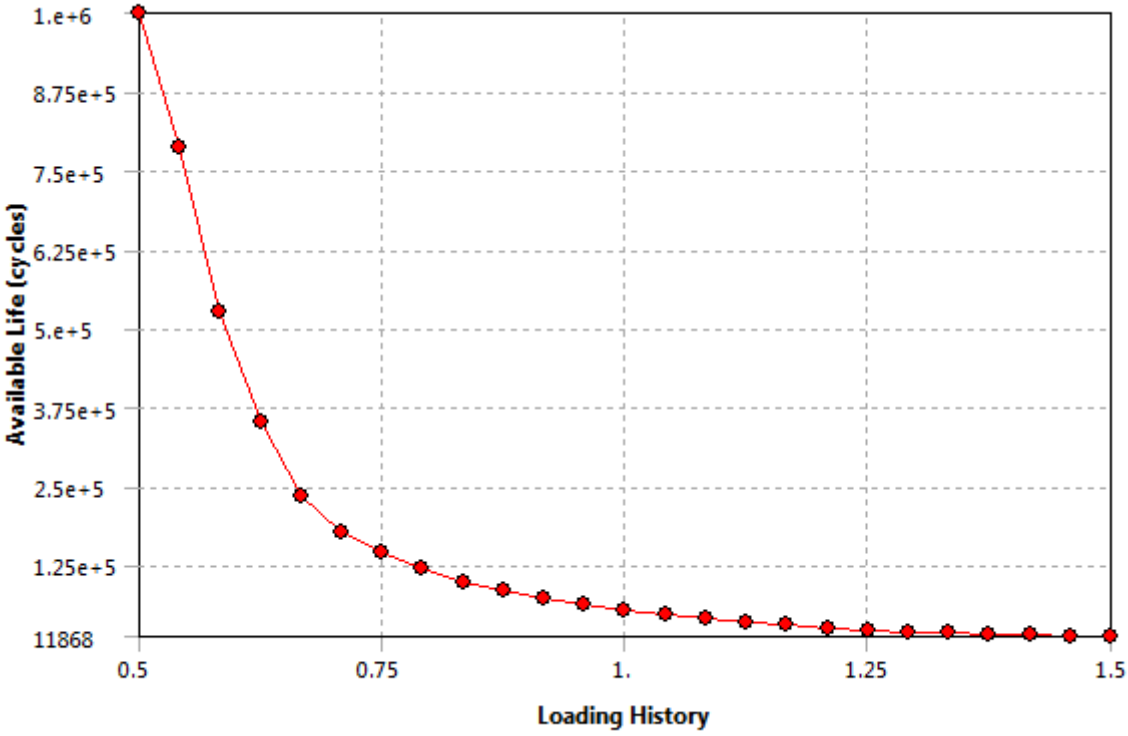

Figure 4.35: Fatigue sensitivity at autobistera during morning peak hour.

As shown in the figure 4.35 above the maximum fatigue sensitivity is $1e^6$cycle and minimum fatigue sensitivity is 11868cycle at autobistera during morning peak hour.

3.2. Autobistera during day flat hour.

3.2.1. Fatigue life.

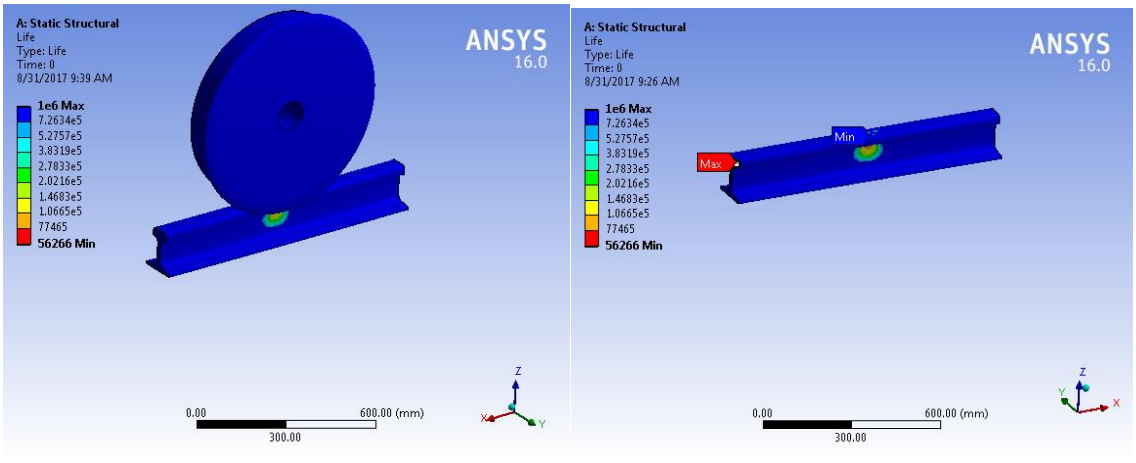

Figure 4.36: Fatigue life at autobistera during day flat hour.

As shown in the figure 4.36 above the maximum fatigue life is $1e^6$cycle and minimum fatigue life is 56266cycle at autobistera during day flat hour.

3.2.2. Fatigue damage.

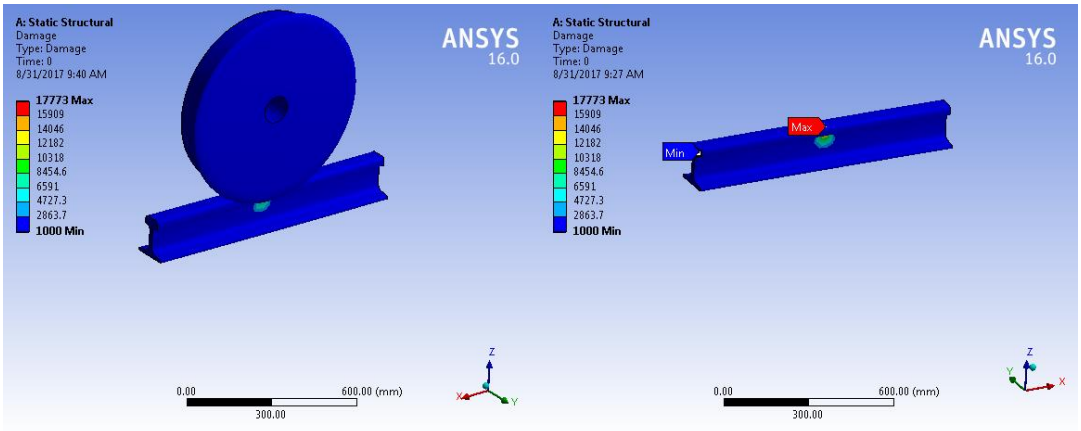

Figure 4.37: Fatigue damage at autobistera during day flat hour.

As shown in the figure 4.37 above the maximum fatigue damage is 17773 and minimum fatigue damage is1000 at autobistera during day flat hour.

3.2.3. Safety Factor.

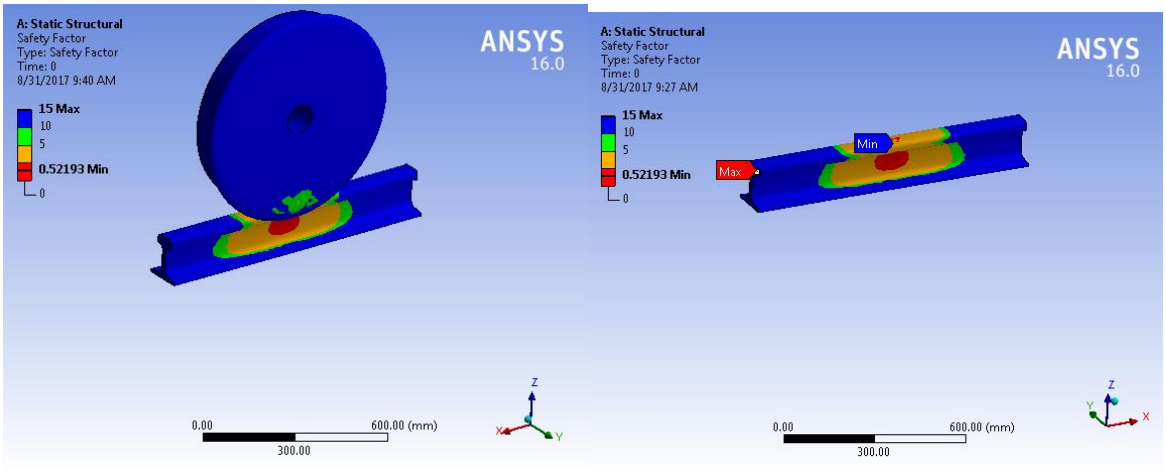

Figure 4.38: Safety factor at autobistera during day flat hour.

As shown in the figure 4.38 above the maximum fatigue safety factor is 15 and minimum fatigue safety factor is 0.52193 at autobistera during day flat hour.

3.2.4. Equivalent Alternating Stress.

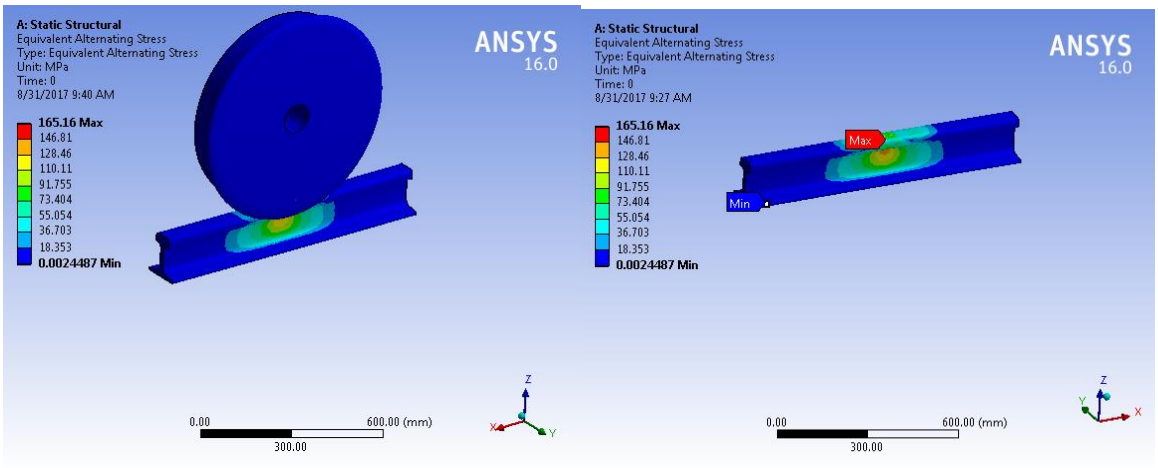

Figure 4.39: Equivalent alternating stress at autobistera during day flat hour.

As shown in the figure 4.39 above the maximum equivalent alternating stress is 165.16 MPa and minimum equivalent alternating stress is 0.0024487 MPa at autobistera during day flat hour.

3.2.5. Fatigue Sensitivity.

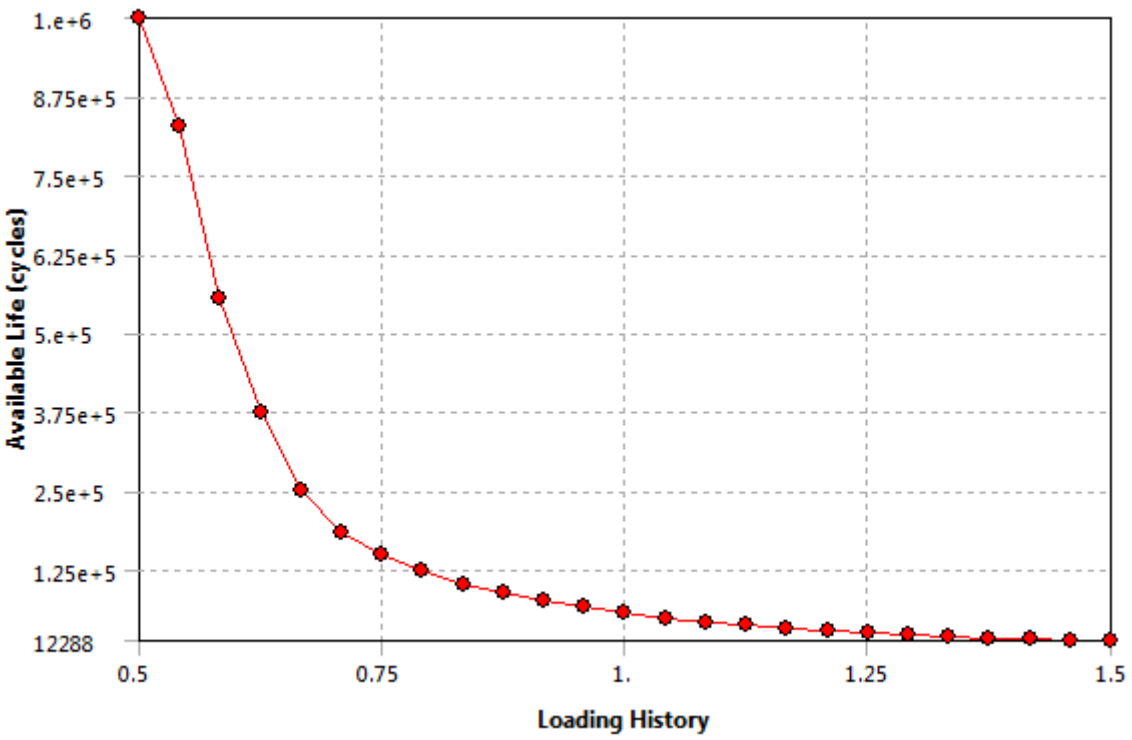

Figure 4.40: Fatigue sensitivity at autobistera during day flat hour.

As shown in the figure 4.40 above the maximum fatigue sensitivity is 1e6cycle and minimum fatigue sensitivity is 12288cycle at autobistera during day flat hour.

3.3. Autobistera during afternoon peak hour.

3.3.1. Fatigue life.

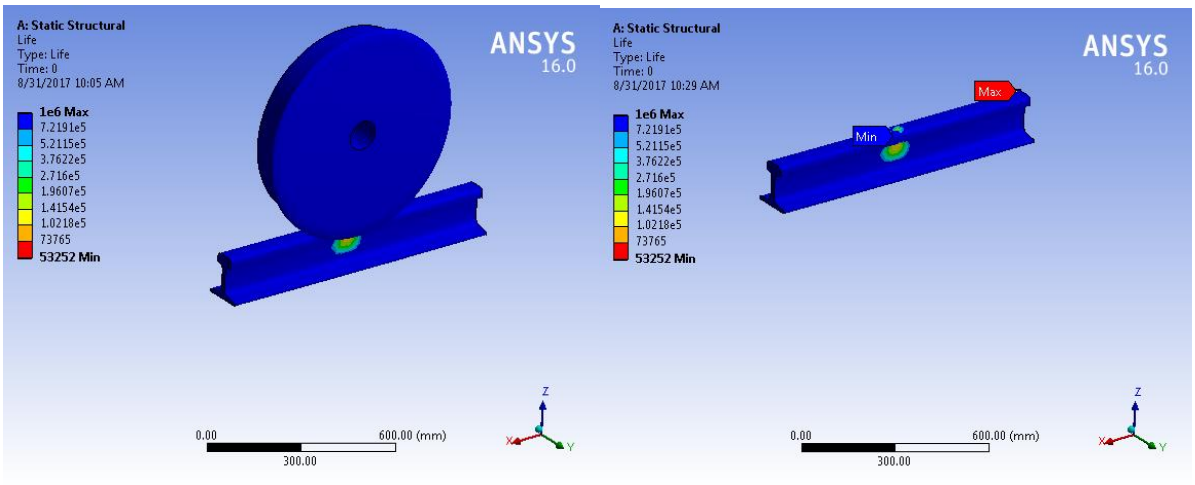

Figure 4.41: Life at autobistera during afternoon peak hour.

As shown in the figure 4.41 above the maximum fatigue life is $1e^6$cycle and minimum fatigue life is 53252cycle at autobistera during afternoon peak hour.

3.3.2. Fatigue damage.

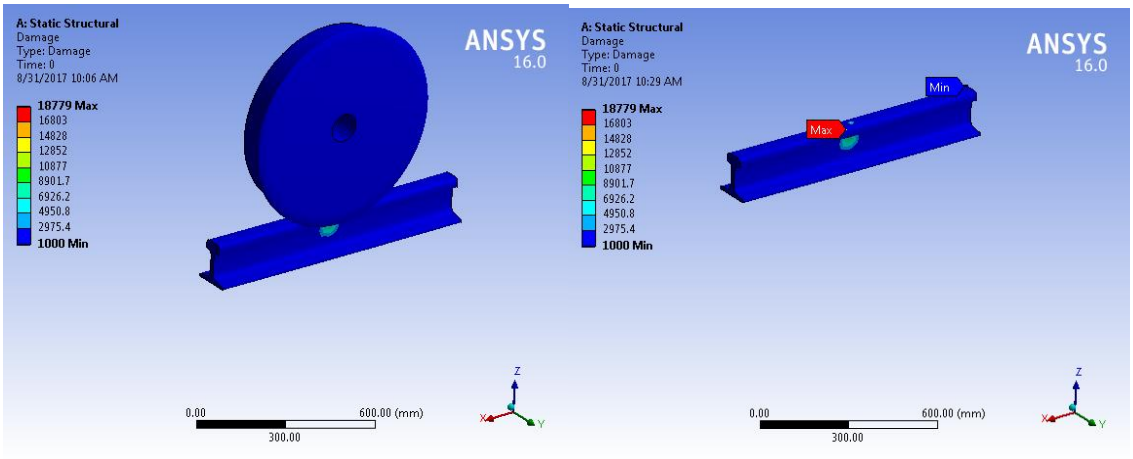

Figure 4.42: Damage at autobistera afternoon peak hour.

As shown in the figure 4.42 above the maximum fatigue damage is 18779 and minimum fatigue damage is 1000 at autobistera during afternoon peak hour.

3.3.3. Safety Factor.

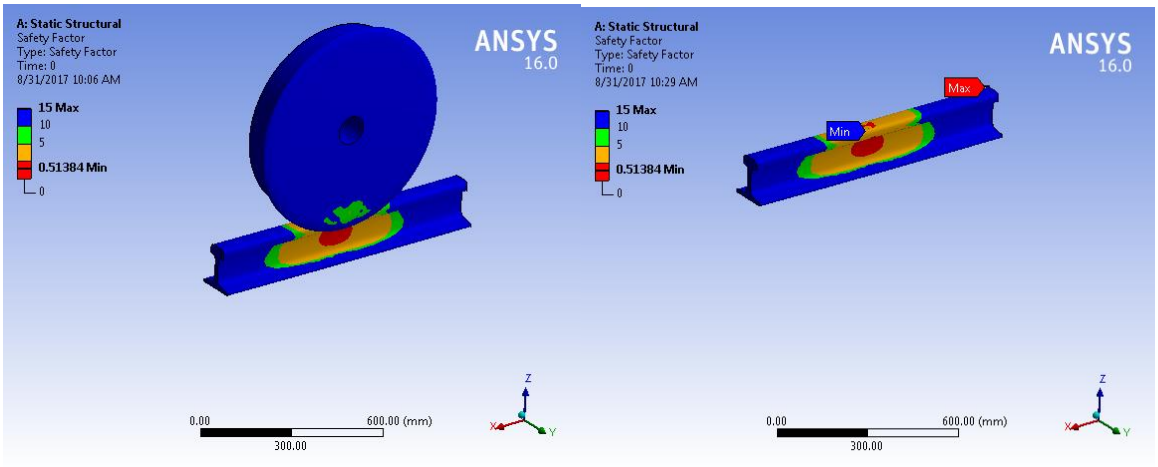

Figure 4.43: Safety factor at autobistera during afternoon peak hour.

As shown in the figure 4.43 above the maximum fatigue safety factor is 15 and minimum fatigue safety factor is 0.51384 at autobistera during afternoon peak hour.

3.3.4. Equivalent Alternating Stress.

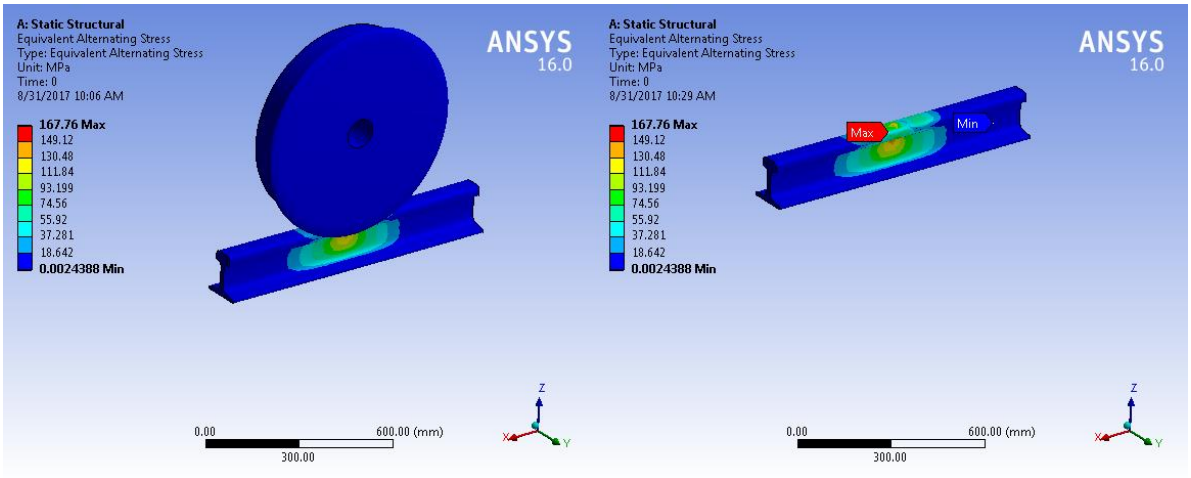

Figure 4.44: Equivalent alternating stress at autobistera during afternoon peak hour.

As shown in the figure 4.44 above the maximum equivalent alternating stress is 167.76 MPa and minimum equivalent alternating stress is 0.0024388 MPa at autobistera during afternoon peak hour.

3.3.5. Fatigue Sensitivity.

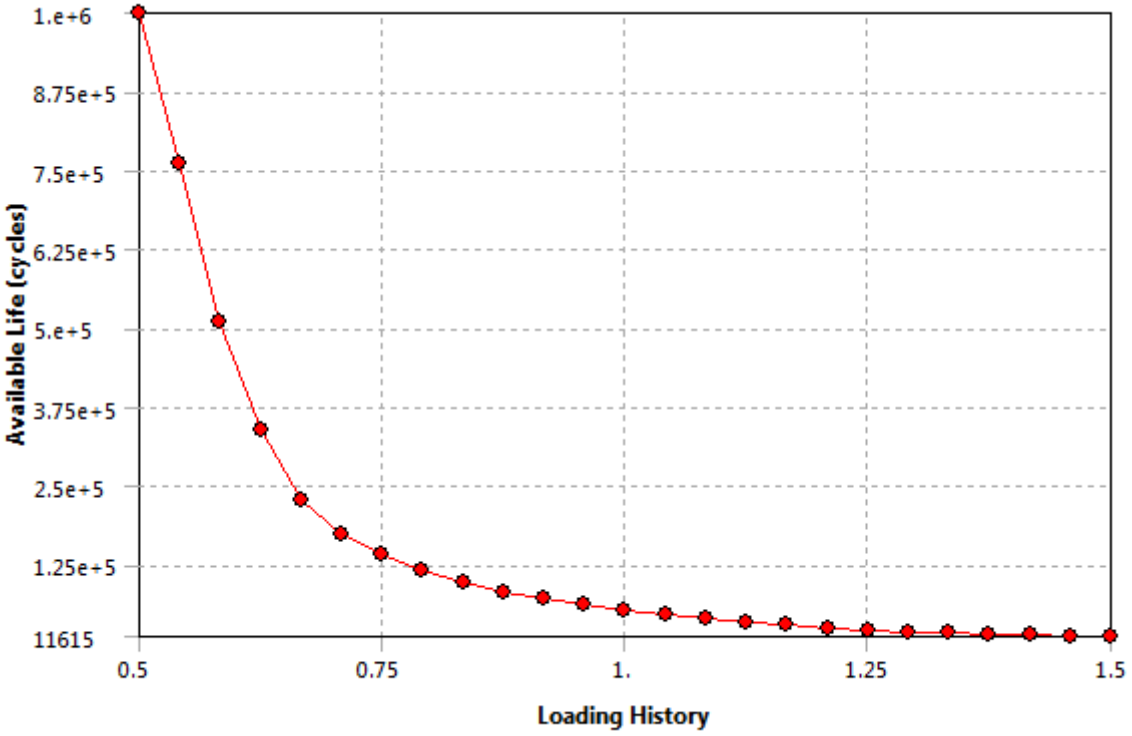

Figure 4.45: Fatigue sensitivity at autobistera during afternoon peak hour.

As shown in the figure 4.45 above the maximum fatigue sensitivity is $1e^6$cycle and minimum fatigue sensitivity is 11615cycle at autobistera during afternoon peak hour.

II. Pressure.

Case 1: Stadium.

1.1.Stadium during morning peak hour.

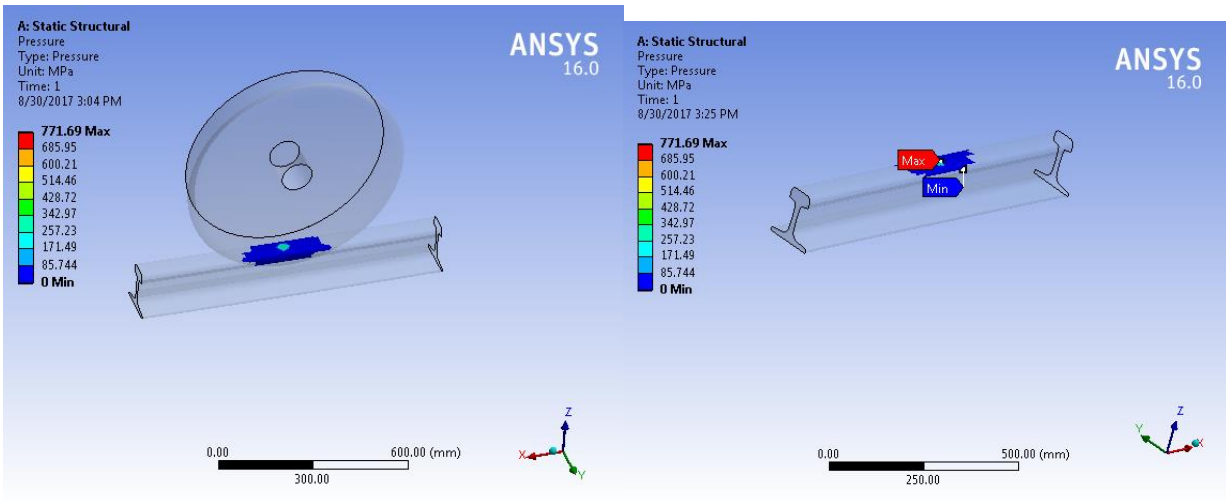

Figure 4.46: Pressure distribution at stadium during morning peak hour.

As shown in above figure 4.46 the maximum pressure is 771.69 MPa and the minimum pressure is 0MPa at stadium during morning peak hour.

1.2.Stadium day flat hour.

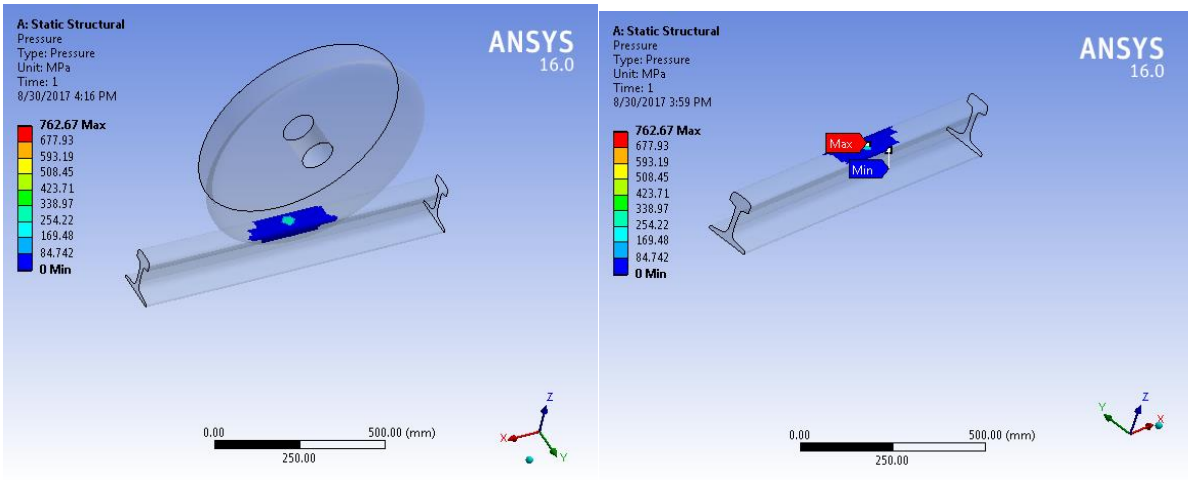

Figure 4.47: Pressure distribution at stadium during day flat hour.

As shown in above figure 4.47 the maximum pressure is 762.67 MPa and the minimum pressure is 0MPa at stadium during day flat hour.

1.3. Stadium during afternoon pick hour.

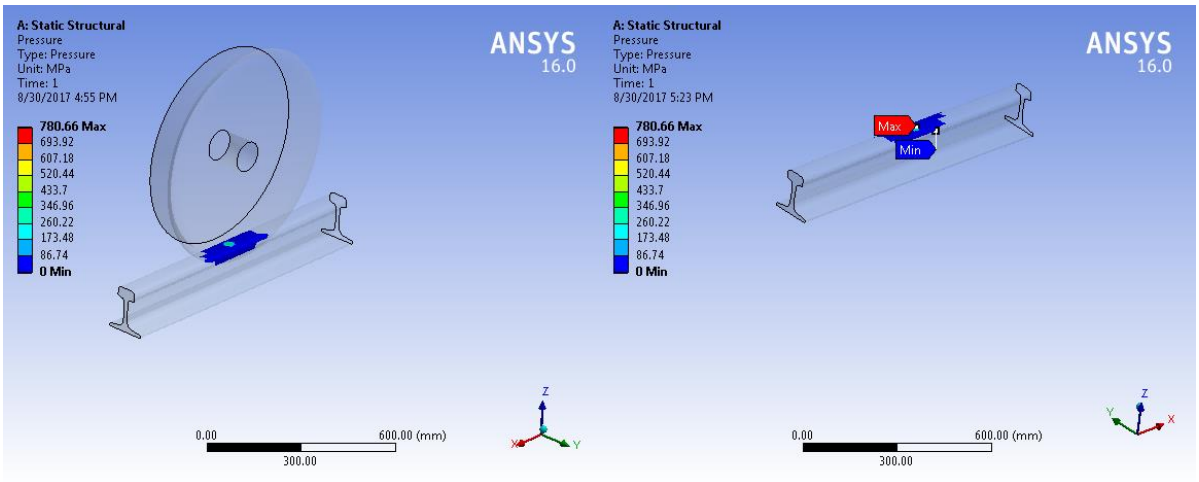

Figure 4.48: Pressure distribution at stadium during afternoon peak hour.

As shown in above figure 4.48 the maximum pressure is 780.66 MPa and the minimum pressure is 0MPaat stadium during afternoon peak hour.

Case 2: Saint Lideta.

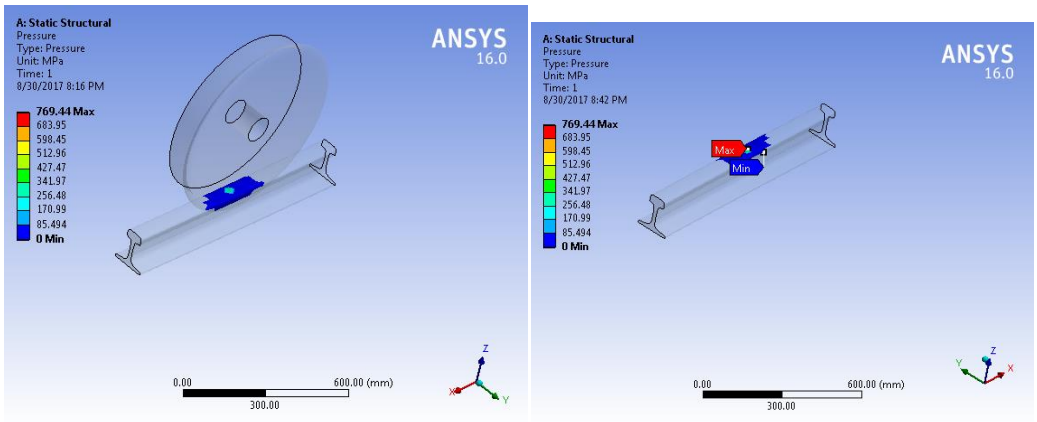

2.1. Saint Lideta during morning peak hour.

Figure 4.49: Pressure distribution saint lideta morning peak hour.

As shown in above figure 4.49 the maximum pressure is769.44MPa and the minimum pressure is 0MPa at saint lideta during morning peak hour.

2.2. Saint Lideta during day flat hour.

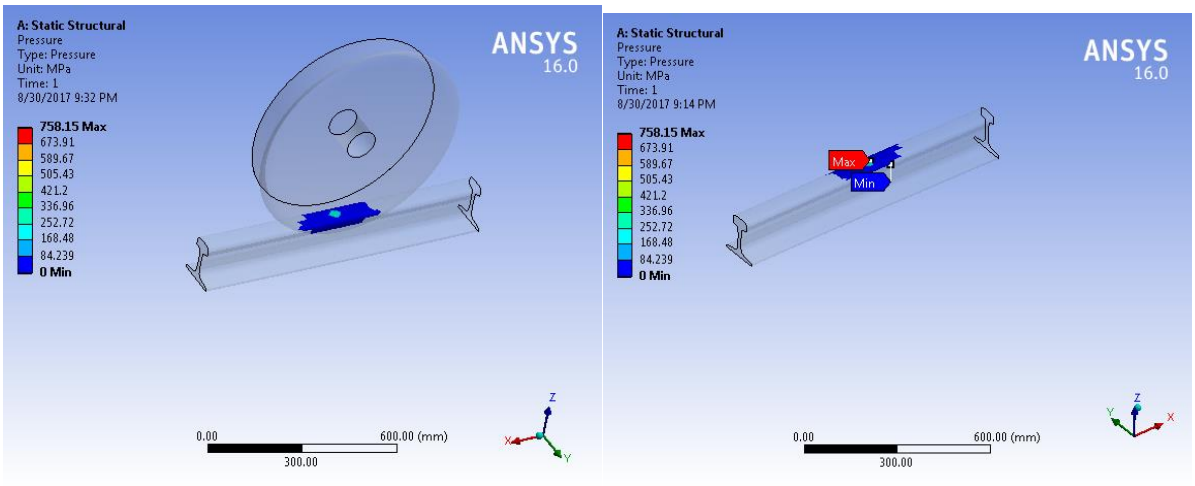

Figure 4.50: Pressure distribution at saint lideta during day flat hour.

As shown in above figure 4.50 the maximum pressure is 758.15 MPa and the minimum pressure is 0MPa at saint lideta during day flat hour.

2.3. Saint Lideta afternoon peak hour.

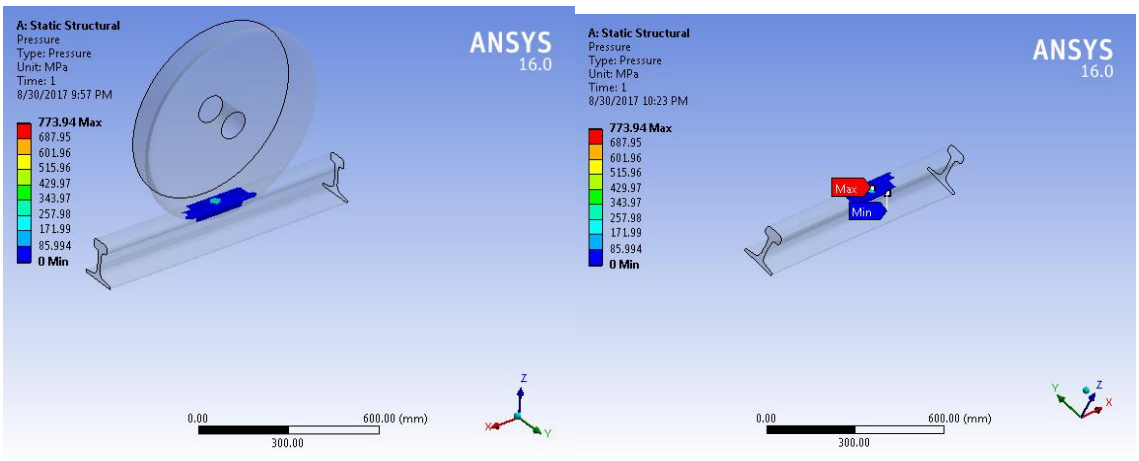

Figure 4.51: Pressure distribution at saint lideta during afternoon peak hour.

As shown in above figure 4.51 the maximum pressure is 773.94MPa and the minimum pressure is 0MPa at saint lideta during afternoon peak hour.

Case 3: Autobistera.

2.1. Autobistera during morning peak hour.

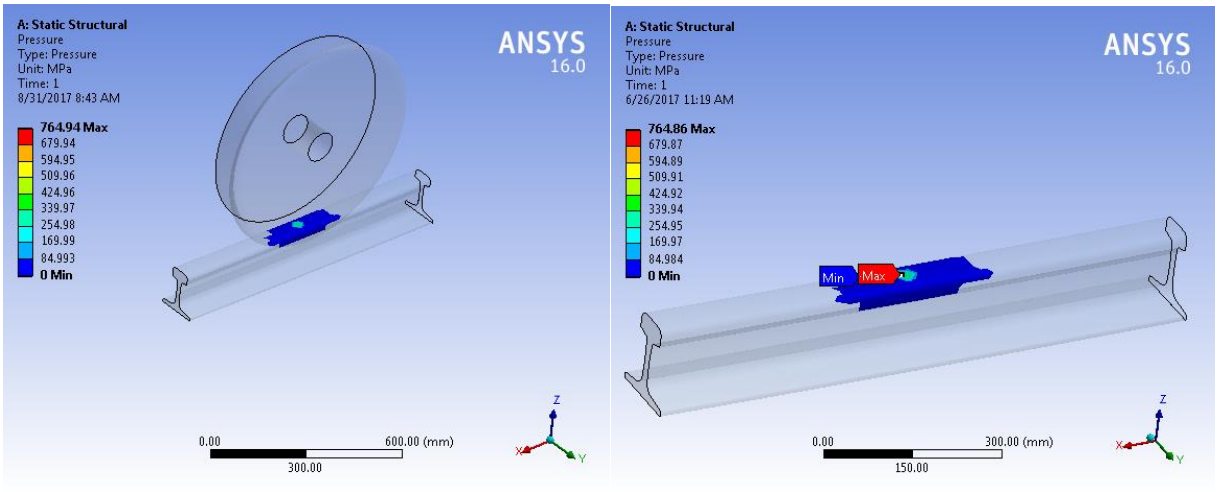

Figure 4.52: Pressure distribution at autobistera during morning peak hour.

As shown in above figure 4.52 the maximum pressure is 764.94MPa and the minimum pressure is 0MPa at autobistera during morning peak hour.

2.2. Autobistera day flat hour.

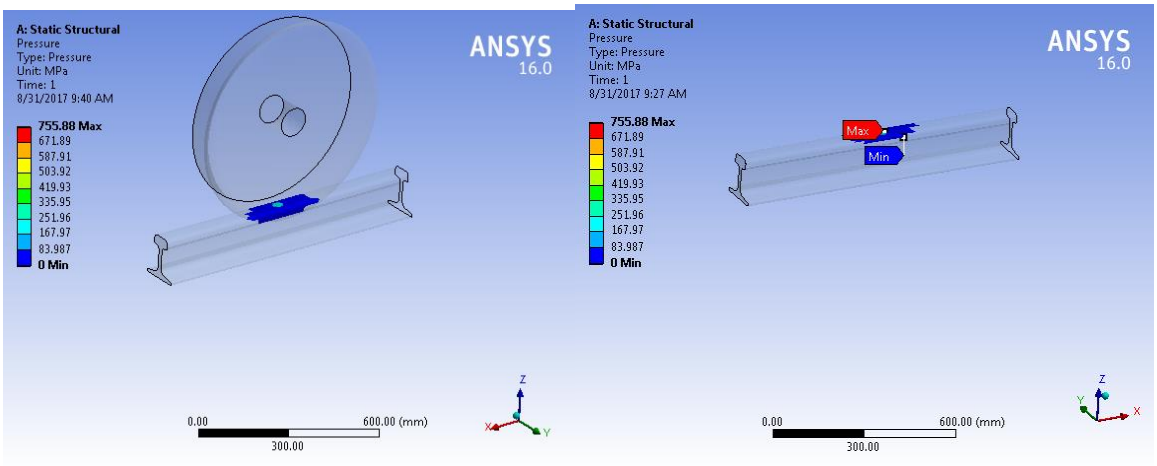

Figure 4.53: Pressure distribution at autobistera during day flat hour.

As shown in above figure 4.53 the maximum pressure is 755.88 MPa and the minimum pressure is 0MPa at autobistera during day flat hour.

3.3. Autobistera afternoon peak hour.

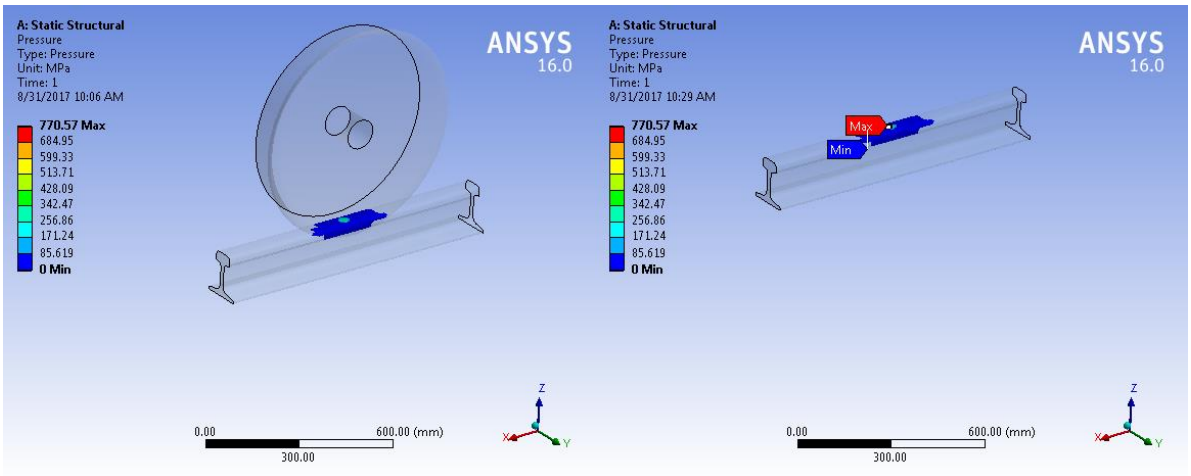

Figure 4.54: Pressure distribution at autobistera during afternoon peak hour.

As shown in above figure 4.54 the maximum pressure is 770.57MPa and the minimum pressure is 0MPa at autobistera during afternoon pick hour.

The analysis is done for minimum curved rail of AALRT reduced the first five millimeter radius from the top of the rail due wear.

1.1. Stadium during morning peak hour for worn rail.

1.1.1. Fatigue Life.

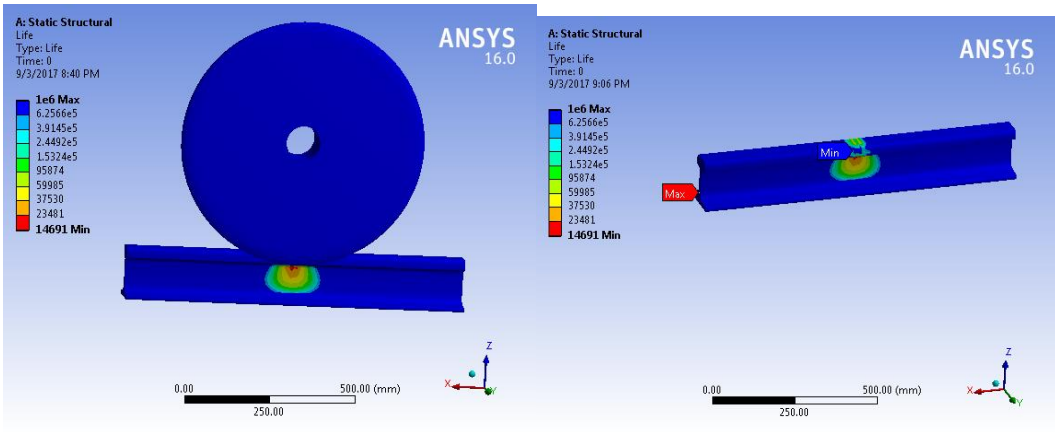

Figure 4.55: Fatigue life at stadium during morning peak hour for worn rail.

As shown in above figure 4.55 the maximum fatigue life is $1e^6$cycles and the minimum fatigue life is 14691 cycles at stadium during morning peak hour.

1.1.2. Fatigue Damage

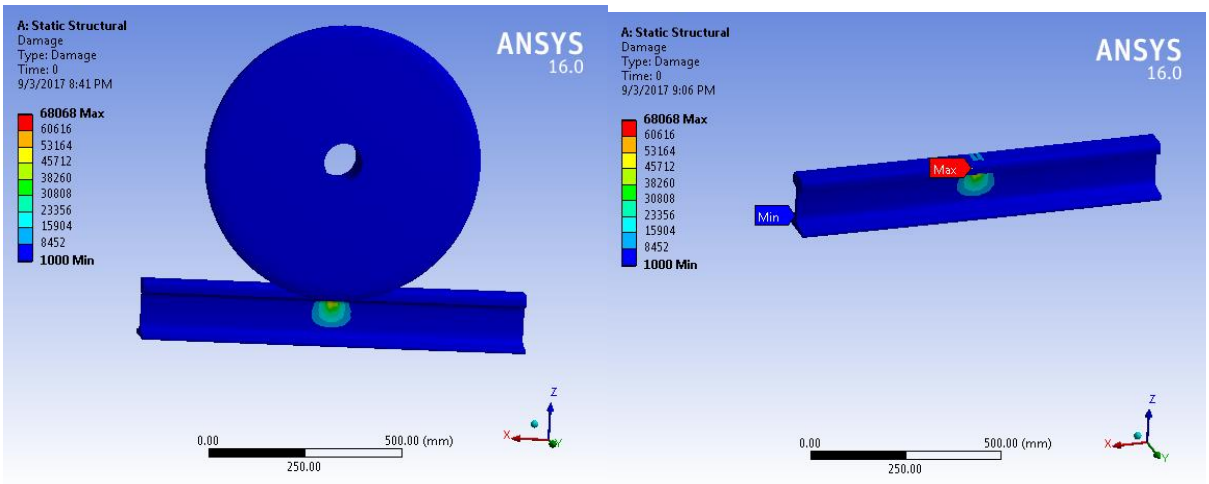

Figure 4.56: Damage at stadium during morning peak hour for worn rail.

As shown in the figure 4.56 above the maximum fatigue damage is 68068 and minimum fatigue damage is 1000 at stadium during morning peak hour.

1.1.3. Fatigue Safety factor.

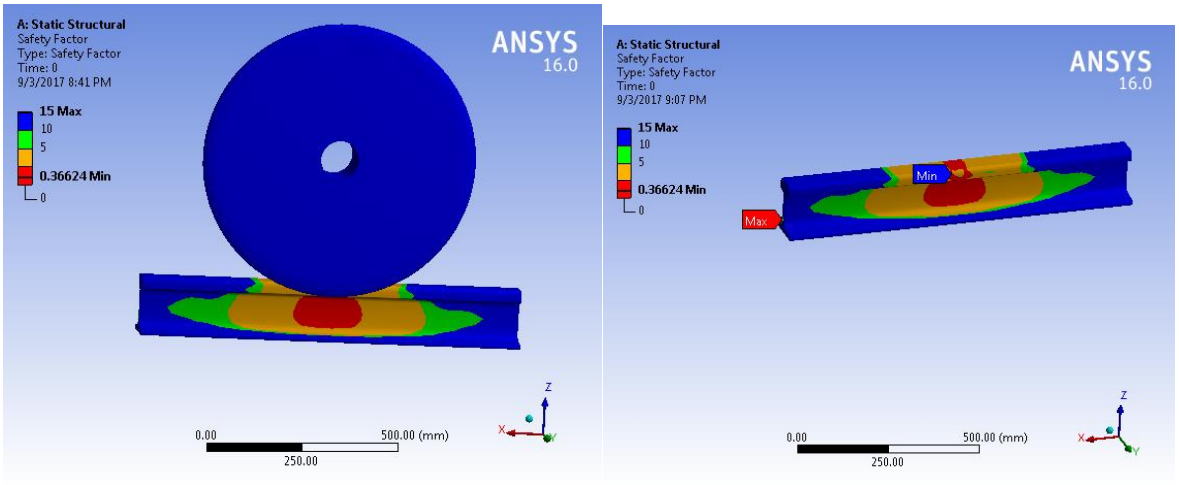

Figure 4.57: Safety factor at stadium morning peak hour for worn rail.

As shown in the figure 4.57 above the maximum fatigue safety factor is 15 and minimum fatigue safety factor is 0.36624 at stadium during morning peak hour.

1.1.4. Equivalent alternating stress.

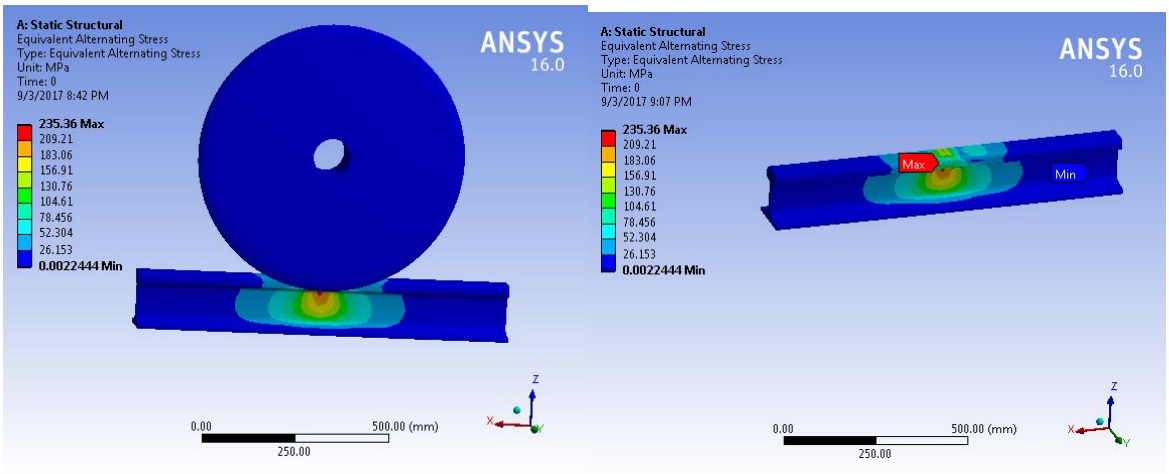

Figure 4.58: Equivalent alternating stress at stadium during morning peak hour for worn rail.

As shown in the figure4.58 above the maximum equivalent alternating stress is 235.36 MPa and minimum equivalent alternating stress is 0.002444 MPa at stadium during morning peak hour.

1.1.5. Fatigue sensitivity

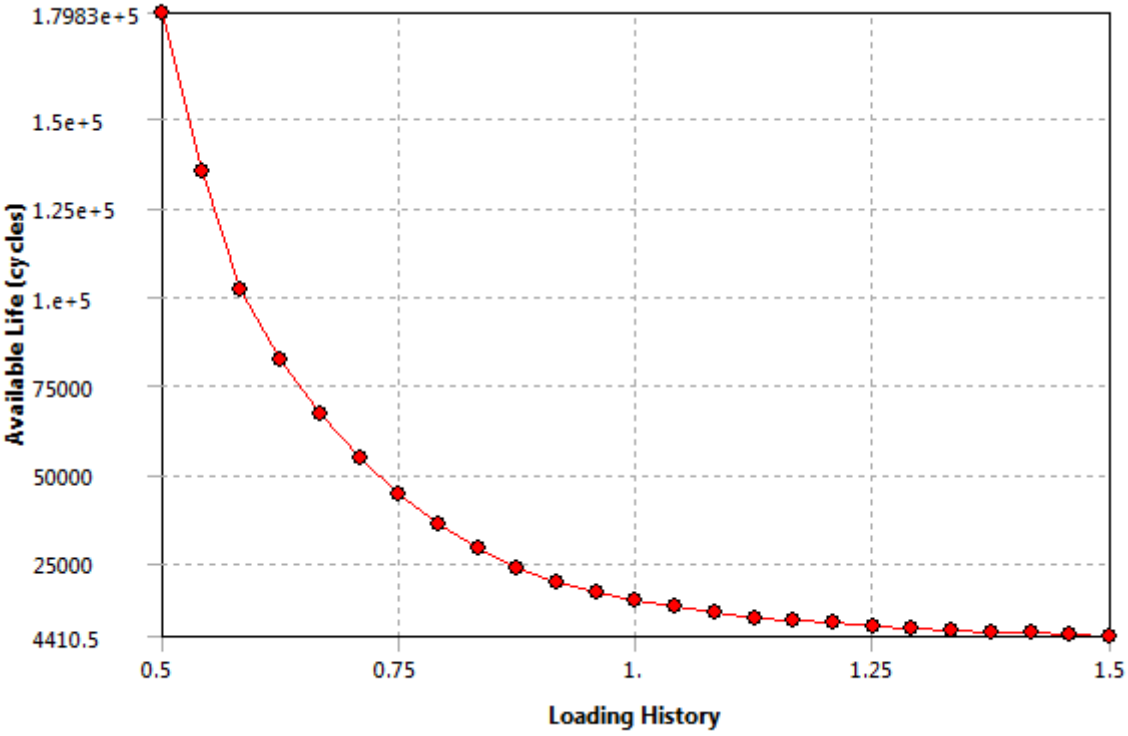

Figure 4.59: Fatigue sensitivity at stadium during morning peak hour for worn rail.

As shown in the figure4.59 above the maximum fatigue sensitivity is $1.7983e^5$ cycles and minimum fatigue sensitivity is 4410.5 cycles at stadium during morning peak hour.

1.2. Stadium during day flat hour for worn rail.

1.2.1. Fatigue life.

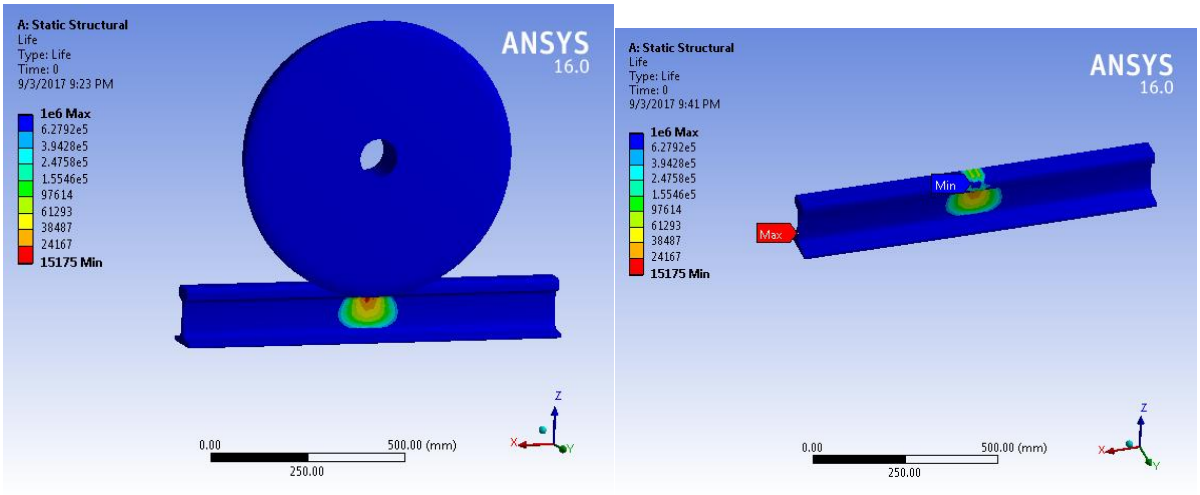

Figure 4.60: Fatigue life at stadium during day flat hour for worn rail.

As shown in the figure4.60 above the maximum fatigue life is $1e^6$cycle and minimum fatigue life is 15175 cycle at stadium during day flat hour.

1.2.2. Fatigue Damage.

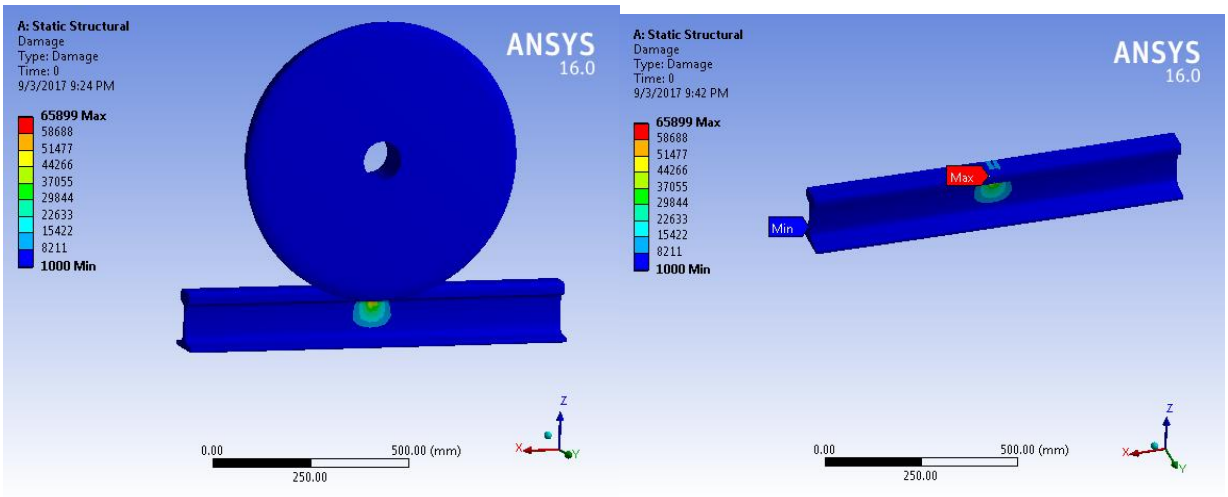

Figure 4.61: Fatigue damage at stadium day flat hour for worn rail.

As shown in the figure4.61 above the maximum fatigue damage is65899 and minimum fatigue damage is 1000 at stadium during day flat hour.

1.2.3. Fatigue Safety factor.

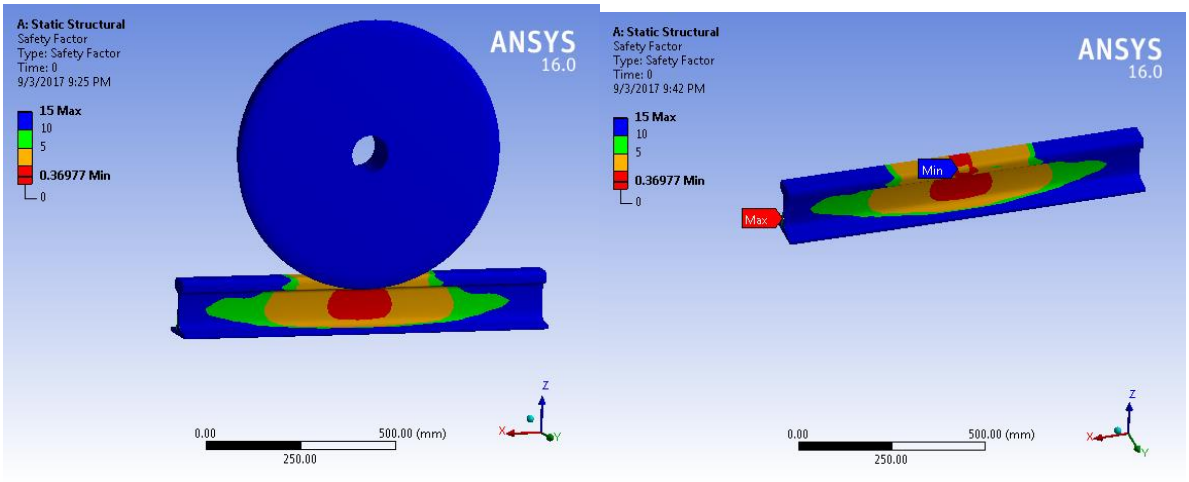

Figure 4.62: Safety factor at stadium during day flat hour for worn rail.

As shown in the figure4.62 above the maximum fatigue safety factor is 15 and minimum fatigue safety factor is 0.36977 at stadium during day flat hour.

1.2.4. Equivalent alternating stress.

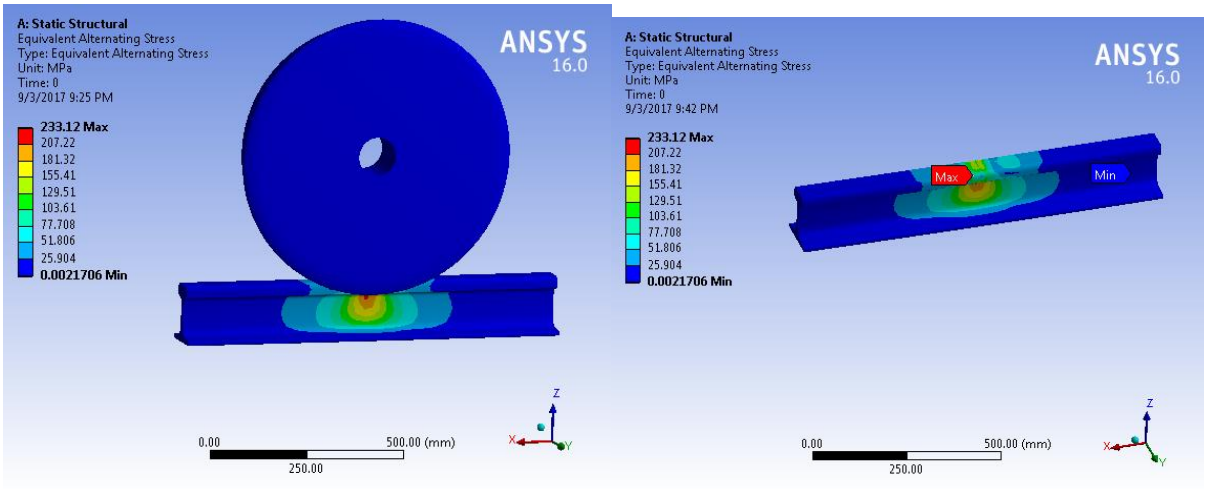

Figure 4.63: Equivalent alternating stress at stadium day flat hour for worn rail.

As shown in the figure4.63 above the maximum equivalent alternating stress is 233.12 MPa and minimum equivalent alternating stress is 0.0021706 MPa at stadium during day flat hour.

1.2.5. Fatigue sensitivity.

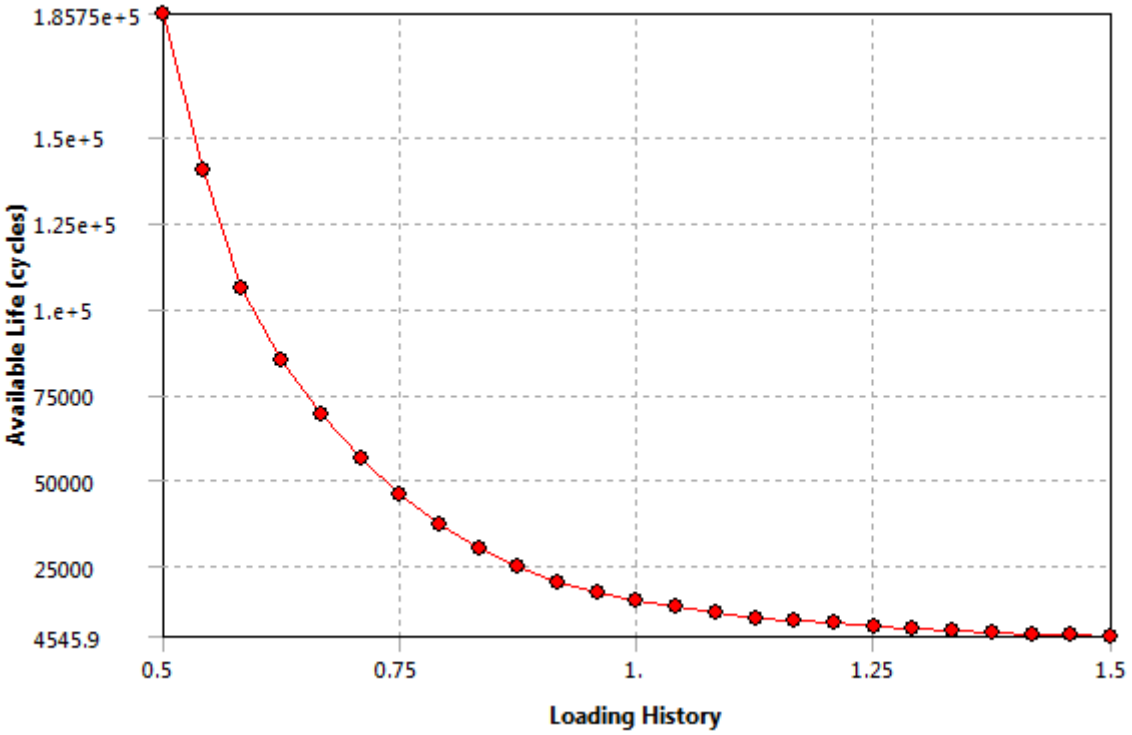

Figure 4.64: Fatigue sensitivity at stadium day flat hour for worn rail.

As shown in the figure4.64 above the maximum fatigue sensitivity is$1.8575e^5$ cycleand minimum fatigue sensitivity is 4545.9 at stadium during day flat hour.

1.3. Stadium during afternoon peak hour for worn rail

1.3.1. Fatigue life

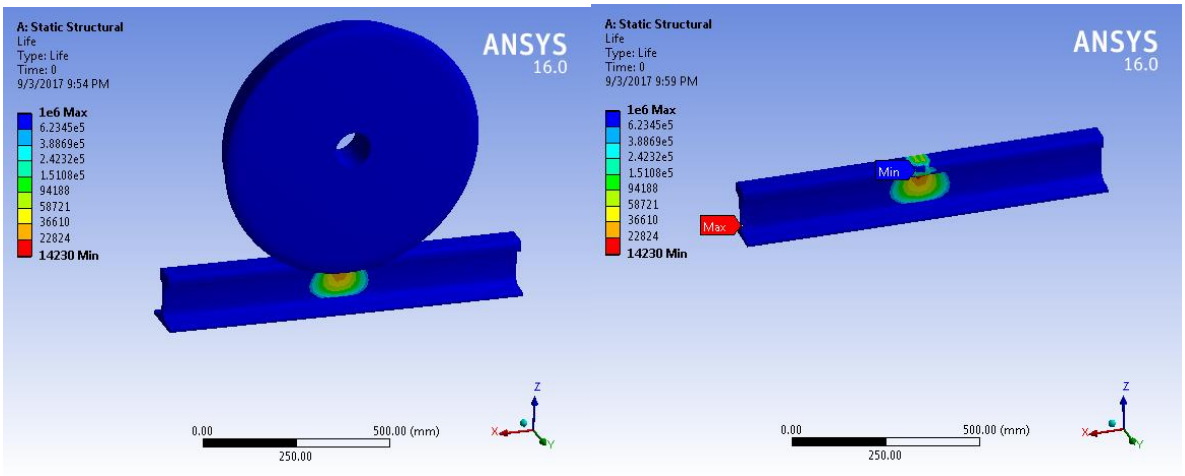

Figure 4.65: Fatigue life at stadium during afternoon peak hour for worn rail.

As shown in the figure 4.65 above the maximum fatigue life is $1e^6$cycle and minimum fatigue life is 14230 cycle at stadium during afternoon peak hour.

1.3.2. Fatigue damage.

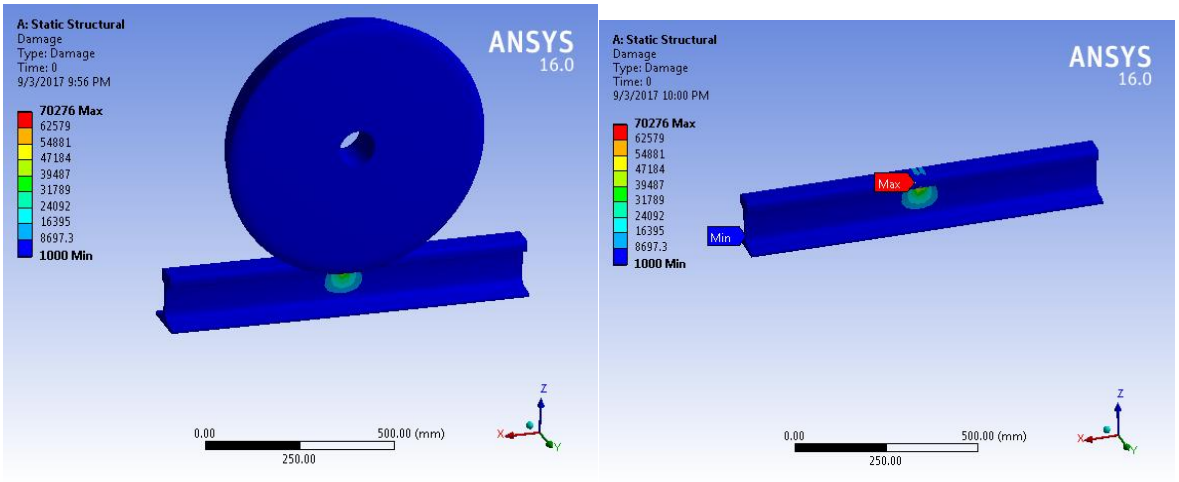

Figure 4.66: Damage at stadium during afternoon peak hour for worn rail.

As shown in the figure4.66 above the maximum fatigue damage is 70276and minimum fatigue damage is 1000 at stadium during afternoon peak hour.

1.3.3. Fatigue safety factor

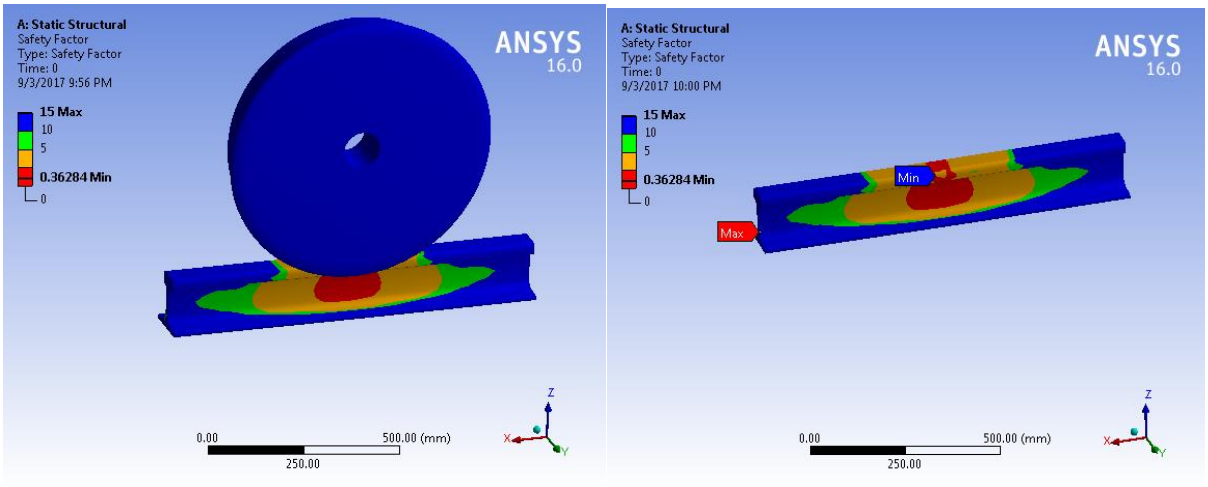

Figure 4.67: Fatigue safety factor at stadium afternoon peak hour for worn rail.

As shown in the figure4.67 above the maximum fatigue safety factor is 15and minimum fatigue safety factor is 0.36284 at stadium during afternoon peak hour.

1.3.4. Equivalent alternating stress.

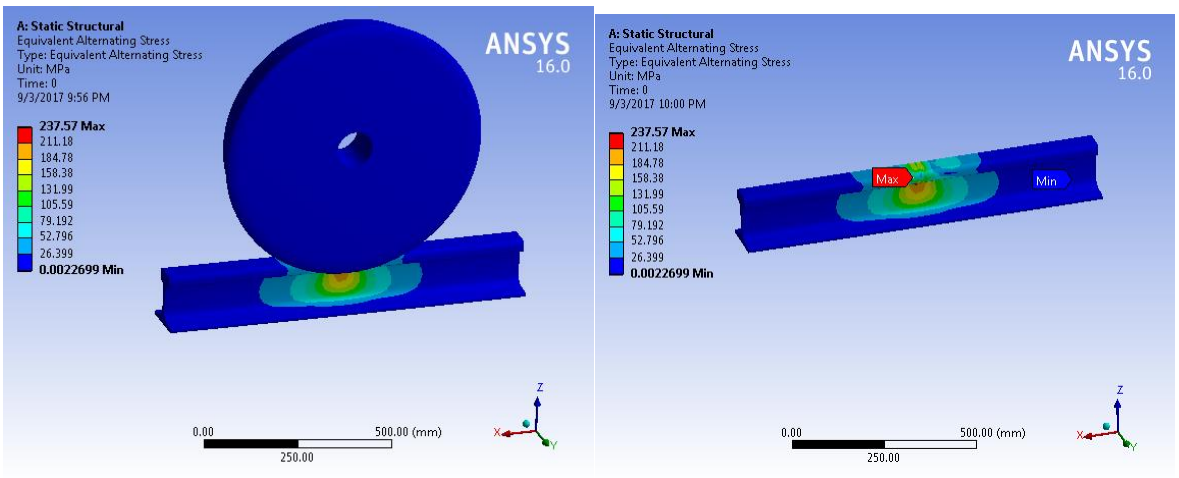

Figure 4.68: Equivalent alternating stress. at stadium afternoon peak hour for worn rail.

As shown in the figure4.68 above the maximum equivalent alternating stress is 237.57 MPa and minimum equivalent alternating stress is 0.0022699 MPa at stadium during afternoon peak hour.

1.3.5. Fatigue sensitivity.

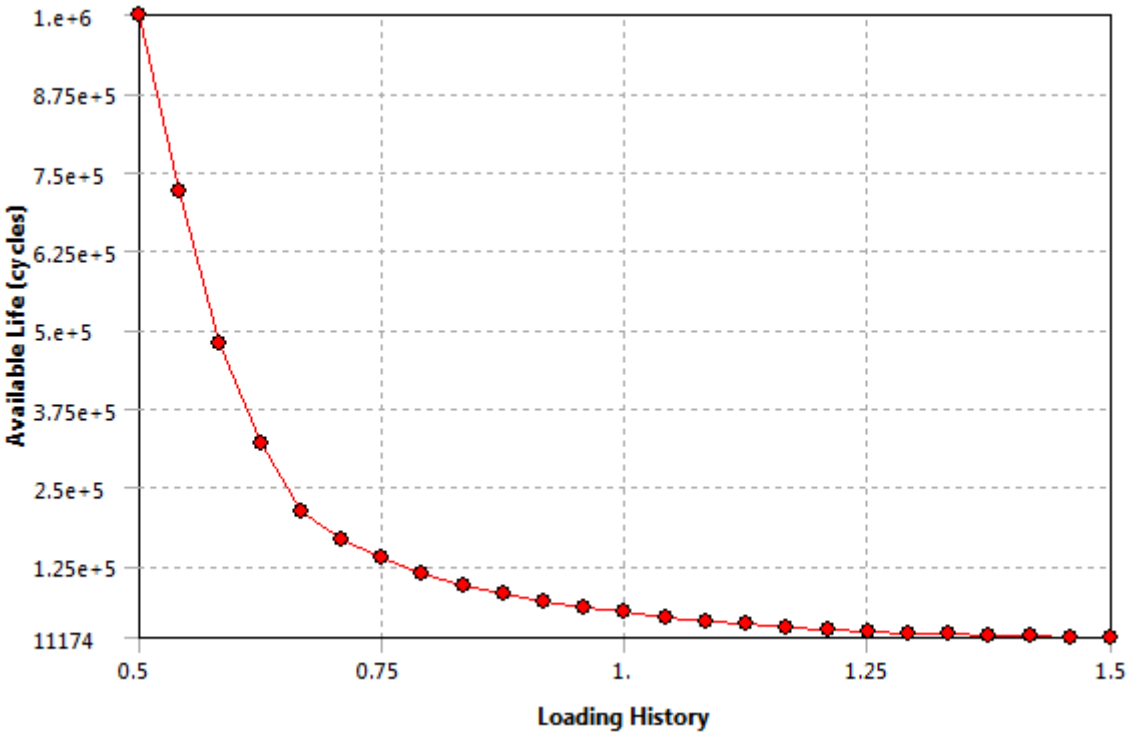

Figure 4.69: Fatigue sensitivity at stadium during afternoon peak hour for worn rail.

As shown in the figure4.69 above the maximum fatigue sensitivity is $1e^5$ cycles and minimum fatigue sensitivity is 11174 cycles at stadium during afternoon peak hour.

Case 2: Saint Lideta.

2.1. Saint Lideta during morning peak hour for worn rail.

2.1.1. Fatigue life.

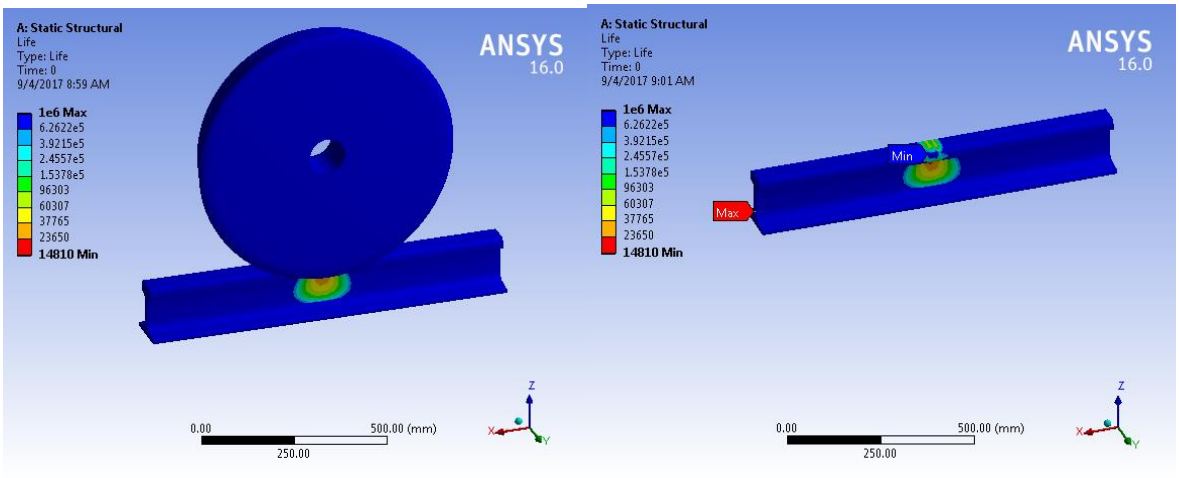

Figure 4.70: Fatigue life at saint lideta during morning peak hour for worn rail.

As shown in the figure4.70above the maximum fatigue life is $1e^6$cycle and minimum fatigue life is 14810 cycle at saint lideta during morning peak hour.

2.1.2. Fatigue damage

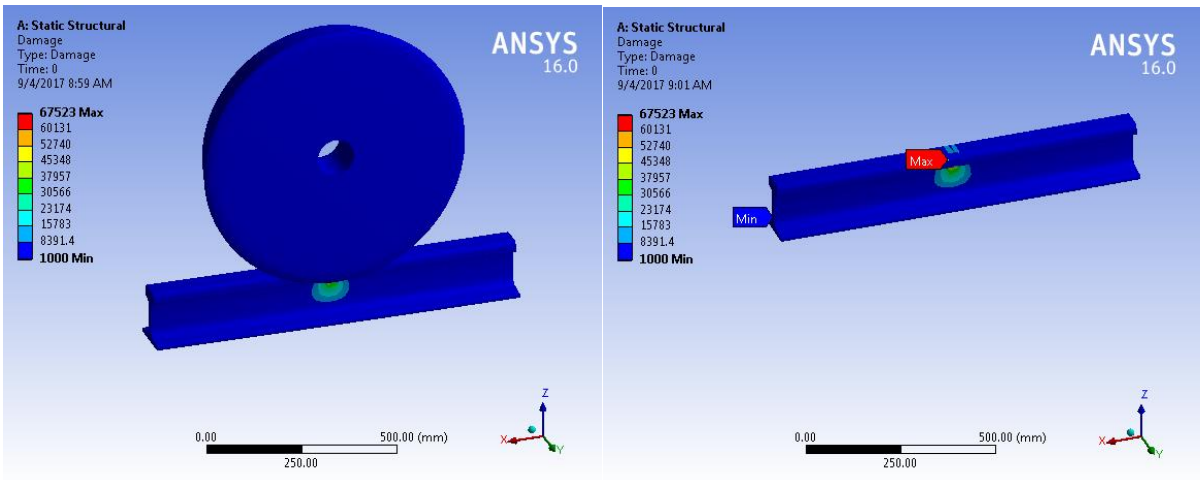

Figure 4.71: Damage at saint lideta morning peak hour for worn rail.

As shown in the figure4.71 above the maximum fatigue damage is 67523and minimum fatigue damage is 1000 at saint lideta during morning peak hour.

2.1.3. Safety factor.

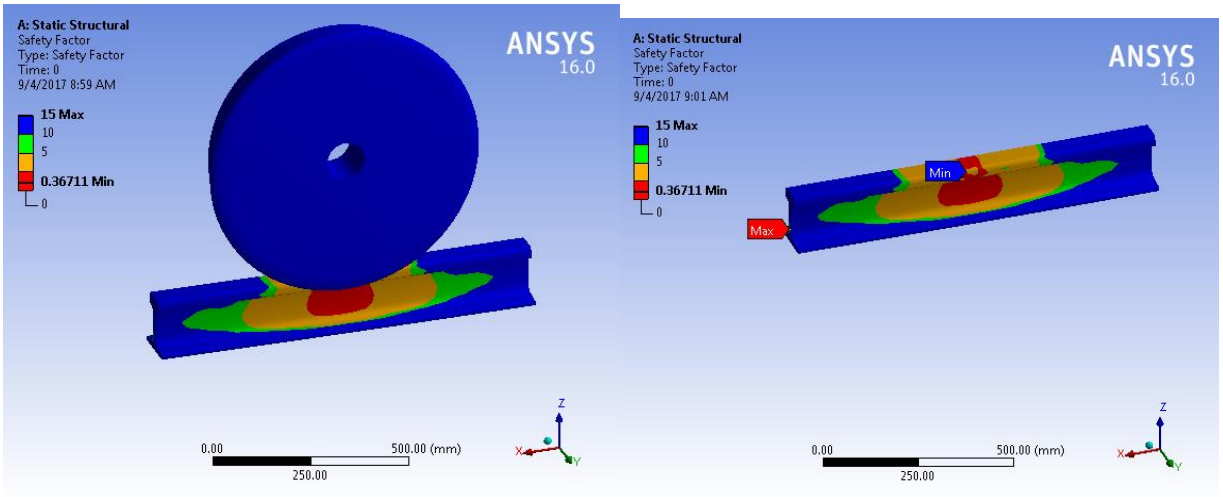

Figure 4.72: Safety factor at saint lideta morning peak hour for worn rail.

As shown in the figure4.72 above the maximum fatigue safety factor is 15and minimum fatigue safety factor is 0.36711at saint lideta during morning peak hour.

2.1.4. Equivalent alternating stress.

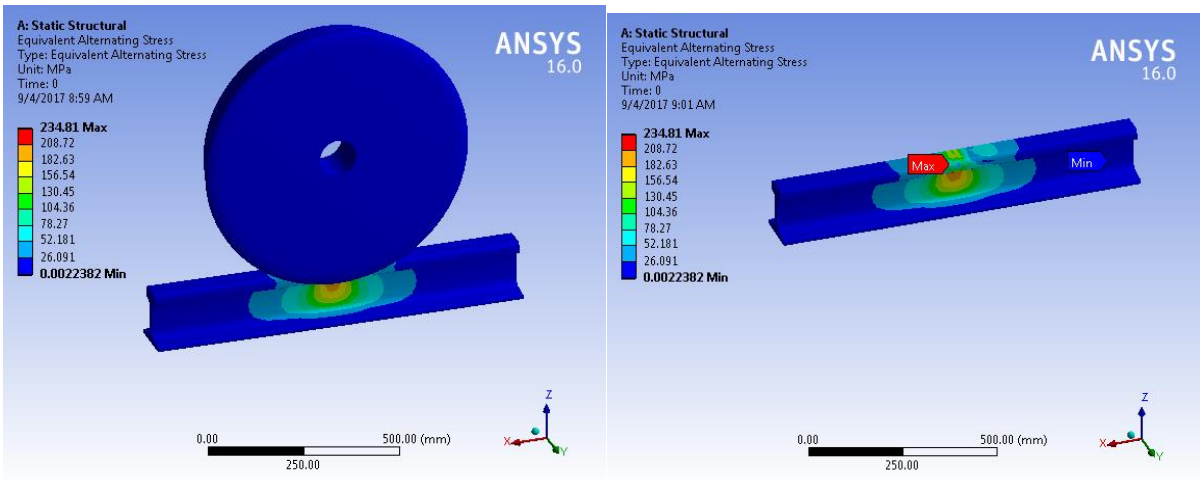

Figure 4.73: Equivalent alternating stress at saint lideta during morning peak hour for worn rail.

As shown in the figure4.73above the maximum equivalent alternating stress is 234.81 MPa and minimum equivalent alternating stress is 0.0022382 MPa at saint lideta during morning peak hour.

2.1.5. Fatigue sensitivity.

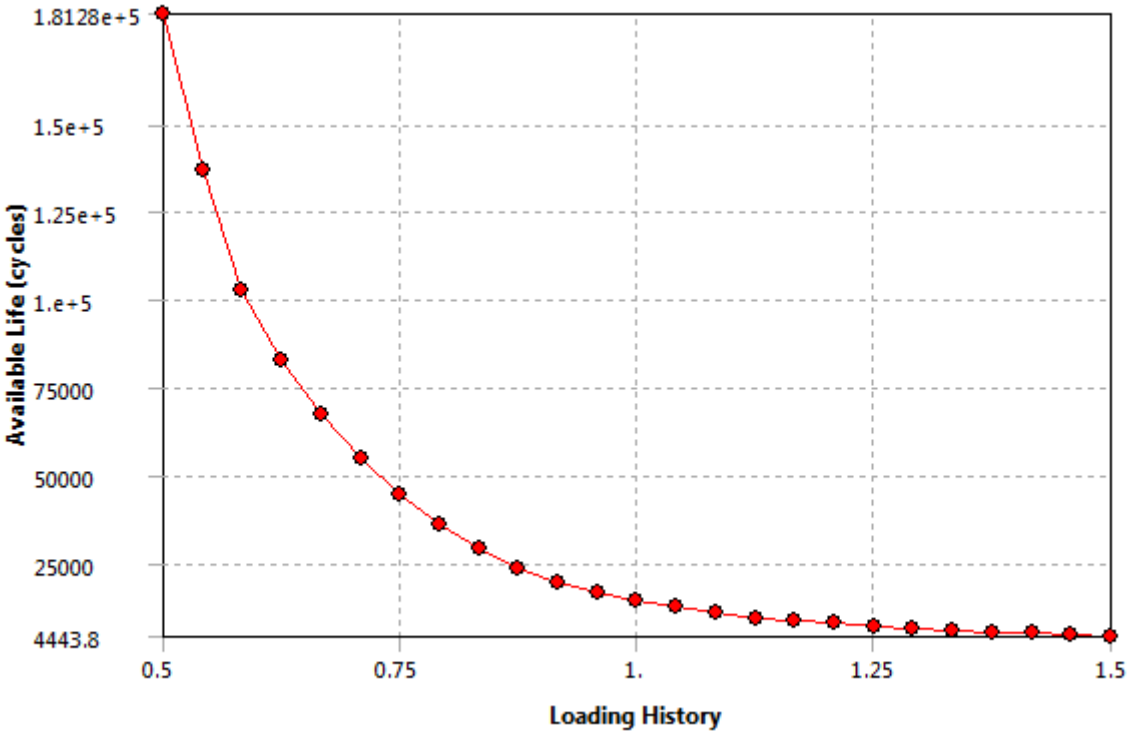

Figure 4.74: Fatigue sensitivity at saint lideta during morning peak hour for worn rail.

As shown in the figure4.74 above the maximum fatigue sensitivity is $1.8128e^5$ cycle and minimum fatigue sensitivity is 4443.8 cycle at saint lideta during morning peak hour.

2.2. Saint Lideta during day flat hour day flat hour for worn rail.

2.2.1. Fatigue life.

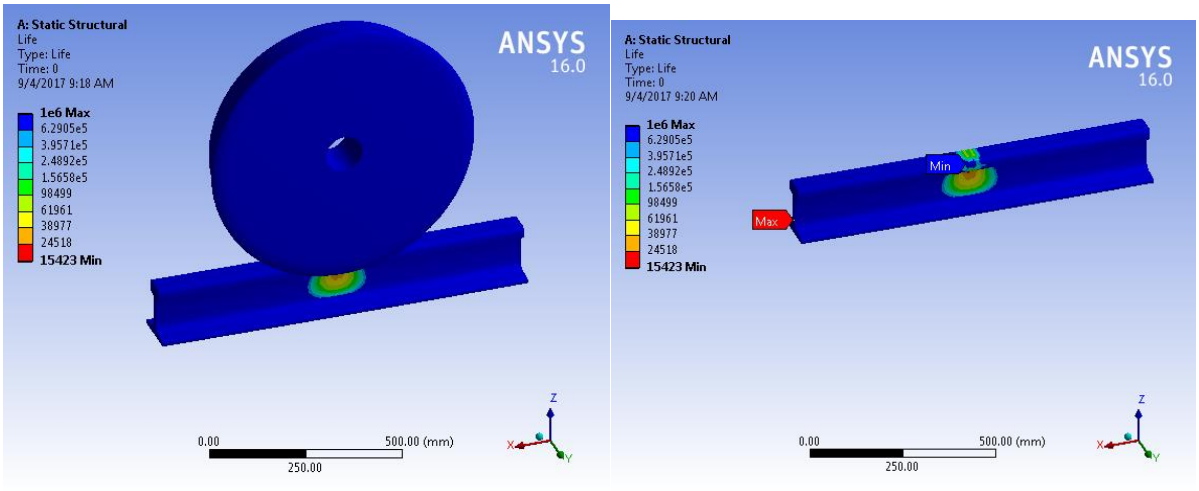

Figure 4.75: Fatigue life at saint lideta during day flat hour for worn rail.

As shown in the figure4.75 above the maximum fatigue life is $1e^6$cycles and minimum fatigue life is 15423 cycle at saint lideta during day flat hour.

2.2.2.Fatigue damage.

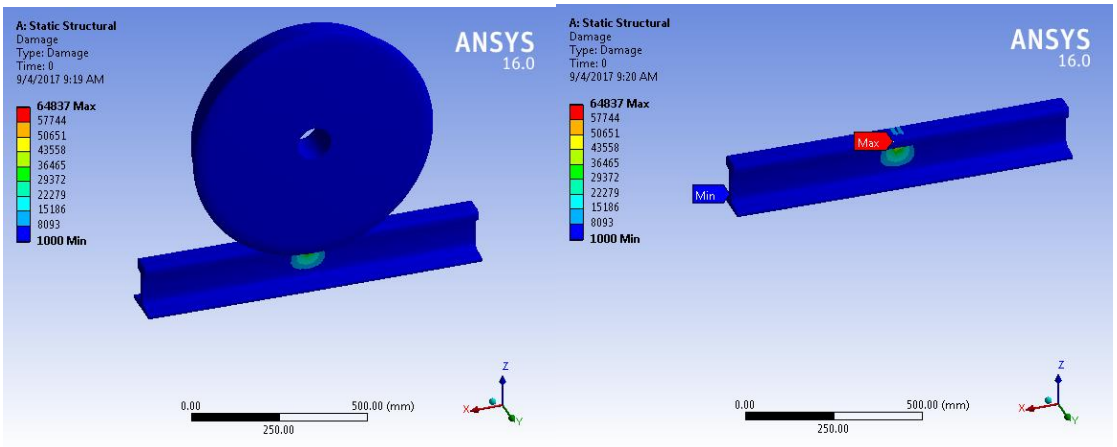

Figure 4.76: Fatigue damage at saint lideta during day flat hour for worn rail.

As shown in the figure4.76 above the maximum fatigue damage is 64837 and minimum fatigue damage is 1000 at saint lideta during day flat hour.

2.2.3. Safety factor.

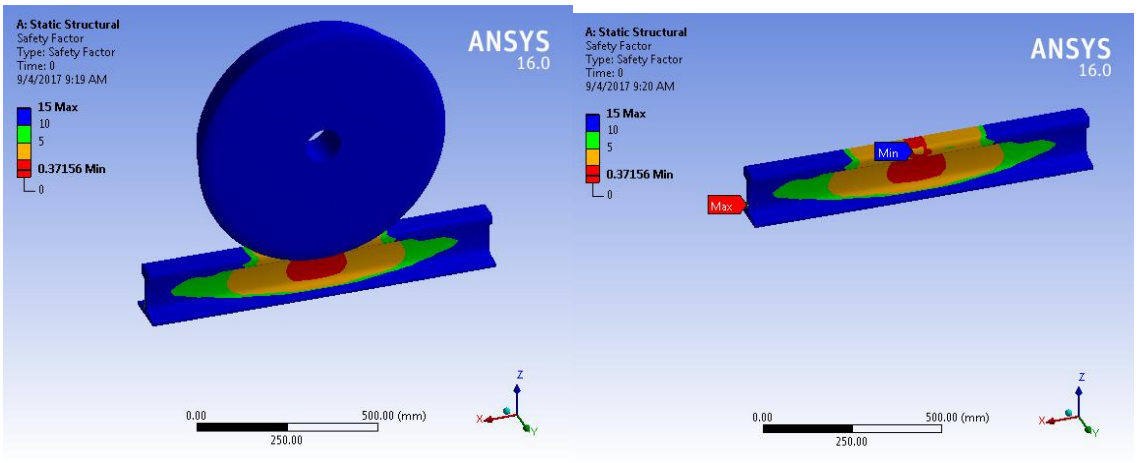

Figure 4.77: Safety factor at saint lideta during day flat hour for worn rail.

As shown in the figure4.77 above the maximum fatigue safety factor is 15and minimum fatigue safety factor is 0.37156 at sait lideta during day flat hour.

2.2.4. Equivalent alternating stress.

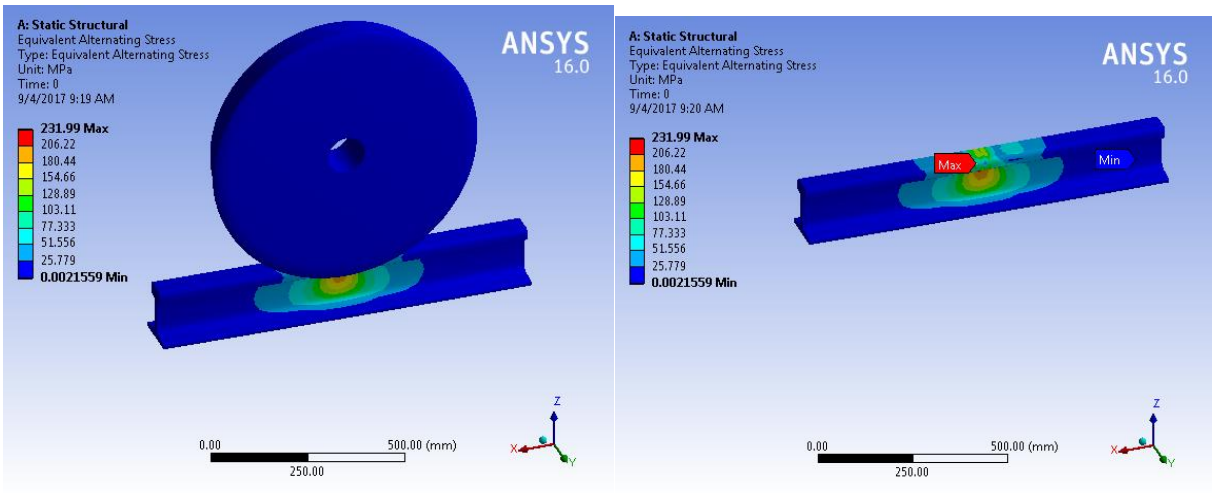

Figure 4.78: Equivalent alternating stress at saint lideta during day flat hour for worn rail.

As shown in the figure4.78 above the maximum equivalent alternating stress is 231.99 MPaand minimum equivalent alternating stress is 0.0021559 MPa at saint lideta during day flat hour.

2.2.5. Fatigue sensitivity.

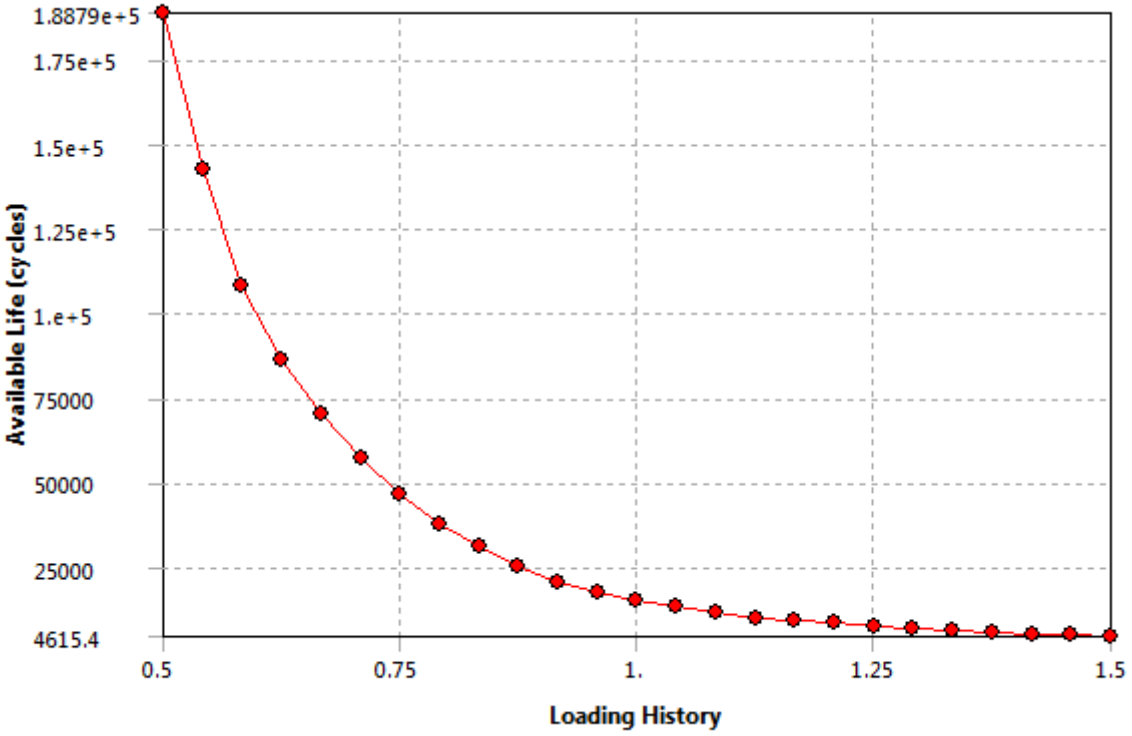

Figure 4.79: Safety factor at saint lideta during day flat hour for worn rail.

As shown in the figure4.79 above the maximum fatigue safety factor is $1.8879e^5$ cycles and minimum fatigue safety factor is 4615.4 at saint lideta during day flat hour.

2.3. Saint Lideta during afternoon peak hour for worn rail.

3.3.1. Fatigue life.

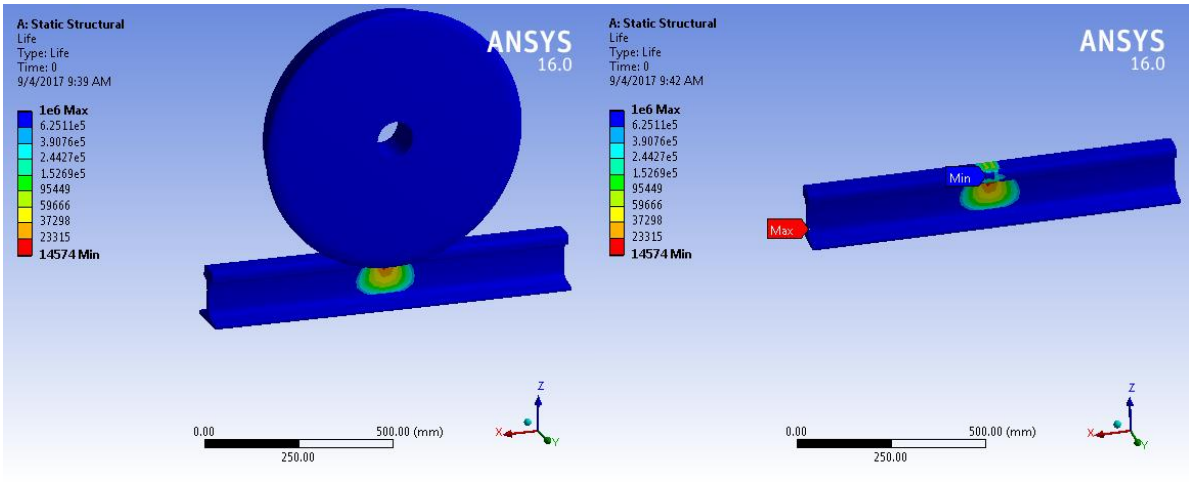

Figure 4.80: Fatigue life at saint lideta during afternoon peak hour for worn rail.

As shown in the figure4.80 above the maximum fatigue life is $1e^6$cycle and minimum fatigue life is 14574 cycle at saint lideta during afternoon peak hour.

3.3.2. Fatigue damage.

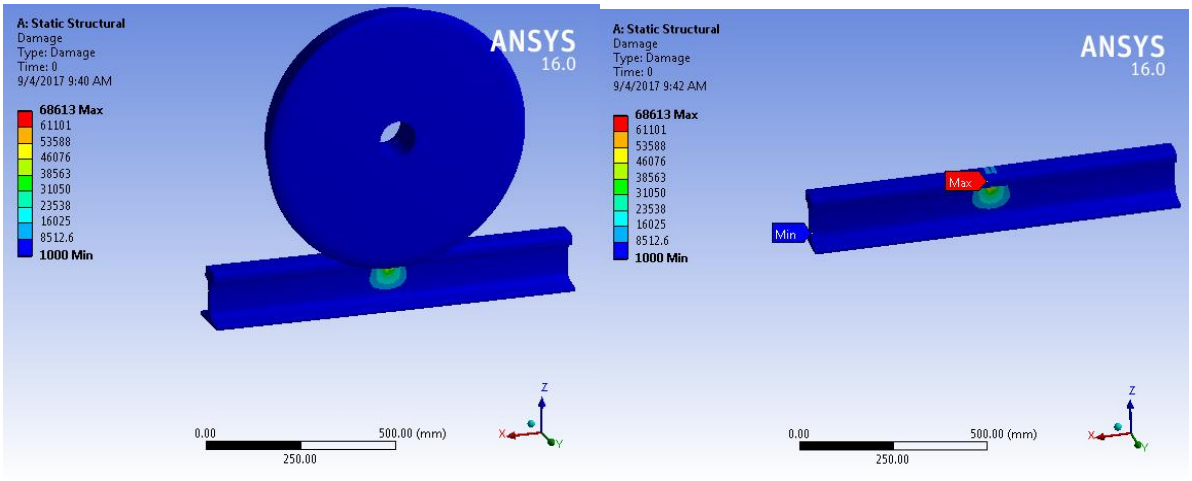

Figure 4.81: Damage at saint lideta afternoon peak hour for worn rail.

As shown in the figure4.81 above the maximum fatigue damage is 68613and minimum fatigue damage is 1000 at saint lideta during afternoon peak hour.

3.3.3. Safety factor.

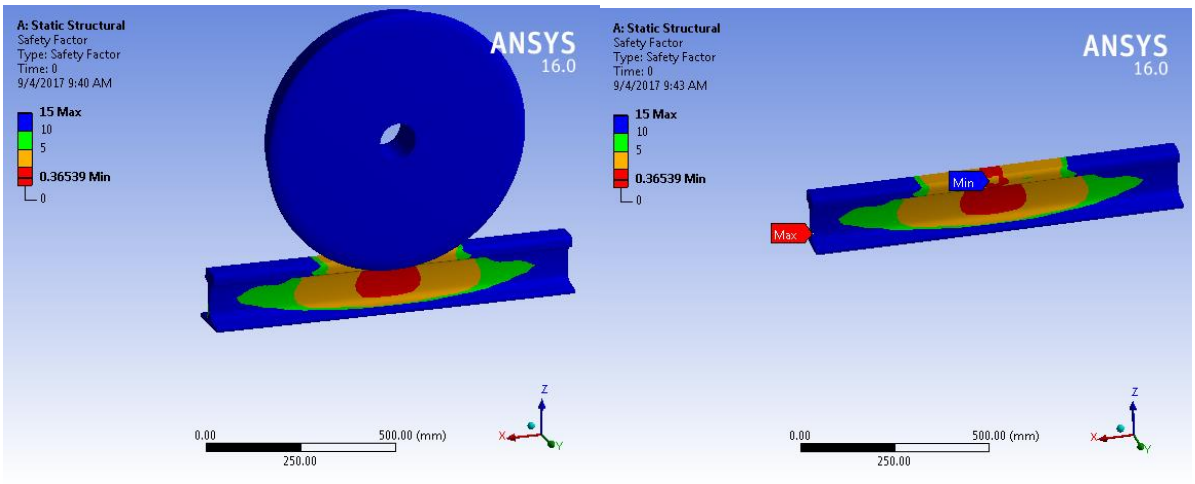

Figure 4.82: Safety factor at saint lideta during morning peak hour for worn rail.

As shown in the figure4.82 above the maximum safety factor is 15and minimum safety factor is 0.36539 at saint lideta during afternoon peak hour.

3.3.4. Equivalent alternating stress.

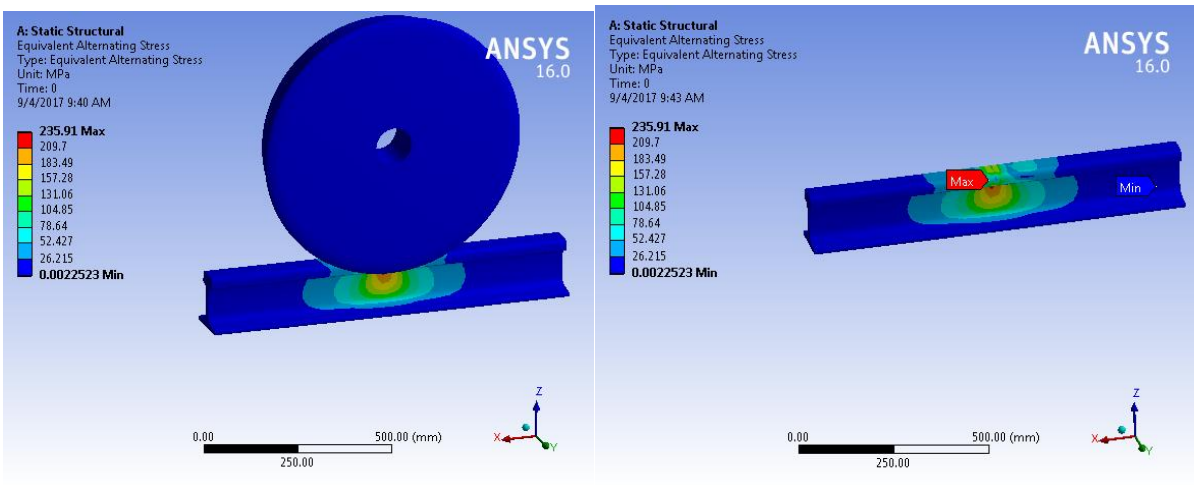

Figure 4.83: Equivalent alternating stress at saint lideta during afternoon peak hour for worn rail.

As shown in the figure4.83 above the maximum equivalent alternating stress is 235.91 MPa and minimum equivalent alternating stress is 0.0022523 MPa at saint lideta during afternoon peak hour.

3.3.5. Fatigue sensitivity.

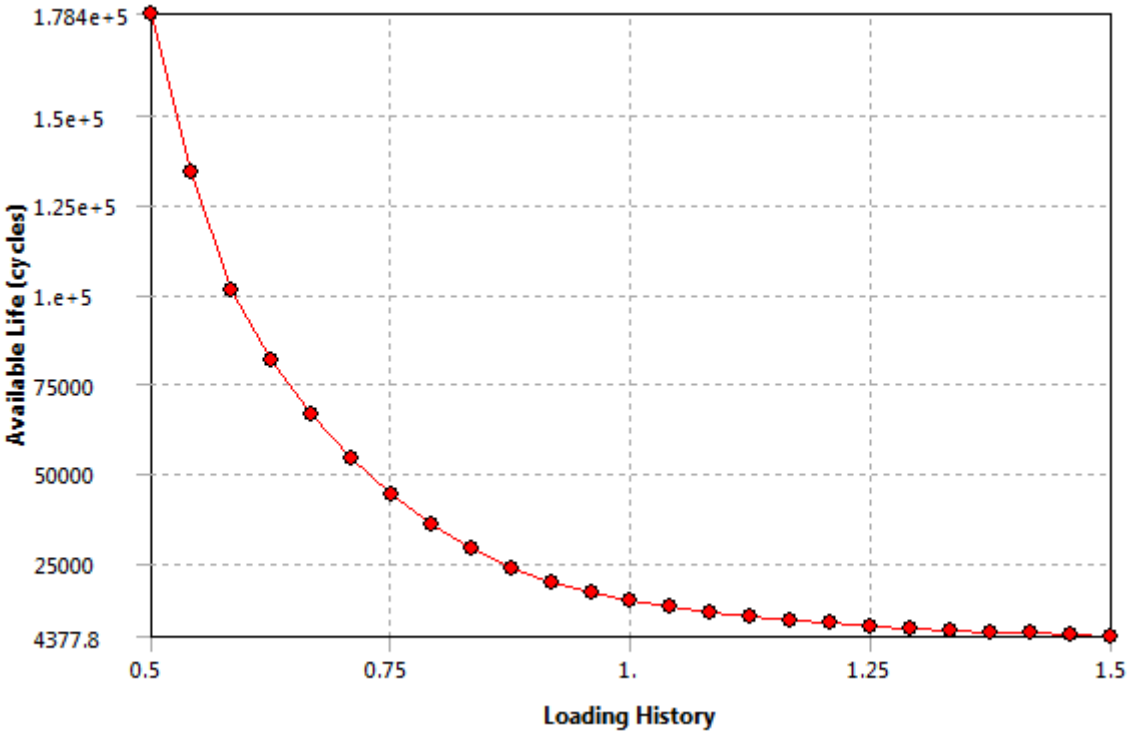

Figure 4.84: Fatigue sensitivity at saint lideta during afternoon peak hour for worn rail.

As shown in the figure4.84 above the maximum fatigue sensitivity is $1.784e^5$ cycle and minimum fatigue sensitivity is4377.8 cycle at saint lideta during afternoon peak hour.

Case 3: Autobistera.

3.1. Autobistera during morning peak hour for worn rail.

3.1.1. Fatigue life.

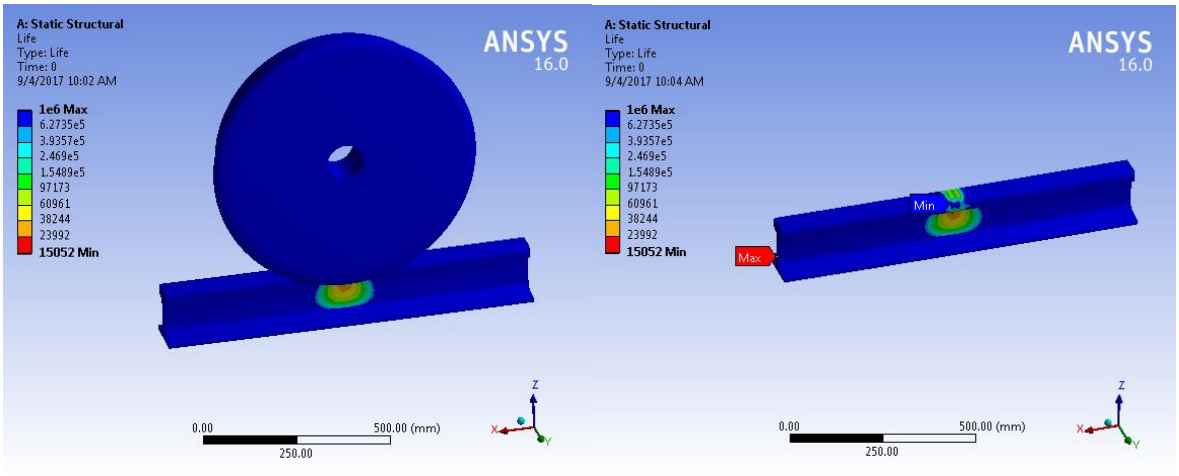

Figure 4.85: Fatigue life at autobistera during morning peak hour for worn rail.

As shown in the figure4.85 above the maximum fatigue life is $1e^6$cycle and minimum fatigue life is 15052 cycle at autobistera during morning peak hour.

3.1.2. Fatigue damage.

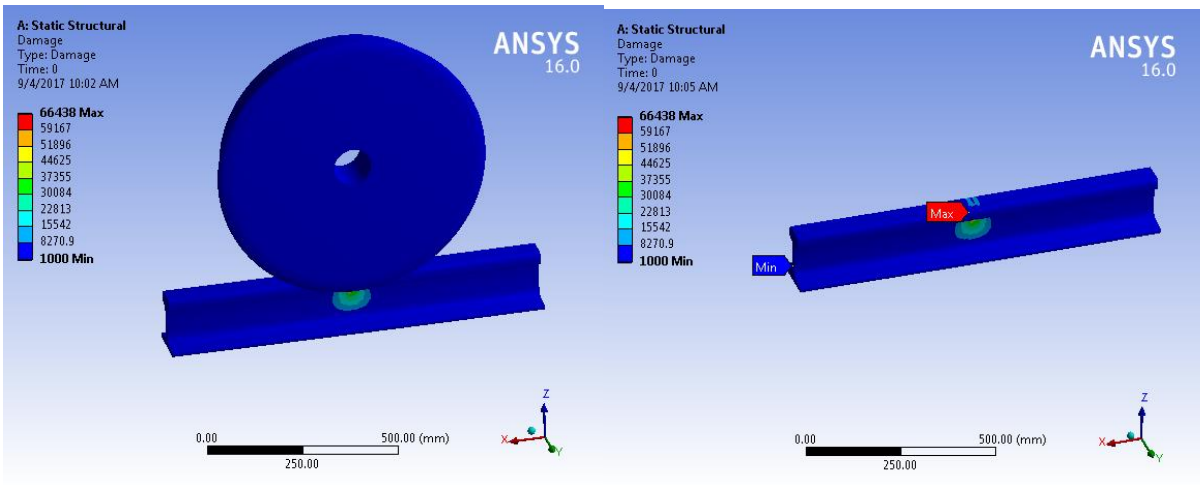

Figure 4.86: Fatigue damage at Autobistera during morning peak hour for worn rail.

As shown in the figure 4.86above the maximum fatigue damage is 66438 and minimum fatigue damage is 1000 at autobistera during morning peak hour.

3.1.3. Safety Factor.

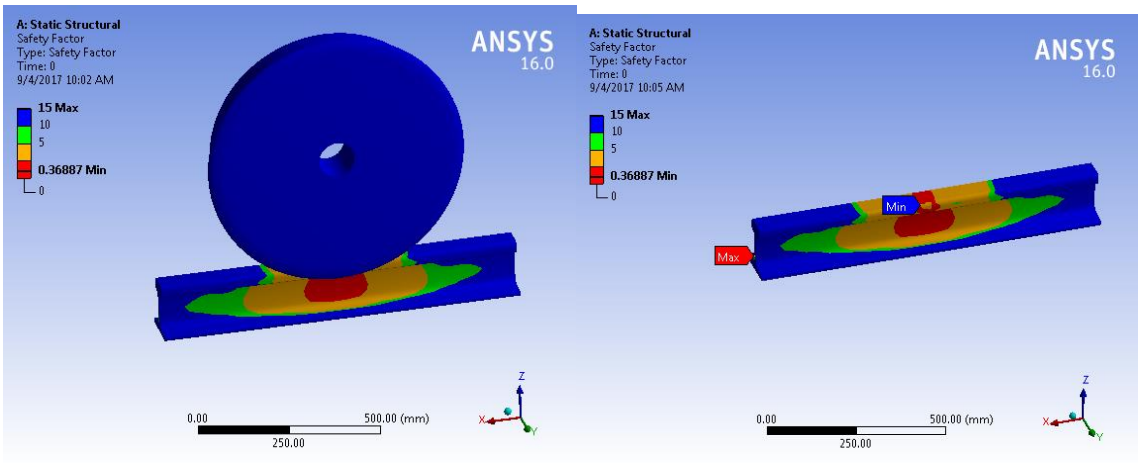

Figure 4.87: Safety factory at autobistera morning peak hour for worn rail.

As shown in the figure 4.87above the maximum fatigue safety factor is 15 and minimum fatigue safety factor is 0.36887 at autobistera during morning peak hour.

3.1.4. Equivalent Alternating Stress.

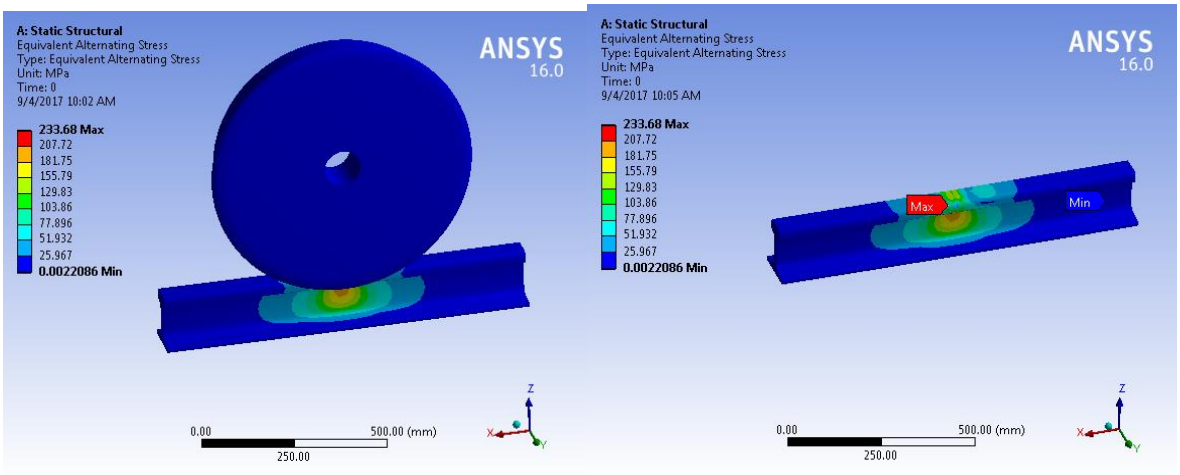

Figure 4.88: Equivalent alternating stress at autobistera during morning peak hour for worn rail.

As shown in the figure 4.88 above the maximum equivalent alternating stress is 233.67 MPa and minimum equivalent alternating stress is 0.0022086 MPa at autobistera during morning peak hour.

3.1.5. Fatigue Sensitivity.

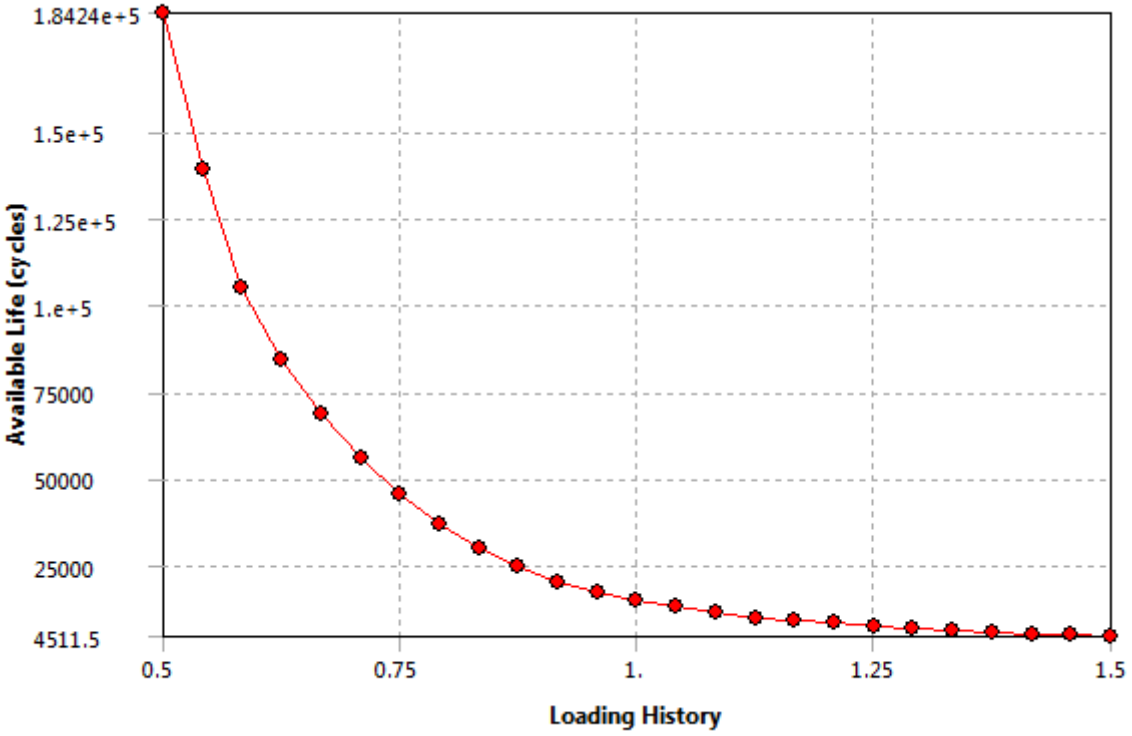

Figure 4.89: Fatigue sensitivity at autobistera during morning peak hour for worn rail.

As shown in the figure 4.89 above the maximum fatigue sensitivity is $1.8424e^5$ cycle and minimum fatigue sensitivity is 4511.5 cycle at autobistera during morning peak hour.

3.2. Autobistera during day flat hour.

3.2.1. Fatigue life.

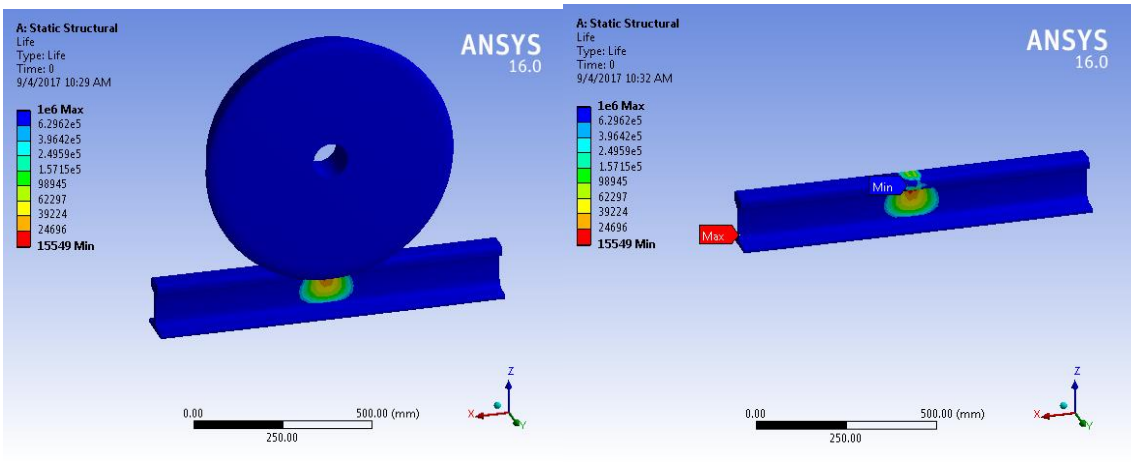

Figure 4.90: Fatigue life at autobistera during day flat hour for worn rail.

As shown in the figure 4.90 above the maximum fatigue life is $1e^6$cycle and minimum fatigue life is 15549 cycle at autobistera during day flat hour.

3.2.2. Fatigue damage.

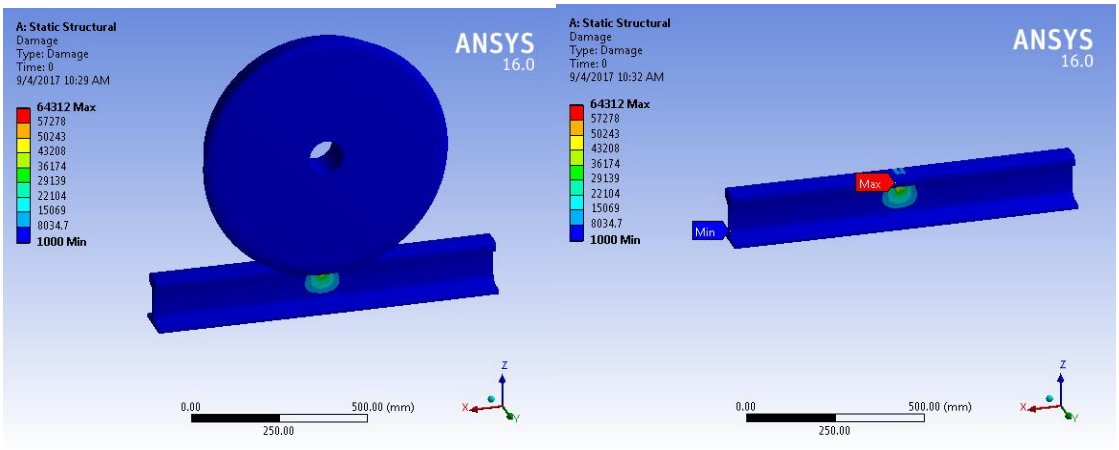

Figure 4.91: Fatigue damage at autobistera during day flat hour for worn rail.

As shown in the figure 4.91 above the maximum fatigue damage is 64312 and minimum fatigue damage is 1000 at autobistera during day flat hour.

3.2.3. Safety Factor.

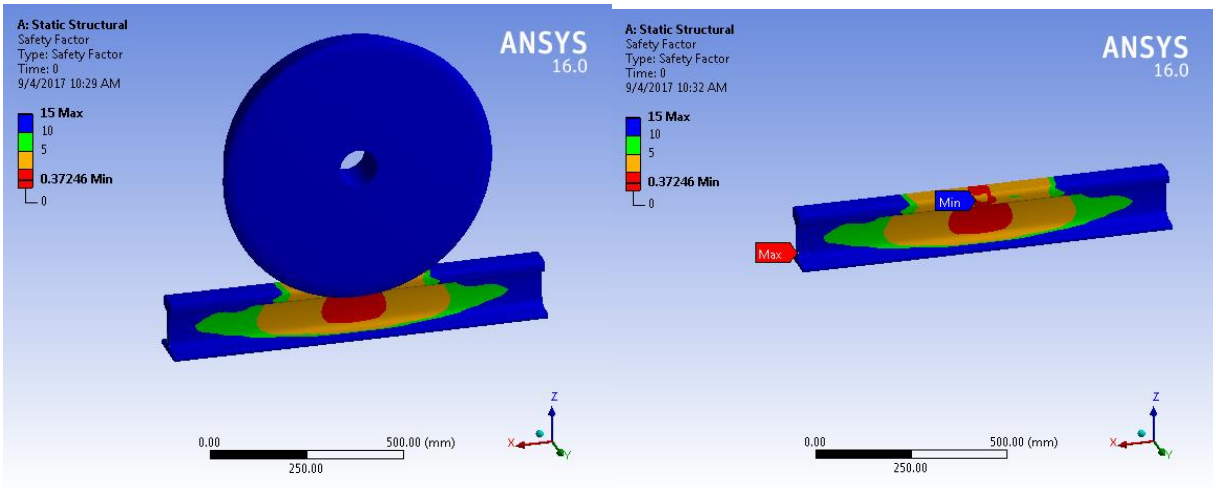

Figure 4.92: Safety factor at autobistera during day flat hour for worn rail.

As shown in the figure 4.92 above the maximum fatigue safety factor is 15 and minimum fatigue safety factor is 0.37246 at autobistera during day flat hour.

3.2.4. Equivalent Alternating Stress.

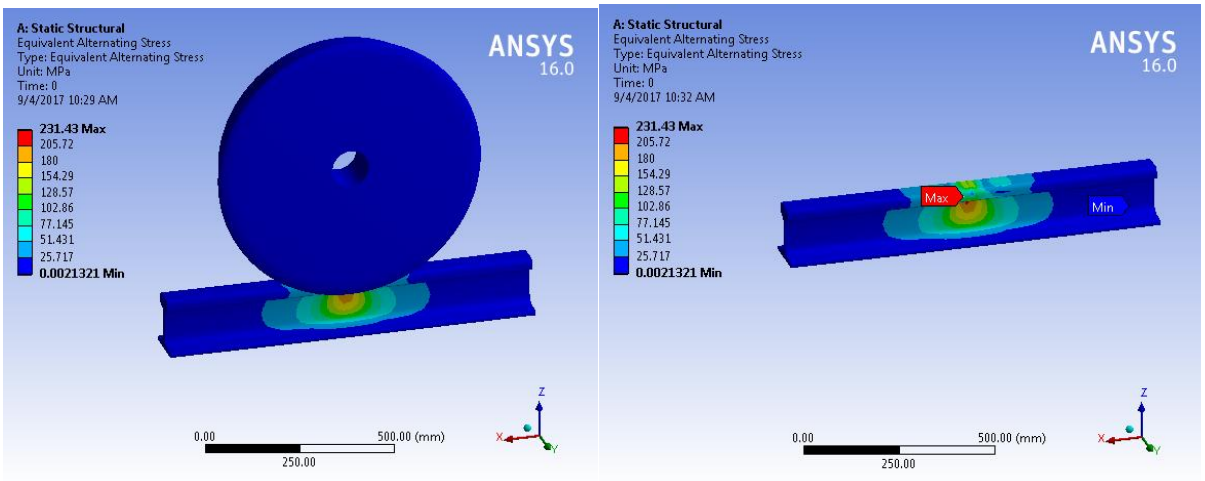

Figure 4.93: Equivalent alternating stress at autobistera during day flat hour for worn rail.

As shown in the figure 4.93 above the maximum equivalent alternating stress is 231.43 MPa and minimum equivalent alternating stress is 0.0021321 MPa at autobistera during day flat hour.

3.2.5. Fatigue Sensitivity.

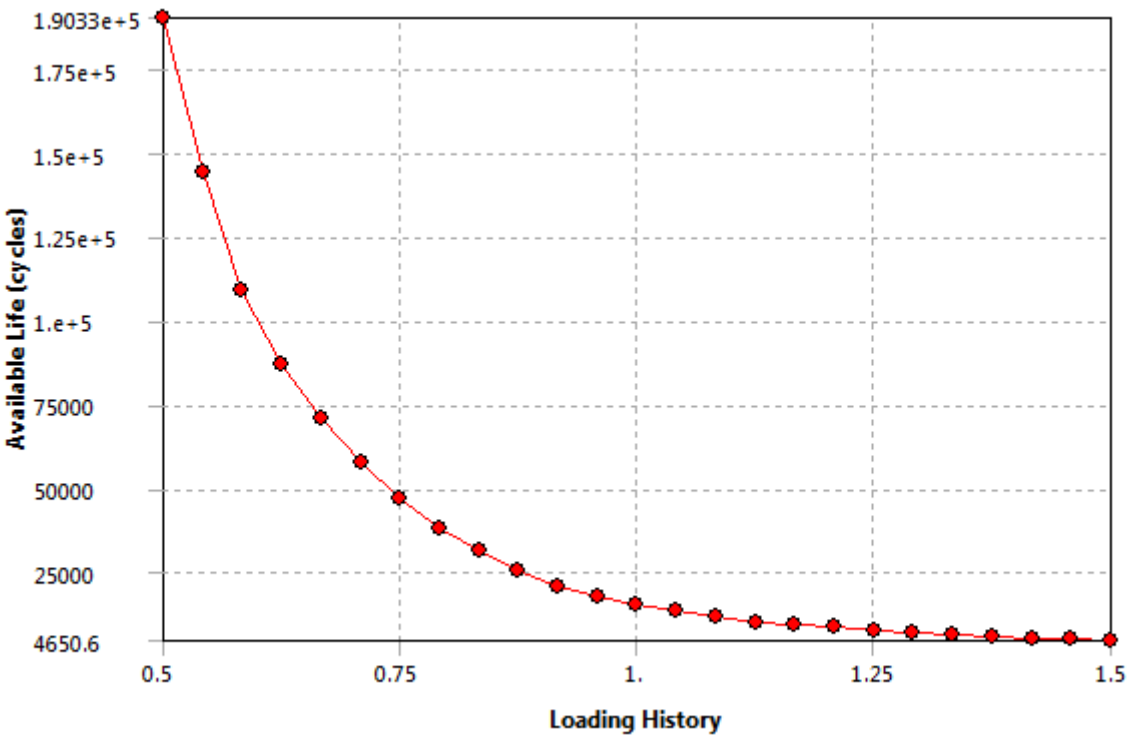

Figure 4.94: Fatigue sensitivity at autobistera during day flat hour for worn rail.

As shown in the figure 4.94 above the maximum fatigue sensitivity is $1.9033e^5$cycle and minimum fatigue sensitivity is 4650.6 cycle at autobistera during day flat hour.

3.3. Autobistera during afternoon peak hour for worn rail.

3.3.1. Fatigue life.

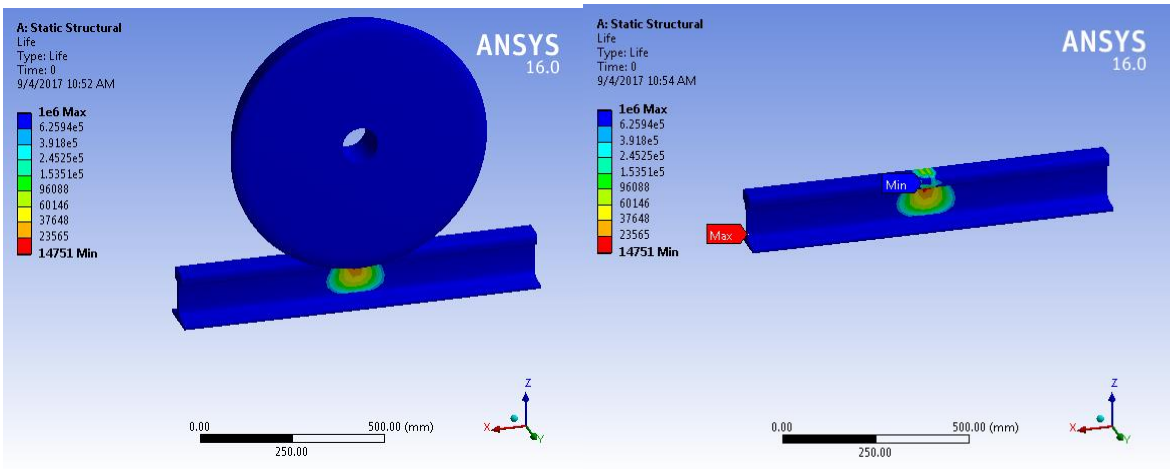

Figure 4.95: Life at autobistera during afternoon peak hour for worn rail.

As shown in the figure 4.95 above the maximum fatigue life is $1e^6$cycle and minimum fatigue life is 14751 cycle at autobistera during afternoon peak hour.

3.3.2. Fatigue damage.

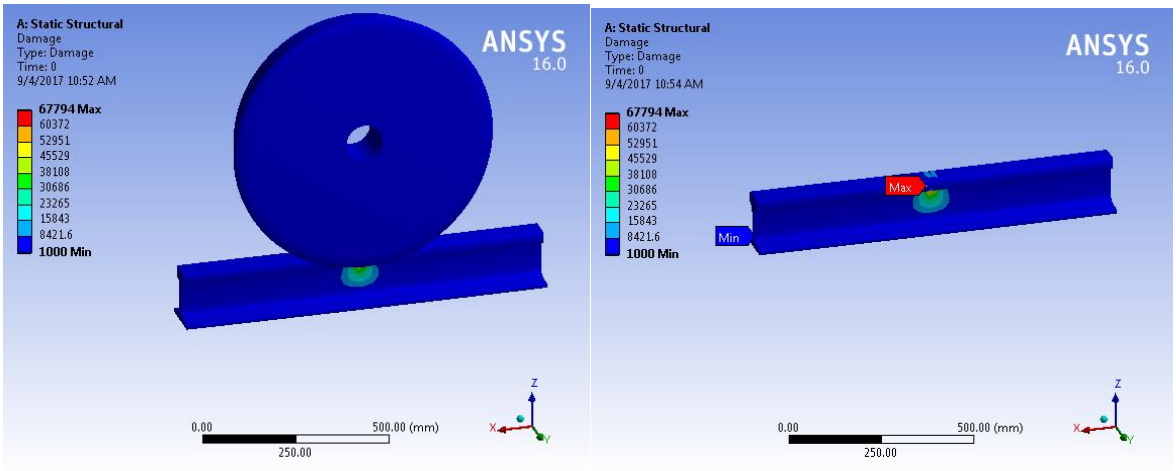

Figure 4.96: Damage at autobistera afternoon peak hour for worn rail.

As shown in the figure 4.96 above the maximum fatigue damage is 67794 and minimum fatigue damage is 1000 at autobistera during afternoon peak hour.

3.3.3. Safety Factor.

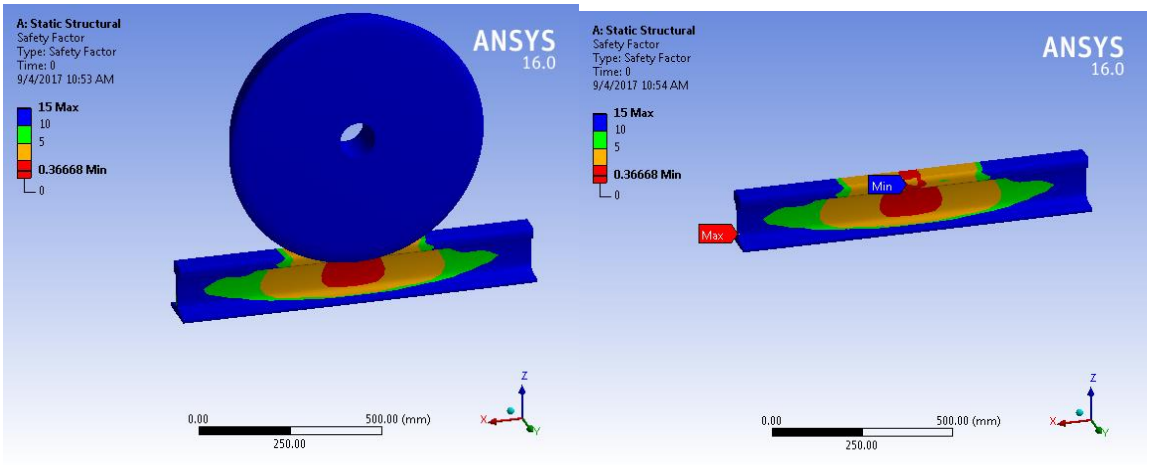

Figure 4.97: Safety factor at autobistera during afternoon peak hour for worn rail.

As shown in the figure 4.97 above the maximum fatigue safety factor is 15 and minimum fatigue safety factor is 0.36668 at autobistera during afternoon peak hour.

3.3.4. Equivalent Alternating Stress.

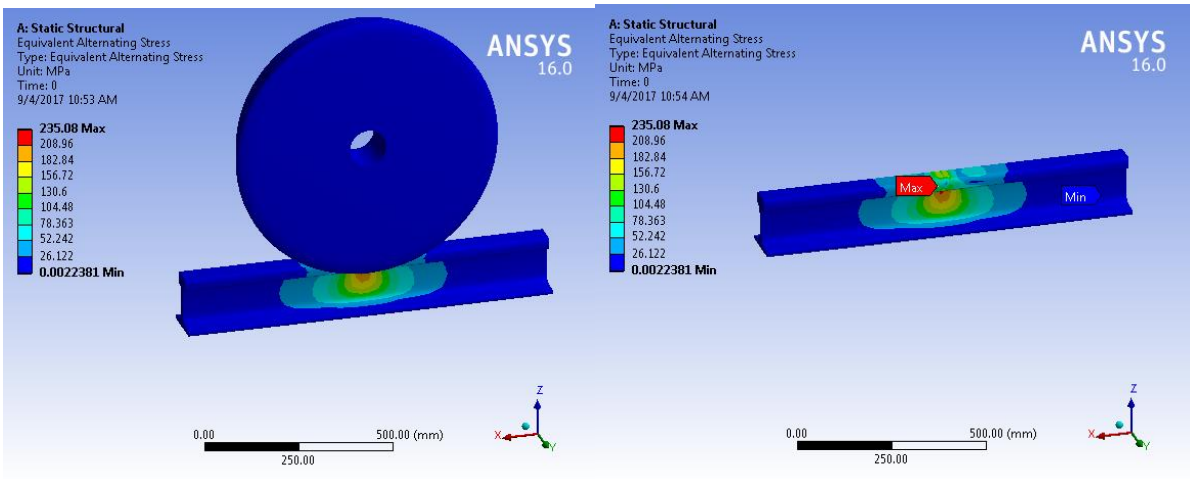

Figure 4.98: Equivalent alternating stress at autobistera during afternoon peak hour for worn rail.

As shown in the figure 4.98 above the maximum equivalent alternating stress is 235.08 MPa and minimum equivalent alternating stress is 0.0022381 MPa at autobistera during afternoon peak hour.

3.3.5. Fatigue Sensitivity.

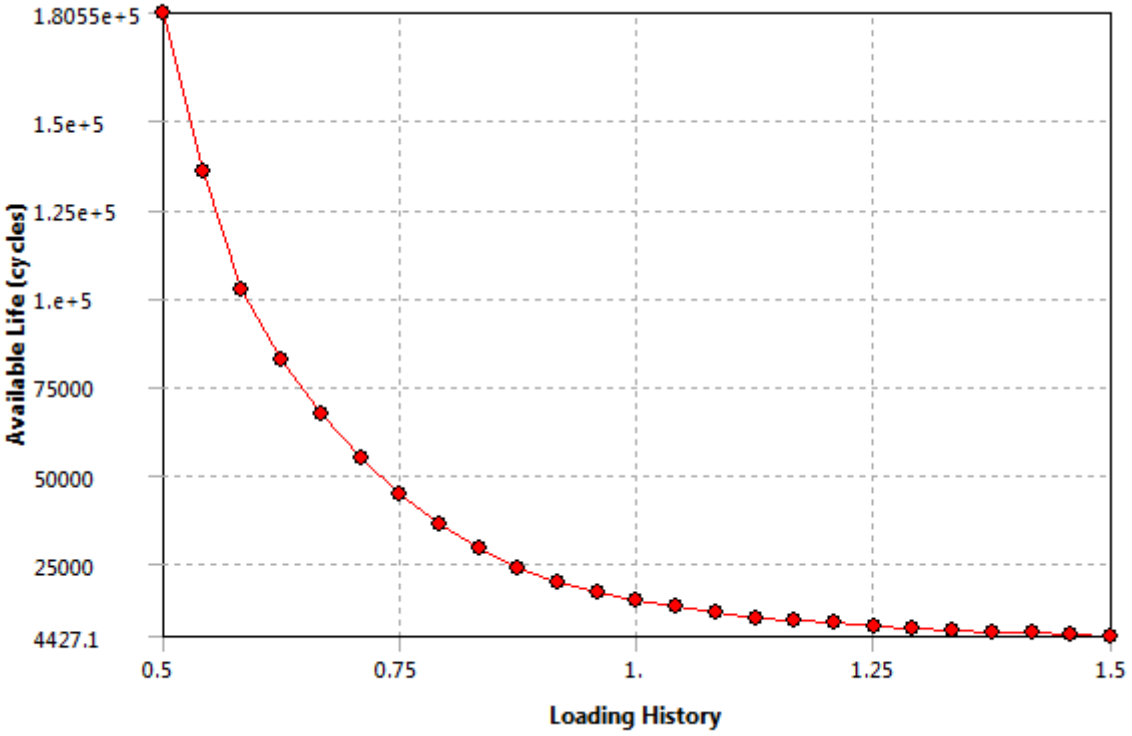

Figure 4.99: Fatigue sensitivity at autobistera during afternoon peak hour for worn rail.

As shown in the figure 4.99 above the maximum fatigue sensitivity is $1.8055e^5$ cycle and minimum fatigue sensitivity is 11615cycle at autobistera during afternoon peak hour.

III. Pressure for worn rail.

Case 1: Stadium.

1.3.Stadium during morning peak hour for worn rail.

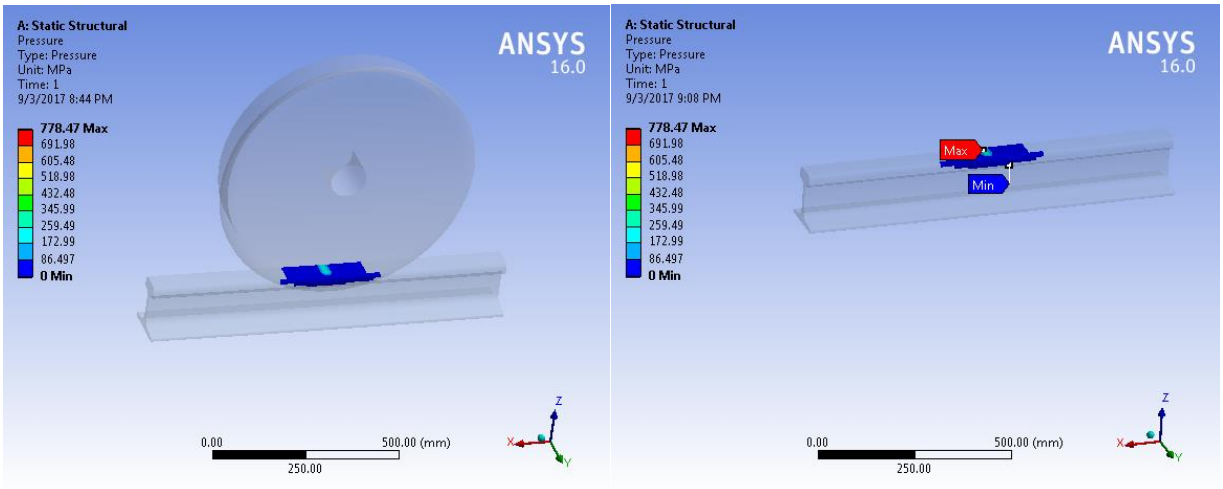

Figure 4.100: Pressure distribution at stadium during morning peak hour for worn rail.

As shown in above figure 4.100 the maximum pressure is 778.47 MPa and the minimum pressure is 0MPa at stadium during morning peak hour.

1.4.Stadium day flat hour for worn rail.

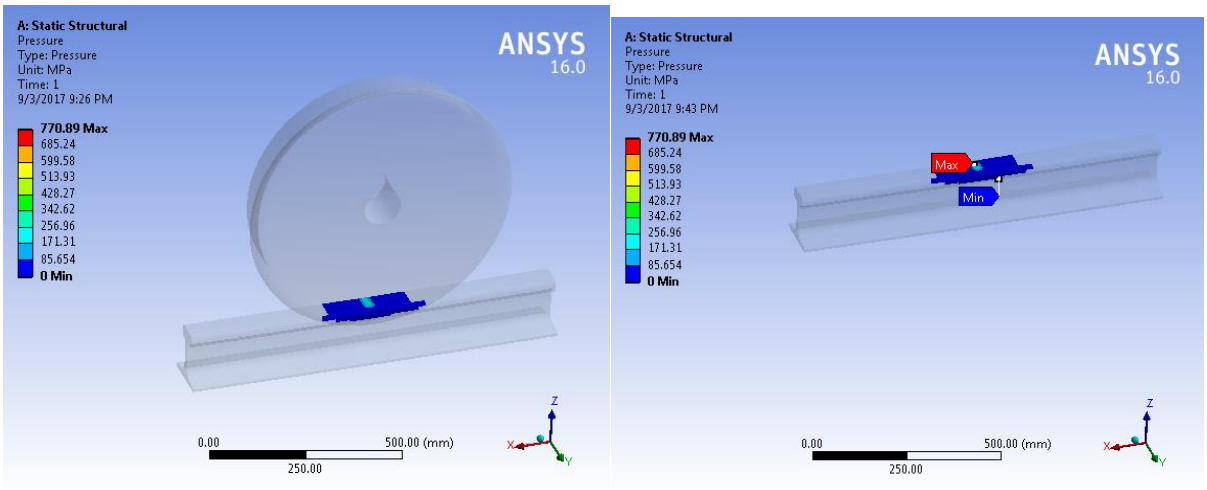

Figure 4.101: Pressure distribution at stadium during day flat hour for worn rail.

As shown in above figure 4.101 the maximum pressure is 770.89 MPa and the minimum pressure is 0MPa at stadium during day flat hour.

1.3. Stadium during afternoon pick hour for worn rail.

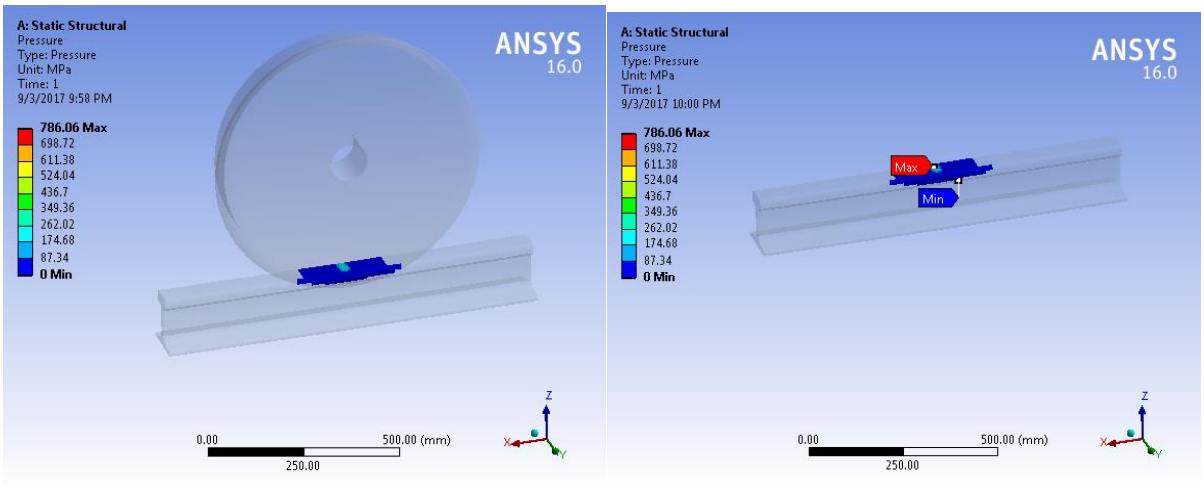

Figure 4.102: Pressure distribution at stadium during afternoon peak hour for worn rail.

As shown in above figure 4.102 the maximum pressure is 786.06 MPa and the minimum pressure is 0MPa at stadium during afternoon peak hour.

Case 2: Saint Lideta

2.1.Saint Lideta during morning peak hour for worn rail.

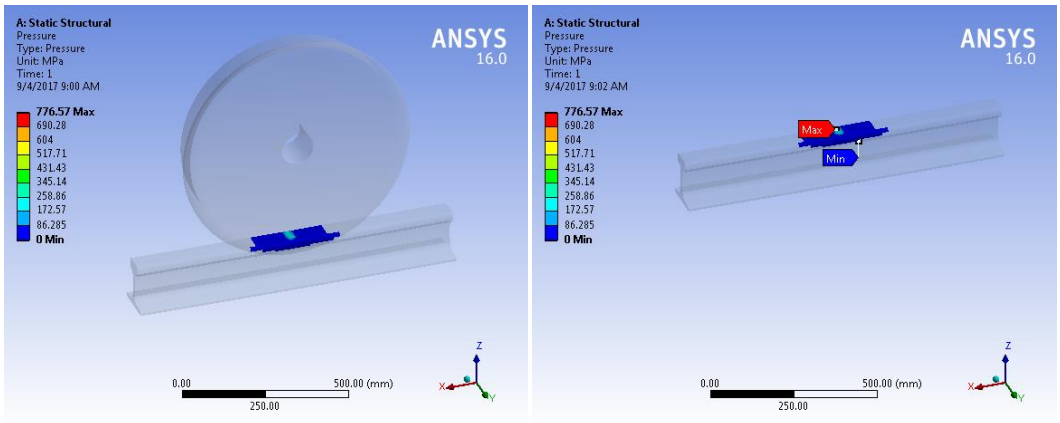

Figure 4.103: Pressure distribution saint lideta morning peak hour for worn rail.

As shown in above figure 4.103 the maximum pressure is776.57 MPa and the minimum pressure is 0 MPa at saint lideta during morning peak hour.

2.2. Saint Lideta during day flat hour for worn rail.

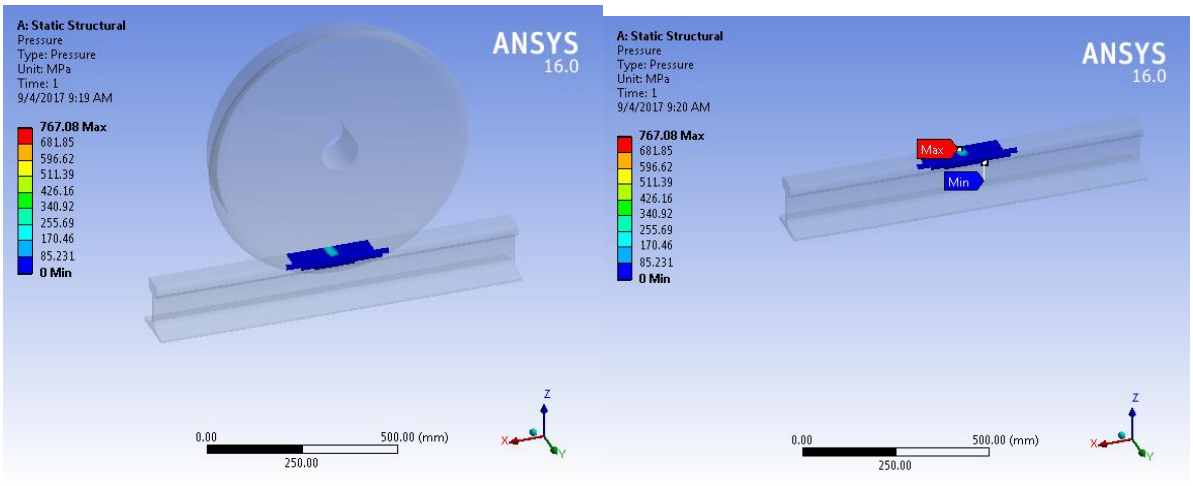

Figure 4.104: Pressure distribution at saint lideta during day flat hour for worn rail.

As shown in above figure 4.104 the maximum pressure is 767.08 MPa and the minimum pressure is 0MPa at saint lideta during day flat hour.

2.3. Saint Lideta afternoon peak hour for worn rail.

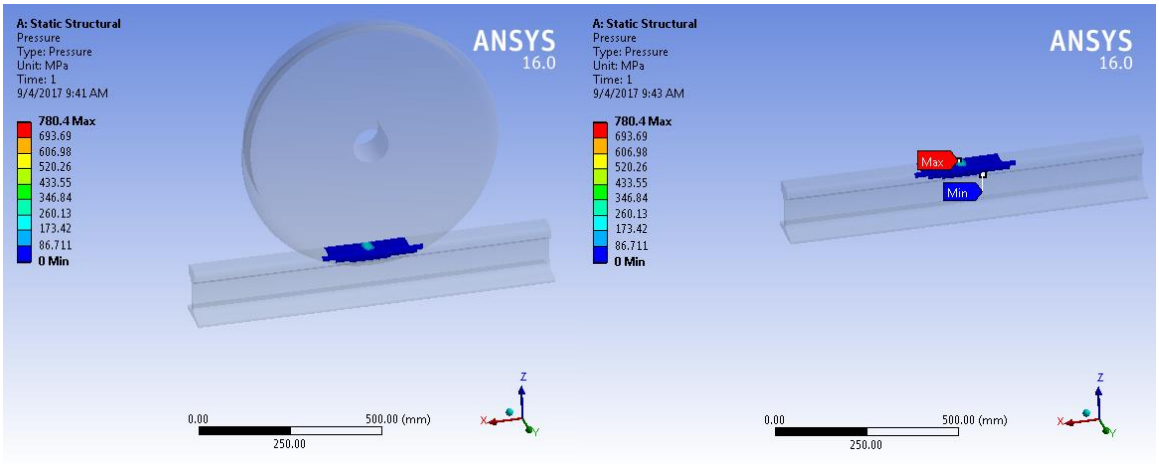

Figure 4.105: Pressure distribution at saint lideta during afternoon peak hour for worn rail.

As shown in above figure 4.105 the maximum pressure is 780.4 MPa and the minimum pressure is 0MPa at saint lideta during afternoon peak hour.

Case 3: Autobistera.

2.1. Autobistera during morning peak hour for worn rail.

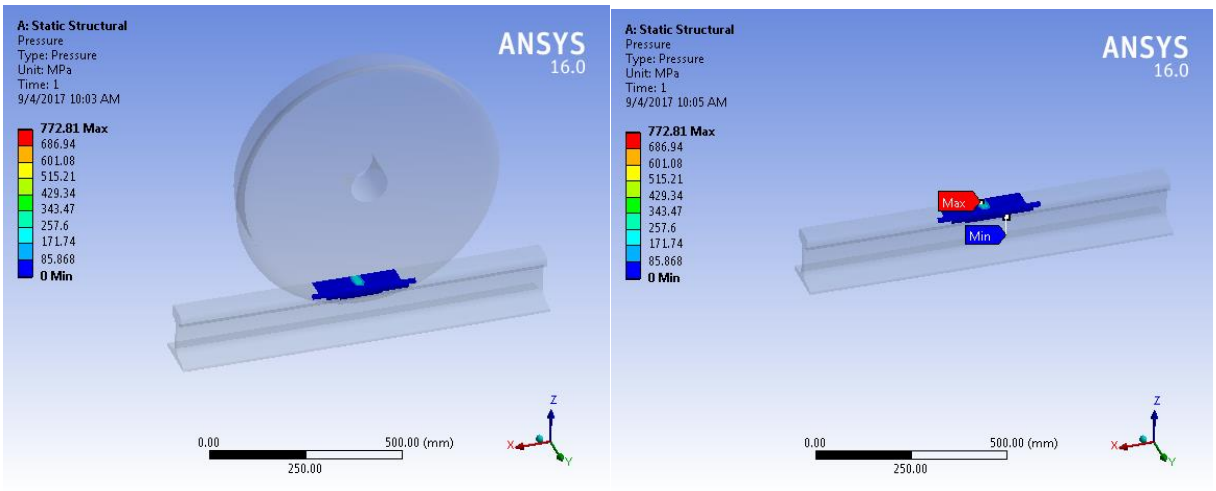

Figure 4.106: Pressure distribution at autobistera during morning peak hour for worn rail.

As shown in above figure 4.106 the maximum pressure is 772.81 MPa and the minimum pressure is 0MPa at autobistera during morning peak hour.

2.2. Autobistera day flat hour for worn rail.

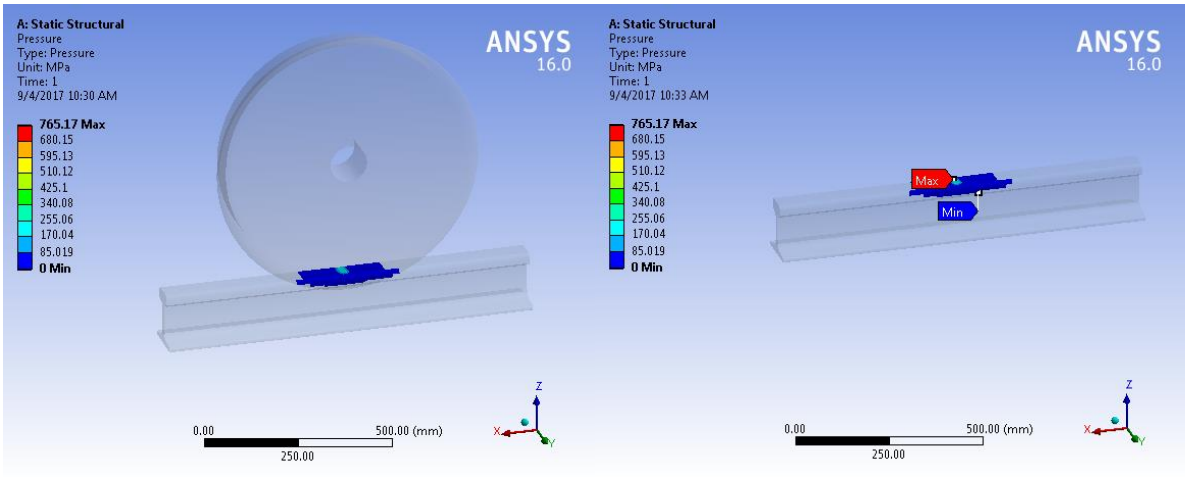

Figure 4.107: Pressure distribution at autobistera during day flat hour for worn rail.

As shown in above figure 4.107 the maximum pressure is 765.17 MPa and the minimum pressure is 0MPa at autobistera during day flat hour.

3.3. Autobistera afternoon peak hour for worn rail.

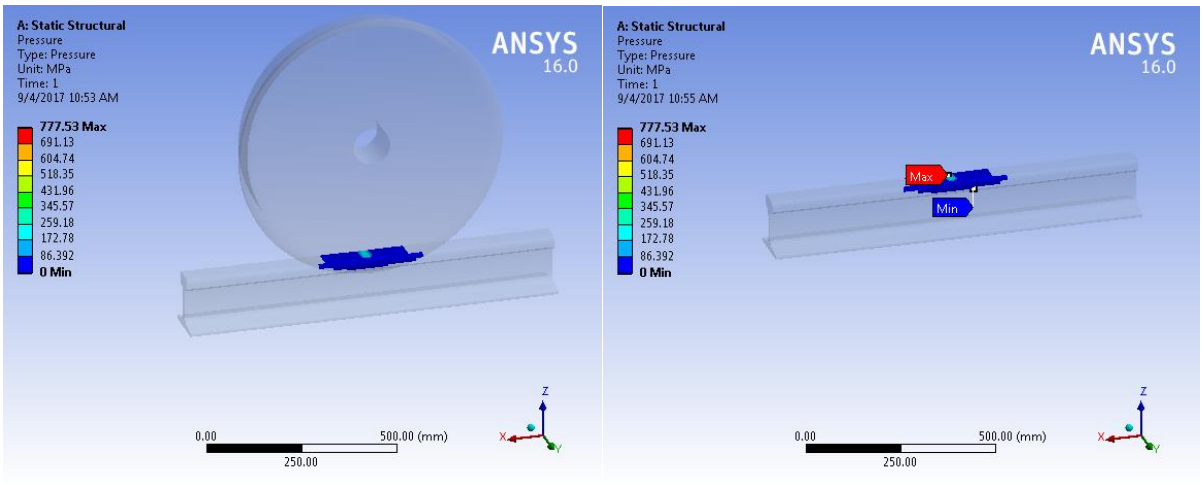

Figure 4.108: Pressure distribution at autobistera during afternoon peak hour of worn rail.

As shown in above figure 4.108 the maximum pressure is 777.53 MPa and the minimum pressure is 0MPa at autobistera during afternoon pick hour.

4.2. Discussion

This part of the paper specifies the result obtained from ANSYS software based on hertzian contact theory. The above result shows different fatigue life, damage and pressure due to vertical and lateral wheel load applied at minimum curved rail and for five millimeter worn rail of Addis Ababa light rail transit. There are three different stations and three working periods compared with each other as follows.

Case 1: Minimum curved rail at stadium (during morning peak hour (7am-9am), day flat hour (9am-5pm), and afternoon peak hour (5pm-7pm).
Case 2: Minimum curved rail at saint lideta (during morning peak hour (7am-9am), day flat hour (9am-5pm), and afternoon pick hour (5pm-7pm).
Case 3: Minimum curved rail at autobistera (during morning peak hour (7am-9am), day flat hour (9am-5pm), and afternoon peak hour (5pm-7pm)).

Table 4.1: Result summary.

Working period	Types of load		Case 1	Case 2	Case 3
Morning peak hour.	Fatigue life	Max.	$1e^6$	$1e^6$	$1e^6$
		Min.	53028	53476	54387
	Fatigue damage	Max.	18858	18700	18387
		Min.	1000	1000	1000
	Safety factor	Max.	15	15	15
		Min.	0.51323	0.51445	0.51691
	Equivalent alternating stress (MPa).	Max.	167.95	167.56	166.76
		Min.	0.0024382	0.0024393	0.002442
	Fatigue sensitivity	Max.	$1e^6$	$1e^6$	$1e^6$
		Min.	11565	11665	11868
	Pressure (MPa).	Max.	771.69	769.44	764.94
		Min.	0	0	0

Working period	Types of load		Case 1	Case 2	Case 3
Day flat hour.	Fatigue life (cycle)	Max.	$1e^6$	$1e^6$	$1e^6$
		Min.	54849	55788	56266
	Fatigue damage	Max.	18232	17925	17773
		Min.	1000	1000	1000
	Safety factor	Max.	15	15	15
		Min.	0.51815	0.52066	0.52193
	Equivalent alternating stress (MPa).	Max.	166.36	165.56	165.16
		Min.	0.0024435	0.0024469	0.0024487
	Fatigue sensitivity (cycle).	Max.	$1e^6$	$1e^6$	$1e^6$
		Min.	11971	12181	12288
	Pressure (MPa).	Max.	762.67	758.15	755.88
		Min.	0	0	0
Afternoon peak hour.	Fatigue life (cycle)	Max.	$1e^6$	$1e^6$	$1e^6$
		Min.	51274	52584	53252
	Fatigue damage	Max.	19503	19017	18779
		Min.	1000	1000	1000
	Safety factor	Max.	15	15	15
		Min.	0.50842	0.51202	0.51384
	Equivalent alternating stress (MPa).	Max.	169.54	168.35	167.76
		Min.	0.0024347	0.0024372	0.0024388
	Fatigue sensitivity (cycle).	Max.	$1e^6$	$1e^6$	$1e^6$
		Min.	11174	11466	11615
	Pressure (MPa).	Max.	780.66	773.94	770.57
		Min.	0	0	0

The above result contains both the curved rail and wheel due to the reason of the analysis performed using the contact mechanism. The paper mainly focuses on the curved rail result and ignores the result of the wheel part.

As shown on the above static ANSYS result the fatigue tools (life, damage, safety factor, equivalent alternating stress and fatigue sensitivity), and pressure vary for one case to case and for one working period to other working period. In case1 as shown in the figure 4.1, figure 4.2, figure 4.4, figure 4.5, the minimum fatigue life, maximum fatigue damage, maximum equivalent alternating stress, minimum fatigue sensitivity 53028 cycles, 18858mm,167.95MPa, 11565cycles, during morning peak hour. In case 2 as shown in figure 4.16, figure 4.17, figure 4.19, figure 4.20, the minimum fatigue life, maximum fatigue damage, maximum equivalent alternating stress, minimum fatigue sensitivity, 53476 cycles, 18700mm,167.56MPa, 11665cycles, during morning peak hour. Incase 3 as shown in the figure 4.31, figure 4.32, figure 4.34, figure 4.35, minimum fatigue life, minimum maximum fatigue damage, maximum equivalent alternating stress, fatigue sensitivity, 54387 cycles, 18387mm, 166.76MPa, 11868cycles, during morning peak hour. Due to the contact there is a pressure on curved rail.

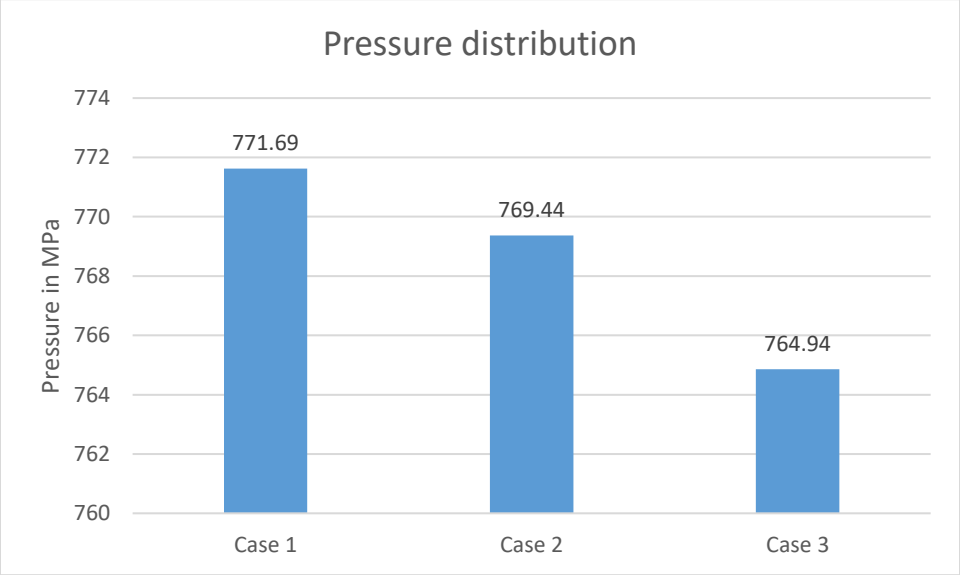

Figure 4.109: Pressure distribution graph during morning peak hour.

As shown in above figure 4.109, the maximum and minimum contact pressure distribution on rail head is given for three different location of minimum curved rail during morning peak hour working period of Addis Ababa light rail transit. Case1 has greater contact pressure than the remaining cases.Case3 has the smallest contact pressure distribution than the rest of cases.

In case1 as shown in the figure 4.6, figure 4.7, figure 4.9, figure 4.10, the minimum fatigue life, maximum fatigue damage, maximum equivalent alternating stress, minimum fatigue sensitivity, 54849 cycles, 18232 mm,166.36MPa,11971cycles, during day flat hour. In case 2 as shown in

figure 4.21, figure 4.22, figure 4.24, figure 4.25, the minimum fatigue life, maximum fatigue damage, maximum equivalent alternating stress, minimum fatigue sensitivity, 55788 cycles, 17925mm,165.56MPa, 12181cycles,during day flat hour. Incase 3 as shown in the figure 4.36, figure 4.37, figure 4.39, figure 4.40, minimum fatigue life, maximum fatigue damage, maximum equivalent alternating stress, minimum fatigue sensitivity, 56266 cycles, 12288cycles, 17773 mm, 165.16 MPa during day flat hour. Due to the contact there is a pressure on curved rail.

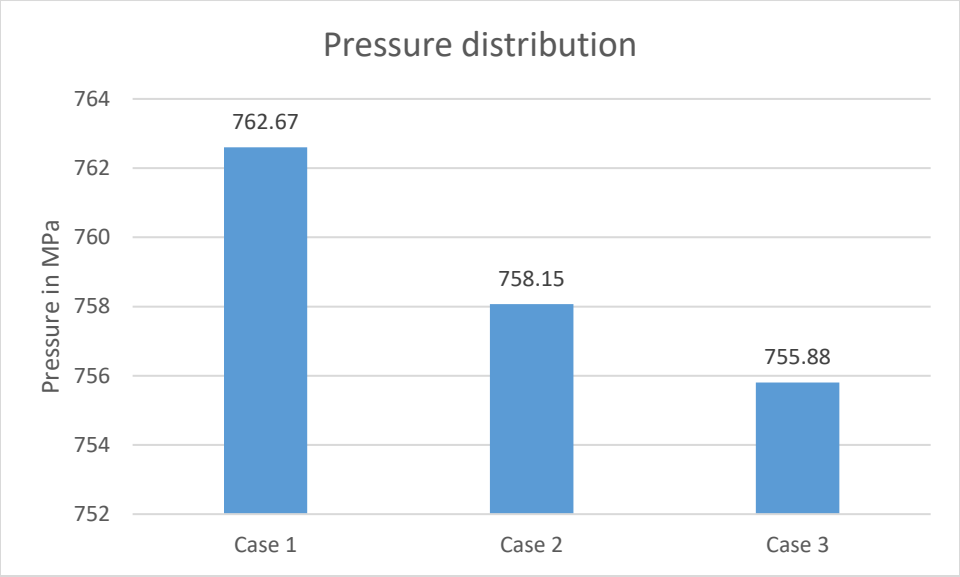

Figure 4.110: Pressure distribution graph during day flat hour.

As shown in above figure 4.110, the maximum and minimum contact pressure distribution on rail head is given for three different location of minimum curved rail during day flat hour working period of Addis Ababa light rail transit. Case1 has greater contact pressure than the remaining cases.Case3 has the smallest contact pressure distribution than the rest of cases.

In case1 as shown in the figure 4.11, figure 4.12, figure 4.14, figure 4.15, the minimum fatigue life, maximum fatigue damage, maximum equivalent alternating stress, minimum fatigue sensitivity, 51274 cycles, 19503 mm,169.54MPa, 11174 cycles, during afternoon peak hour. In case 2 as shown in figure 4.26, figure 4.27, figure 4.29, figure 4.30, the minimum fatigue life, maximum fatigue damage, maximum equivalent alternating stress, minimum fatigue sensitivity, 52584 cycles, 19017mm,168.35MPa, 11466cycles,during afternoon peak hour. Incase 3 as shown in the figure 4.41, figure 4.42, figure 4.44, figure 4.45, minimum fatigue life, maximum fatigue damage, maximum equivalent alternating stress, minimum fatigue sensitivity, 53252

cycles, 18779 mm, 167.76MPa 11615cycles, during afternoon peak hour. Due to the contact there is a pressure on curved rail.

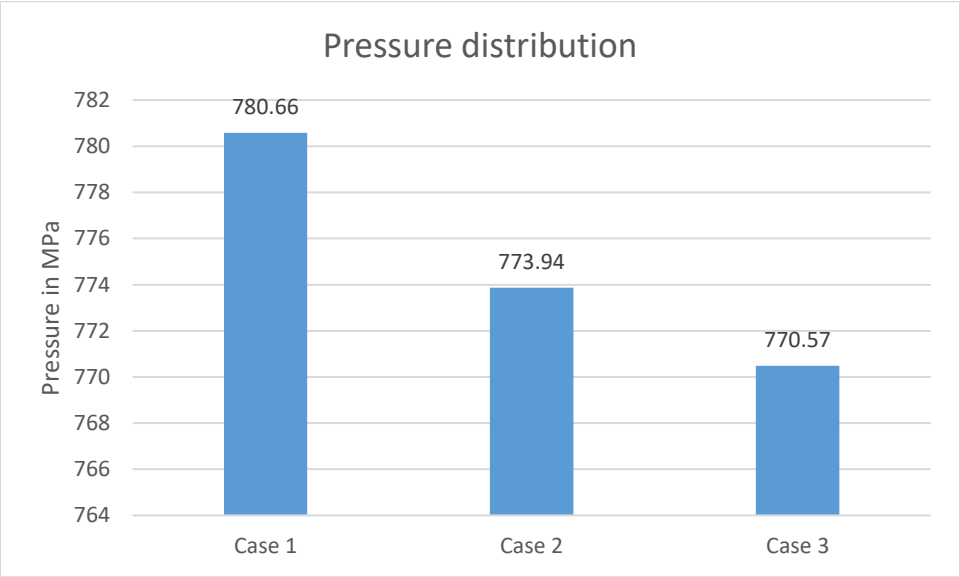

Figure 4.111: Pressure distribution graph during afternoon peak hour.

As shown in above figure 4.111, the maximum and minimum contact pressure distribution on rail head is given for three different location of minimum curved rail during morning peak hour working period of Addis Ababa light rail transit. Case1 has greater contact pressure than the remaining cases.Case3 has the smallest contact pressure distribution than the rest of cases.

Factor of safety in case1 is shown in Figure 4.3, the value of safety factor amounted to be 0.51336 during morning peak hour. Factor of safety in case2 is shown in Figure 4.18, the value of safety factor amounted to be 0.51457 during morning peak hour. Factor of safety in case3 is shown in Figure 4.33, the value of safety factor amounted to be 0.51703 during morning pick hour.

Factor of safety in case1 is shown in Figure 4.8, the value of safety factor amounted to be 0.51828 during day flat hour. Factor of safety in case2 is shown in Figure 4.23, the value of safety factor amounted to be 0.52078 during day flat hour. Factor of safety in case3 is shown in Figure 4.38, the value of safety factor amounted to be 0.52206 during day flat hour.

Factor of safety in case1 is shown in Figure 4.13, the value of safety factor amounted to be 0.50854 during afternoon peak hour. Factor of safety in case2 is shown in Figure 4.28, the value of safety factor amounted to be 0.51214 during afternoon pick hour. Factor of safety in case3 is

shown in Figure 4.43, the value of safety factor amounted to be 0.51396 during afternoon peak hour.

This part of the paper specifies the result obtained from ANSYS software based on hertzian contact theory. The result shows different fatigue life, damage and pressure due to vertical and lateral wheel load applied at minimum curved five millimeter worn rail of Addis Ababa light rail transit. There are three different stations and three working periods compared with each other as follows.

Case 1: Minimum curved worn rail at stadium (during morning peak hour (7am-9am), day flat hour (9am-5pm), and afternoon peak hour (5pm-7pm).
Case 2: Minimum curved worn rail at saint lideta (during morning peak hour (7am-9am), day flat hour (9am-5pm), and afternoon pick hour (5pm-7pm).
Case 3: Minimum curved worn rail at autobistera (during morning peak hour (7am-9am), day flat hour (9am-5pm), and afternoon peak hour (5pm-7pm)).

Table 4.2: Result summary for worn rail.

Working period	Types of load		Case 1	Case 2	Case 3
Morning peak hour.	Fatigue life	Max.	$1e^6$	$1e^6$	$1e^6$
		Min.	14691	14810	15052
	Fatigue damage	Max.	68068	67523	66438
		Min.	1000	1000	1000
	Pressure (MPa).	Max.	778.47	776.57	772.81
		Min.	0	0	0
Day flat hour.	Fatigue life (cycle)	Max.	$1e^6$	$1e^6$	$1e^6$
		Min.	15175	15423	15549
	Fatigue damage	Max.	65899	64837	64312
		Min.	1000	1000	1000
	Pressure (MPa).	Max.	770.89	767.08	765.17
		Min.	0	0	0
Afternoon peak	Fatigue life (cycle)	Max.	$1e^6$	$1e^6$	$1e^6$

hour.		Min.	14230	14574	14751
	Fatigue damage	Max.	70276	68613	67794
		Min.	1000	1000	1000
	Pressure (MPa).	Max.	786.06	780.4	777.53
		Min.	0	0	0

The above result contains both the curved worn rail and wheel due to the reason of the analysis performed using the contact mechanism. The paper mainly focuses on the curved worn rail result and ignores the result of the wheel part.

As shown on the above static ANSYS result the fatigue tools (life, damage) and pressure vary for one case to case and for one working period to other working period. In case1 as shown in the figure 4.55 and figure 4.56the minimum fatigue life and maximum fatigue damage are 14691 cycles and 68068during morning peak hour respectively. In case 2 as shown in the figure 4.70 and figure 4.71the minimum fatigue life and maximum fatigue damage are 14810 cycles and 67523during morning peak hour respectively. In case 3 as shown in the figure 4.85 and figure 4.86the minimum fatigue life and maximum fatigue damage are 15052 cycles and 66438during morning peak hour respectively. Due to the contact there is a pressure on curved worn rail.

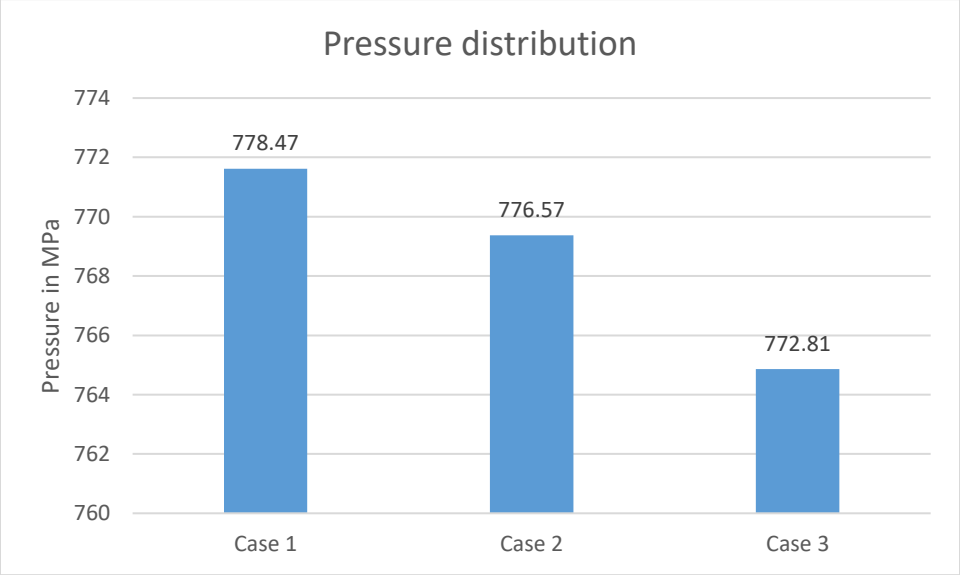

Figure 4.112: Pressure distribution graph during morning peak hour for worn rail.

As shown in above figure 4.12, the maximum and minimum contact pressure distribution on rail head is given for three different location of minimum curved worn rail during morning peak hour working period of Addis Ababa light rail transit. Case1 has greater contact pressure than the remaining cases.Case3 has the smallest contact pressure distribution than the rest of cases.

In case1 as shown in the figure 4.60 and figure 4.61the minimum fatigue life and maximum fatigue damage are 15175 cycles and 65899during day flat hour respectively. In case 2 as shown in the figure 4.75 and figure 4.76the minimum fatigue life and maximum fatigue damage are 15423 cycles and 64837during day flat hour respectively. In case 3 as shown in the figure 4.90 and figure 4.91the minimum fatigue life and maximum fatigue damage are 15549 cycles and 64312during day flat hour respectively.. Due to the contact there is a pressure on curved worn rail.

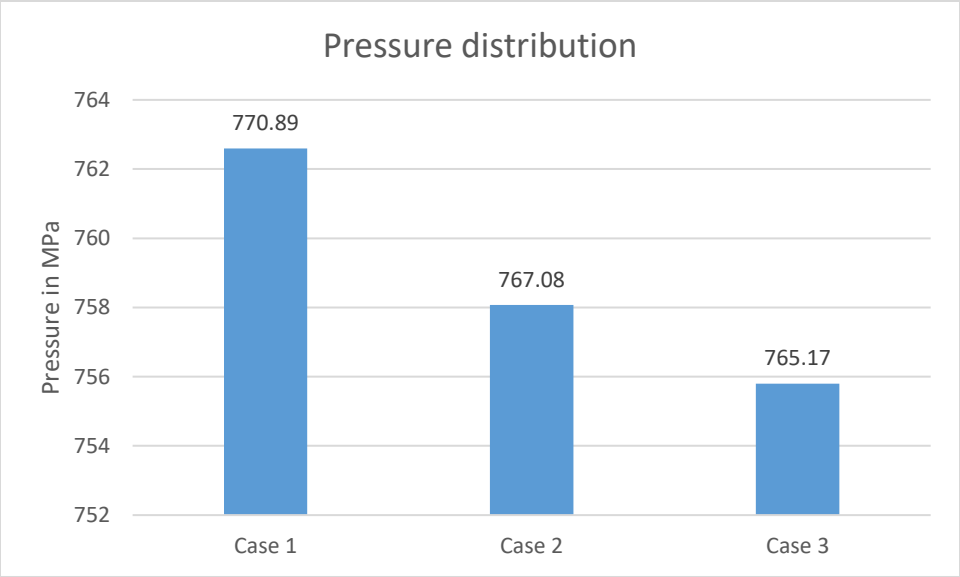

Figure 4.113: Pressure distribution graph during day flat hour for worn rail.

As shown in above figure 4.13, the maximum and minimum contact pressure distribution on worn rail head is given for three different location of minimum curved rail during day flat hour working period of Addis Ababa light rail transit. Case1 has greater contact pressure than the remaining cases.Case3 has the smallest contact pressure distribution than the rest of cases.

In case1 as shown in the figure 4.65 and figure 4.66the minimum fatigue life and maximum fatigue damage are 14230 cycles and 70276during afternoon peak hour respectively. In case 2 as shown in the figure 4.80 and figure 4.81the minimum fatigue life and maximum fatigue damage

are 14574 cycles and 68613during afternoon peak hour respectively In case 3 as shown in the figure 4.95 and figure 4.96the minimum fatigue life and maximum fatigue damage are 14751 cycles and 67794during afternoon peak hour respectively. Due to the contact there is a pressure on curved worn rail.

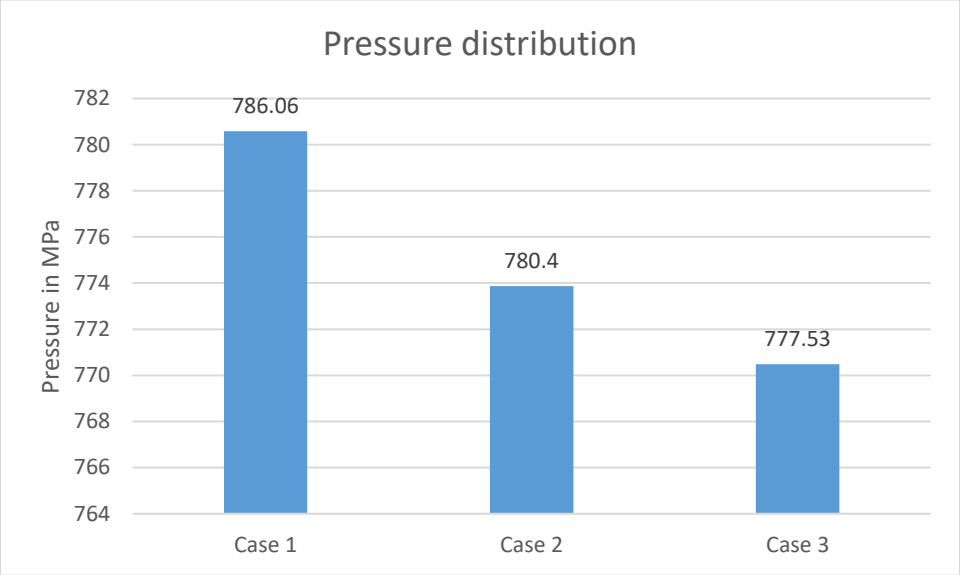

Figure 4.114: Pressure distribution graph during afternoon peak hour for worn rail.

As shown in above figure, the maximum and minimum contact pressure distribution on rail head is given for three different location of minimum curved rail during morning peak hour working period of Addis Ababa light rail transit. Case1 has greater contact pressure than the remaining cases.Case3 has the smallest contact pressure distribution than the rest of cases.

CHAPTER FIVE

5. CONCLUSION, RECOMMENDATION AND FUTURE WORK.

5.1. Conclusion.

In this study, the responses of curved rail are determined under static cyclic vertical and lateral wheel load, the results are assumed to be significant. The analysis included determining fatigue life, fatigue damage, equivalent alternating stress, and pressure distribution response of curved rail and curved worn rail caused by vertical and lateral cyclic wheel load. The analysis considers minimum curve radius of rails located at three places (stadium, saint lideta and autobistera) with three different working periods (during morning peak hours (7am-9am), day flat hours (9am-5pm) and afternoon peak hours (5pm-7pm)) in Addis Ababa light rail transit. In addition the paper makes analysis on minimum curved rail reduced five millimeter from the top of the rail due to wear.

From the results obtained in the static analysis, the three cases have different fatigue life on the curved rail. Fatigue life of the curved rail at stadium is less in comparison to fatigue life of curved rail at saint lideta and fatigue life of curved rail at autobistera. The fatigue life at autobistera is more in comparison to the fatigue life at stadium and fatigue life at saint lideta. The fatigue life during afternoon peak hour (5pm-7pm) is less in comparison to fatigue life during morning peak hour (7am-9am) and fatigue life during day flat hour (9am-5pm). The fatigue life during day flat hour (9am-5pm) is more in comparison to the fatigue life during morning peak hour and fatigue life during afternoon peak hour. The fatigue life of the rail decreases as wear of the rail increases at three minimum curved rail of AALRT (stadium, saint lideta and autobistera) during three working periods (morning peak hour, day flat hour and afternoon peak hour).

From the analysis based on the applied load, the safety factors on curved root at stadium, saint lideta and autobistera are less than one. This indicates that the rail will fail before reaching its design life in service.

5.2. Recommendation.

This part of rail track needed more attention than other parts, to reduce the problem related to the curved rail. This paper recommends curved rail at stadium needs special attention. This paper is also recommend, working period during afternoon pick hour need more attention due to more passenger flow that provides more vertical and lateral loads.

5.3. Future work.

In this paper fatigue failure analysis on curved rail caused by vertical and lateral wheel load are studied for different location of curved rail or/curved root with different working periods. This paper studies mainly on fatigue life, and fatigue damage based up on applied wheel load.

The curved part of the rail needs more attention to minimize the problem related to wheel/rail rolling contact fatigue on curved rail. Finally some suggestion are listed below for future work as extension and continuity of this paper.

- This paper studied fatigue failure analysis on horizontally curved rail. Studying fatigue failure analysis on effect of vertically curved rail route will be a research area.
- Analysis of fatigue failure on curved rail route of switch or crossing.
- Studying fatigue life and fatigue damage on curved rail route is analyzed. Making the analysis of fatigue failure on curved rail joints (welded and bolted joints) needs to be study.
- The more difference between straight and curved rails can be observed by studying and comparing fatigue failure analysis on straight and on curved root.

APPENDIX

Data collection.

The primary data of passenger loads in three tables below: table 3.7, 3.8, and 3.9 are collected through travelling with master trains.

Table1: Passenger Loads at Stadium.

Travelling time	Trains	Passenger loads in tons		
		Motor one	motor two	average
Morning peak hour (7am-9am)	Vehicle no. 205	18.5	18.5	18.5
	Vehicle no.206	18.6	18.5	18.55
	Vehicle no.207	18.4	18.3	18.35
	Average mean			18.46
Day flat hour(9am-5pm)	Vehicle no.210	16.7	16.5	16.6
	Vehicle no.209	16.9	16.6	16.75
	Vehicle no.211	16.5	16.4	16.45
	Average mean			16.6
Afternoon peak hour(5pm-7pm)	Vehicle no.205	19.1	19.0	19.05
	Vehicle no.208	19.3	18.9	19.1
	Vehicle no.212	19.2	19.1	19.15
	Average mean			19.1

Table 2: Passenger Loads at Saint Lideta.

Travelling time	Trains	Passenger loads in tons		
		Motor one	motor two	average
Morning peak hour(7am-9am)	Vehicle no. 205	18.1	18.2	18.15
	Vehicle no.206	18.1	17.9	18.0
	Vehicle no.207	18.2	17.6	17.9

	Average mean			18.0
Day flat hour(9am-5pm)	Vehicle no.210	16.2	16.1	16.15
	Vehicle no.209	16.1	16.3	16.2
	Vehicle no.211	16.4	16.3	16.35
	Average mean			16.23
Afternoon peak hour(5pm-7pm)	Vehicle no.205	18.7	18.6	18.65
	Vehicle no.208	18.8	18.8	18.8
	Vehicle no.212	18.6	18.5	18.55
	Average mean			18.66

Table 3: Passenger Loads at Autobistera.

Travelling time	Trains	Passenger loads in tons		
		Motor one	motor two	average
Morning peak hour(7am-9am)	Vehicle no.205	17.2	16.9	17.05
	Vehicle no.206	17.8	17.5	17.65
	Vehicle no.207	17.9	18.1	18.0
	Average mean			17.56
Day flat hour(9am-5pm)	Vehicle no.210	15.8	15.7	15.75
	Vehicle no.209	15.8	16.0	15.9
	Vehicle no.211	15.3	15.2	15.25
	Average mean			15.63
Afternoon peak hour(5pm-7pm)	Vehicle no.205	18.3	18.3	18.3
	Vehicle no.208	18.4	18.3	18.35
	Vehicle no.212	18.4	18.2	18.3
	Average mean			18.3

Constant amplitude load.

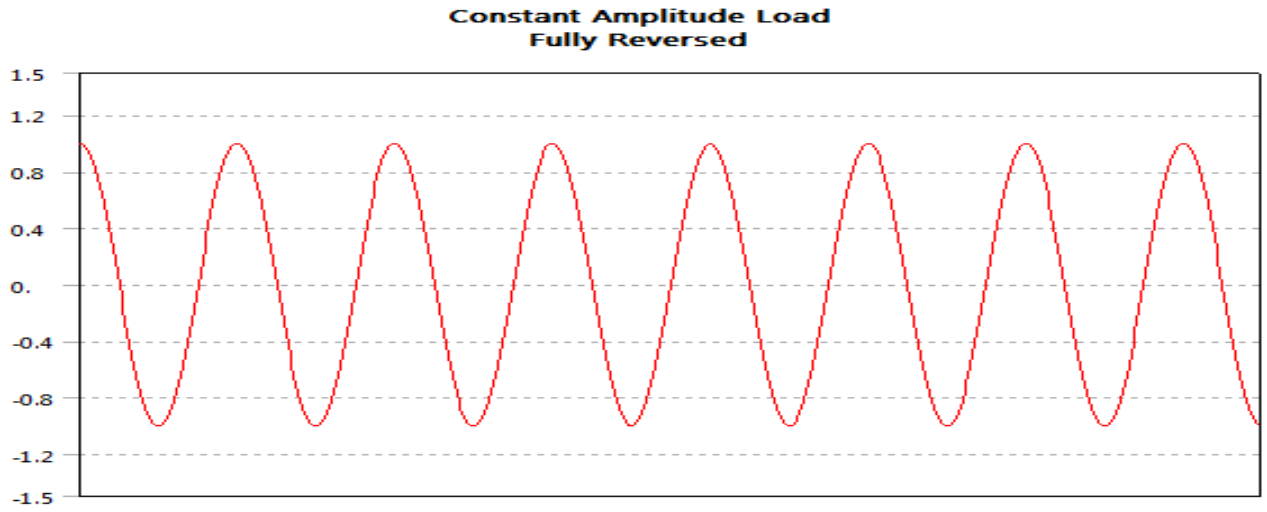

Figure 1: Fatigue constant amplitude load fully reversed.

Fatigue mean stress correction.

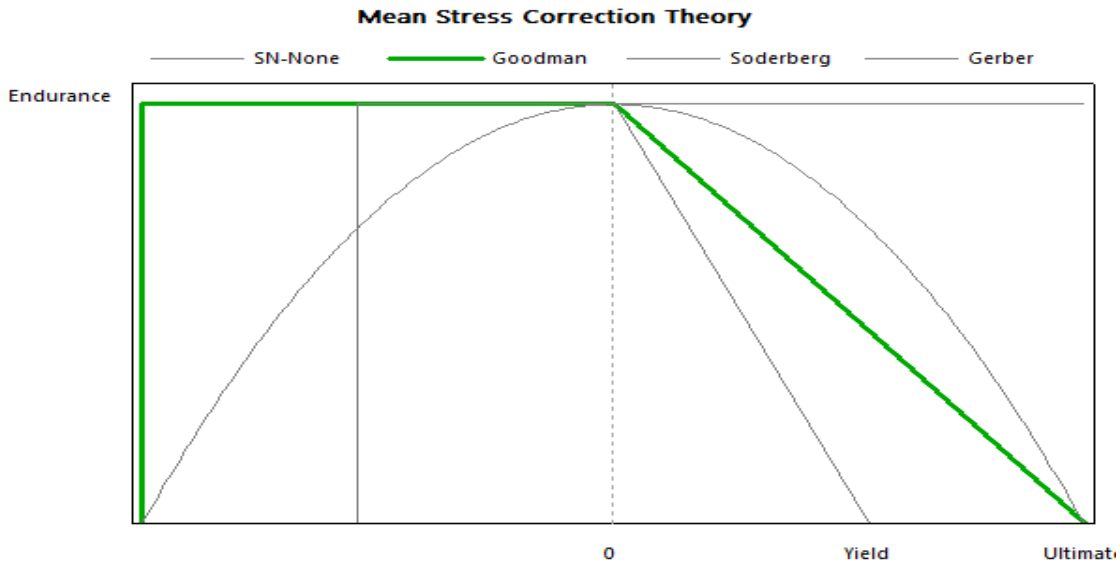

Figure 2: Fatigue mean stress correction theory.

REFERENCE

[1]. Michelangelo Bozzone, A.A. 2009/2010: Dynamic analysis of railway systems using computationally efficient wheel-rail contact models.Università Degli Studi Di Roma.

[2]. Coenraad Esveld, 2001: Modern Railway Track Second Edition, MRT-Productions. Delft University of Technology.

[3]. Saurabh Kumar, August, 2006. Study of Rail Breaks: Associated Risks and Maintenance Strategies. Luleå University of Technology, Luleå, Sweden.

[4]. Zerbst, U.; Lunden, R.; Edel, K.-O.; Smith, R.A. 2009: Introduction to the damage tolerance behaviour of railway rails. DOI: 10.1016.

[5]. R A Smith. 2000,Rolling Contact Fatigue of Rails: Imperial College of Science, Technology and Medicine, London.

[6]. Tiberiu Axinte, Violeta-Vali Ciucur, Rolling Contact Fatigue. Application in Rail-Wheel Interaction Modeling. Department Of General Engineering Sciences Constanta Maritime University 104, Mircea Cel Batran Str, Constanta, 900663Romania.

[7]. ASM International, 2008: Elements of Metallurgy and Engineering Alloys/264(#05224G).

[8].KhoaDuyVo, 2015. Damage analysis of wheel/rail contact associated to high adhesion condition. University of Wollongong.

[9]. Sagheer Abbas Ranjha, on December 2013. Effect of head wear on rail underhead radius stresses and fracture under high axle load conditions. Swinburne University of Technology.

[10].Munidasa Widhana Pathiranage Isuru Udara Wickramasinghe, August 2013. Investigation of Surface Ratchetting Due To Rail/Wheel Contact, Queensland University of Technology.

[11]. Kalle Karttunen, 2015. Influence of Rail, Wheel and Track Geometries on Wheel and Rail Degradation. Chalmers University of Technology Göteborg, Sweden. ISBN 978-91-7597-203-9.

[12]. Ir. R.P.B.J. Dollevoet, 2010. Design of an Anti-Head Check profile based on stress relief. PhD Thesis, University of Twente, Enschede, the Netherlands, ISBN 978-90-365-3073-6.

[13]. Jungwon Seo[a]a*, Seokjin Kwon[a], Deonghyeong Lee[a], 2011.Effects of surface defects on rolling contact fatigue of rail, aKorea Railroad Research Institute, 360-1 Woram-dong, Uiwang, 437-757, Korea.

[14]. Mark C. Burstow, 2011. Improving track geometry alignment to reduce rolling contact fatigue (RCF). 9th world congress on railway research may22-26, 2011.

[15]. Jungwon Seo*, Seokjin Kwon, Hynukyu Jun and Donghyeong Lee, Fatigue 2010. Fatigue crack growth behavior of surface crack in rails. Korea Railroad Research Institute, 360-1Woram-dong, Uiwang, 437-757, Korea.

[16]. Xiangyun Deng*, Maysam Naeimi, Zili Li, Zhiwei Qian, Rolf Dollevoet, May 2014. Residual fatigue life evaluation of rail at squats seeds using 3D explicit finite element analysis. Delft University of Technology, Delft, The Netherlands, Conference on Ageing of Materials & Structures Delft 26 – 28 May 2014, The Netherlands.

[17]. Ajay Kapoor, David I. Fletcher, F. Schmid, K.J. Sawley, M. Ishida, 2001.Tribology of Rail Transport. The University of Sheffield.

[18]. A. Langueh[a,c,d]*, J-F. Brunel[a,c,d], E. Charkaluk[a,b,d], P. Dufrénoy[a,c,d] , F. Demilly[e], 2011. Influence of the steel grades on rolling contact fatigue
of railway wheels.

[19]. De Song Technology Co., Limited, 2009-2017. P50 railway rail steel production, China.[20]. Ethiopian Railway Corporation, Technical Specifications of Vehicles July 2013.

[21]. Test Tracks at Transportation Technology Center, 2000. Inc. (Pueblo, Colorado).

[22]. Jean-Bernard Ayasse and Hugues Chollet, 2006.Hand book of railway vehicle dynamics (wheel/rail contact). By Taylor & Francis Group, LLC.

[23]. Fundamentals of rail vehicle dynamics, by A.H. Wickens, Loughborough University, UK, Swets&Zeitlinger, 2003.

[24] Map of AALRT line showing the respective fifty meter curve radius in the south- north line (kality-Minilik square),2015.

[25] S. Bhat and R. Patibandla (2011). Metal Fatigue and Basic Theoretical Models: A Review, Alloy Steel -Properties and Use, Dr. Eduardo Valencia Morales (Ed.), ISBN: 978-953-307-484-9, InTech,